

**Infection of immune competent macrophages expressing
functional Slc11a1 alters global gene expression, regulation
of metal ions, and infection outcomes**

by

Lara Janiszewski

B.A., University of Colorado, 2015

A thesis submitted to the
Faculty of the Graduate School of the
University of Colorado in partial fulfillment
of the requirements for the degree of
Doctor of Philosophy
Department of Molecular Cellular and Developmental Biology

2021

Committee Members:

Corrie Detweiler, Chair

Amy Palmer

Robin Dowell

Mary Allen

Brad Olwin

Janiszewski, Lara (Ph.D., Molecular, Cellular and Developmental Biology)

Infection of immune competent macrophages expressing functional Slc11a1 alters global gene expression, regulation of metal ions, and infection outcomes

Thesis directed by Prof. Amy Palmer

Nutritional immunity involves cellular and physiological responses to invading pathogens such as limiting iron availability, increasing exposure to bactericidal copper, and manipulating zinc to restrict the growth of pathogens. Manipulation of zinc at the host-pathogen interface depends on both the pathogen's identity and the nature of the host cell. Here I examine infection of bone marrow-derived macrophages from 129S6/SvEvTac mice by *Salmonella* Typhimurium. Unlike Balb/c and C57BL/6 mice, 129S6 mice possess functional Slc11a1 (Nramp-1), a phagosomal transporter of divalent cations. I carried out global RNA sequencing upon treatment with live or heat-killed *Salmonella* at 2 and 18 Hrs post-infection and observed widespread changes in metal transport, metal-dependent, and metal homeostasis genes, suggesting significant remodeling of iron, copper, and zinc availability by host cells. Changes in host cell gene expression suggest infection simultaneously increases cytosolic zinc and limits zinc within the phagosome. Using a genetically encoded sensor, I demonstrate that cytosolic labile zinc increases 36-fold 12 hrs post-infection. Further, manipulation of zinc in the media alters bacterial clearance and replication, with zinc depletion inhibiting both processes. Comparing my results to published data on infection of C57BL/6 macrophages revealed notable differences in metal regulation and the global immune response, with 129S6 macrophages transitioning from M1 to M2 polarization over the course of infection and showing signs of recovery. My results suggest that functional Slc11a1 profoundly affects the transcriptional landscape upon infection. Further, my results indicate that manipulation of zinc at the host-pathogen interface is more nuanced than that of iron or copper. The 129S6 macrophage leverages its intricate means of manipulating zinc availability and distribution to limit the pathogen's access to zinc while simultaneously ensuring sufficient zinc to support the immune response.

Dedication

This work is dedicated to my husband, Andrzej Waclaw Janiszewski, who in 2011 said, "I thought you wanted to do biology. You should go back to school."

Acknowledgements

I must acknowledge my advisor, Amy Palmer, who has supported and believed in me for the past 6 years, and who has been the best PI I could have asked for. Additionally, I could not have completed this work without the unflagging support of my husband Andy, my friend and confidante Jan, and my mother Lorraine. The guidance and mentorship of my committee has also been pivotal, as they all had a role in developing and refining this work. I must also acknowledge my financial support from the National Science Foundation Graduate Research Fellowship Program, which it was an honor to receive. Last but not least, I wish to recognize the developers of Biorender, who have saved me hours of toil and frustration.

Contents

Chapter		
1	Introduction	1
1.1	Zinc Homeostasis	2
1.1.1	Zinc in mammalian cells	2
1.1.2	Intracellular Zinc regulation	4
1.1.3	Zinc Transport	5
1.1.4	Zinc Buffering	9
1.1.5	Zinc Responsive Transcription	10
1.2	Measuring zinc in cells	11
1.2.1	Genetically encoded sensors	11
1.2.2	Small molecule sensors	13
1.3	Nutritional immunity	14
1.3.1	Extracellular nutritional immunity	14
1.3.2	Fe Starvation	15
1.3.3	Cu Toxicity	16
1.3.4	Zn Manipulation	16
1.4	Innate immune functions in macrophages	19
1.4.1	Polarization	20
1.4.2	Immune competent mouse model	22
1.5	Overall project description	22

1.5.1	Research questions	22
1.5.2	Novelty and relevance	24
2	Infection of immune competent macrophages expressing Functional Slc11a1 alters global gene expression, regulation of metal ions, and infection outcomes	25
2.1	Publication status	25
2.2	Introduction	25
2.3	Results	28
2.3.1	Infection induces widespread changes in gene expression	28
2.3.2	GSEA reveals pathways differentially affected by live versus heat-killed bacteria	33
2.3.3	There is significant remodeling of metal homeostasis in response to infection .	36
2.3.4	Cytosolic labile Zn increases at late stages of infection	40
2.3.5	Zn promotes bacterial clearance as well as bacterial replication	41
2.3.6	Macrophages from 129S6 and C57BL/6 differ in nutritional immune response to infection	45
2.4	Discussion	49
2.5	Methods	56
2.5.1	Monocyte extraction from bone marrow	56
2.5.2	Primary cell culture and infection	57
2.5.3	RNA extraction and sequencing	57
2.5.4	Data analysis pipeline	58
2.5.5	Comparison of current study with Stapels et al, Science, 2018	59
2.5.6	Measurement of cytosolic Zn and Imaging analysis	60
2.5.7	Flow cytometry study of infection outcome with varied zinc availability . . .	61
3	Future Directions	71
3.1	Fluorescent imaging of macrophages under Zn manipulation conditions	71

3.2	Long term live imaging of macrophages expressing ZapCV2 and treated with heat killed <i>Salmonella</i>	73
3.3	SpiroZin2 to interrogate Zn levels within the <i>Salmonella</i> containing vacuole	74
	Bibliography	77

Figures

Figure

1.1	Zinc Transporter Localization.	6
1.2	Basic Intra- and Extracellular Nutritional Immunity Mechanisms.	18
1.3	Mouse Macrophage Polarization.	21
2.1	<i>Salmonella</i> treatment of macrophages induces global RNA expression changes across two primary axes: time post exposure and <i>Salmonella</i> status (live vs. heat killed)	29
2.2	Clustered data exposes multiple distinct expression trends in global data .	32
2.3	GSEA reveals enrichment of the hypoxia and complement Hallmark gene sets in BMDMs infected with live <i>Salmonella</i> compared to treatment with heat killed bacteria.	34
2.4	GSEA reveals enrichment of the apoptosis Hallmark gene set at 2 Hrs and the UPR gene set at 18 Hrs in BMDMs treated with live versus heat killed <i>Salmonella</i>	37
2.5	There are widespread changes in metal-transport, -dependent and homeostasis genes.	38
2.6	Changes in labile cytosolic Zn in 129S6 BMDMs upon infection with <i>Salmonella</i>	42
2.7	Bacterial clearance as a function of time and Zn availability.	43
2.8	Bacterial replication as a function of time and Zn availability.	46

2.9	Changes in metal-transport and -homeostasis genes reveal differences in metal regulation in BMDMs derived from Slc11a1-functional mice compared to nonfunctional mice.	48
2.10	Clustered data exposes multiple distinct trends in gene expression (groups 3, 16, 11, 16, 7, 9).	63
2.11	Clustered data exposes multiple distinct trends in gene expression (groups 14, 19, 13, 16).	64
2.12	Clustered data exposes multiple distinct trends in gene expression (groups 4 and 5).	65
2.13	Clustered data exposes multiple distinct trends in gene expression (groups 17, 12, 20, 18).	66
2.14	GSEA analysis of Hallmark gene set TNF α signaling via NF-kB.	67
2.15	FACS analysis of infected 129S6 BMDMs clustered by time post infection.	68
2.16	Heatmaps of the gene clusters III and IV that were defined in Stapels et al.	69
2.17	PCA and dendrogram showing Stapels et al's data analyzed with my pipeline.	70

Chapter 1

Introduction

Metal ions play an important role in influencing how immune cells such as macrophages respond to infection by pathogens. Because metal ions are both essential to survival, as well toxic when present in excessive amounts, the host and the pathogen have evolved diverse strategies to regulate metal acquisition and availability, a concept encompassed by the term nutritional immunity. Here, I show that the metal transporter *slc11a1* plays a critical role in defining the macrophage response to *Salmonella* Typhimurium infection. Within these immune competent macrophages, I demonstrate that infection causes widespread changes in expression of nutritional immunity related genes, including those that remodel zinc to ensure increased zinc in the cytosol and limited zinc for the pathogen. Macrophages expressing functional *slc11a1* have a different profile of metal regulation and vastly different outcomes compared to immune compromised macrophages, demonstrating significantly different nutritional immune responses in immune competent versus immune compromised macrophages.

I am most specifically interested in the role of zinc ions (Zn) within infected macrophages, as Zn's role in immunity is complex and its nutritional use against *Salmonella* is not well understood. As a preface to this I present background on Zn homeostasis in the host, and the methods used in this work to measure intracellular Zn. I also include an in-depth introduction of iron, copper and zinc nutritional immunity, since the landscape of gene expression related to these metals is a key component of my results. I then briefly discuss macrophage polarization in mice, as this topic arose as a unique aspect of my data and a major factor that differentiates my results from those that

predominate in the field.

1.1 Zinc Homeostasis

Ionic zinc (Zn^{2+} , hereafter referred to as Zn) was initially recognized as an essential micronutrient for the fungus *Aspergillus niger* in 1869 and for rats in 1934, but it was not until 1963 that the profound effects of Zn deficiency in humans were revealed[1, 2]. Individuals with chronic, severe Zn deficiency are rare, and exhibit immune dysfunction resulting in a lifespan of about 25 years[1]. However, those with moderate Zn deficiency experience growth retardation, slow wound healing, mental lethargy and immune dysfunction while even mild deficiency has a measurable effect on immune function, including decreased phagocytosis, decreased IFN γ levels and NK cell dysfunction[2]. Mild to moderate Zn deficiency is common in the developing world, and the World Health Organization (WHO) estimates that more than 2 billion people (almost a third of the world's population) falls into this category. Zn deficiency is most prevalent in people with plant-based diets in developing nations. Cereals and legumes in these diets tend to be minimally processed and therefore retain a high level of phytate, a potent cation chelator that can dramatically limit the bioavailability of Zn[3]. However, Zn supplementation can reverse many symptoms of Zn deficiency including immune dysfunction[2].

1.1.1 Zinc in mammalian cells

The diverse effects of Zn deficiency are rooted in the variety of roles Zn plays in basic physiology including cell division[4], fertilization[5], neurological functioning[6, 7], and immune competence[8]. These myriad roles are a consequence of the fact that Zn is a requisite cofactor either structurally or catalytically for approximately 10% of eukaryotic proteins and 6% of prokaryotic proteins[9]. Zn dependent proteins are primarily enzymes and transcription factors, and in mammals Zn touches most aspects of cell biology. As a catalytic cofactor zinc can act to correctly orient a substrate molecule, or function as a Lewis acid, polarizing the substrate so that it binds to the enzyme more readily[9]. Zinc can also regulate catalytic function by blocking the active site of an

enzyme, as is the case in some serine proteases. Some enzymes, including matrix metalloproteinases, require zinc binding at two domains, one acting catalytically and the other acting structurally[9, 10]. Zn's essential role in the cell extends beyond that of a cofactor, as it has oxidative, antioxidative and second messenger functions.

Zn is intricately involved in the modulation of oxidative stress within cells. Despite its redox inactivity in biological systems, Zn has both direct and indirect antioxidant properties. Reactive oxygen species (ROS) are a normal byproduct of cellular respiration which must be neutralized to avoid cellular damage. Zn is key to this neutralization as an essential cofactor for superoxide dismutase, which converts superoxide radicals to the less toxic hydrogen peroxide. Zn can also diminish the overall level of radicals by inhibiting the production of superoxide by NADPH oxidase[11]. Finally, if Zn replaces copper (Cu) or iron (Fe) it could prevent the Fenton reaction, which produces OH radicals, from occurring[12]. Zn binds vulnerable sulfhydryl groups within proteins and lipids in the plasma membrane[13], affording them protection against oxidation. Additionally, increased cytosolic Zn activates metal regulatory transcription factor (Mtf1), inducing the production of metallothionein (Mt) proteins, which themselves are potent antioxidants. Mts effectively scavenge radical species and heavy metals. Thus, there are a variety of ways in which Zn can act to protect cells from oxidative stress.

While the above examples demonstrate that Zn can protect against oxidative stress, altered Zn levels, either too low or high, can also exacerbate oxidative stress. Zn deficiency negates the above antioxidant functions and causes the dysfunction of Zn dependent proteins. These include metalloenzymes that are essential for mitochondrial maturation, as well as resident ER chaperones calnexin and calreticulin, and the GPI-PET transferases[14]. Improper folding contributes to a buildup of misfolded proteins in the ER, which induces the unfolded protein response (UPR). The UPR can impair redox homeostasis and induce oxidative stress[15, 16]. Excess zinc also interferes with glycolysis, by inhibiting the enzyme glyceraldehyde-3-phosphate dehydrogenase (GAPDH)[17], as well as cellular respiration by disrupting the α -ketoglutarate dehydrogenase (KGDHG) in complex 1 of the electron transport chain[11, 18]. Both of these effects lead to decreased ATP production

and increased mitochondrial stress and ROS production[19].

1.1.2 Intracellular Zinc regulation

Given the serious consequences of Zn dysregulation, it is unsurprising that Zn homeostasis is tightly controlled. Mammalian cells contain 0.1-0.5 mM total Zn[14, 20] but much of this is bound to proteins, enzymes and other ligands with high affinity and is therefore unavailable for biological processes[21, 22]. The labile (or exchangeable) Zn pool, as measured by fluorescent sensors, is typically in the hundreds of picomolar range in the cytosol[23, 24, 25]. This labile pool is regulated both by buffering proteins, which can bind or release Zn based on the redox environment, and by transporters that regulate Zn's localization within intracellular compartments. While accurate measurement of Zn within organelles can be challenging, there are solid data indicating that Zn levels differ across organelles, as well as between cell types. Mitochondria maintain labile Zn levels at less than 1 pM in the matrix[26] but closer to 100 pM in the cytosol and between membranes[27]. While there were initially conflicting reports about whether Zn levels in the ER were higher than[28] or lower than[25] the cytosol, optimization of calibration conditions conclusively demonstrated that the Zn concentration in the ER is less than that in the cytosol[29]. Additionally, relative changes in Zn within lysosomes and secretory vesicles have been successfully measured[30, 31].

This tight regulation of Zn is modified within certain cell types, allowing for dynamic Zn fluctuations that have signaling characteristics. Secretory cells in particular maintain Zn rich granules from which Zn is co-released with vesicular cargo, allowing Zn transients to engage in paracrine or autocrine signaling[31]. For example, glutaminergic neurons use vesicular stores of Zn as neurotransmitters, and mouse hippocampal neurons exhibit Zn transients when stimulated with glutamate[7]. Pancreatic beta cells also release Zn in concert with insulin[31], while mast cells secrete Zn during caspase degranulation[32]. Oocytes also release thousands of Zn filled vesicles upon fertilization, creating a Zn 'spark' that hardens the zona pellucida, preventing multiple sperm from entering[5, 33]. Additionally, localized Zn transients are induced within all cells when Zn is bound or released from metallothionein (Mt) buffering proteins. Zn release can be induced by reactive oxygen or nitrogen

species as well as changes in pH and can serve a variety of purposes[34]. These include inducing transcription via Mtf1, participating in negative feedback by inhibiting nitric oxide synthase, or suppressing the activity of protein tyrosine phosphatases[35]. Thus, while labile Zn is in short supply, Zn dynamics have profound intracellular and extracellular effects.

1.1.3 Zinc Transport

Zn's roles in protein structure and function, transcription, cellular homeostasis, and signaling requires regulation of cellular Zn uptake and export, as well as its intracellular localization. These processes are coordinated by twenty-four Zn transporters. In mammals, Slc30a1-10 (also referred to as zinc transporters or ZnTs) transport zinc out of the cytosol either into the extracellular space or lumen of subcellular compartments. This is balanced by Slc39a1-14 (also referred to as Zrt- and Irt-like proteins or Zips), which transport Zn, as well as iron (Fe) and manganese (Mn), into the cytosol. See Figure 1.1.

While there are no crystal structures of mammalian Zn transporters, there is consensus on the general features of these proteins. Models are based on predicted topology, homology, and hydrophobicity plots, as well as lipidic cubic phase crystallography of bacterial transporters[36] including YiiP, an *E. coli* ZnT homolog and BbZip, a bacterial Zip homolog. Phylogenetic trees based on protein sequence homology show that both Zips and ZnTs are highly conserved among mammals, and proteins within each category cluster based on sequence and functional similarities[37].

Structurally ZnTs are likely to have 6 trans membrane domains, which form helical bundles, and tetramer transmembrane Zn binding sites containing conserved histidine and aspartic acid residues[37]. The YiiP homolog functions as a homodimer with monomers bound by salt bridges to maintain the correct conformation, and these structural features are predicted to be conserved in mammalian ZnTs. While ZnTs have cytosolic termini, YiiP also has a cytosolic C terminus Zn binding domain, though this may not be conserved[38].

All Zips and ZnTs can act as secondary active transporters, requiring energy in the form of an electrochemical potential to facilitate Zn transport. YiiP transports protons into the cytosol as

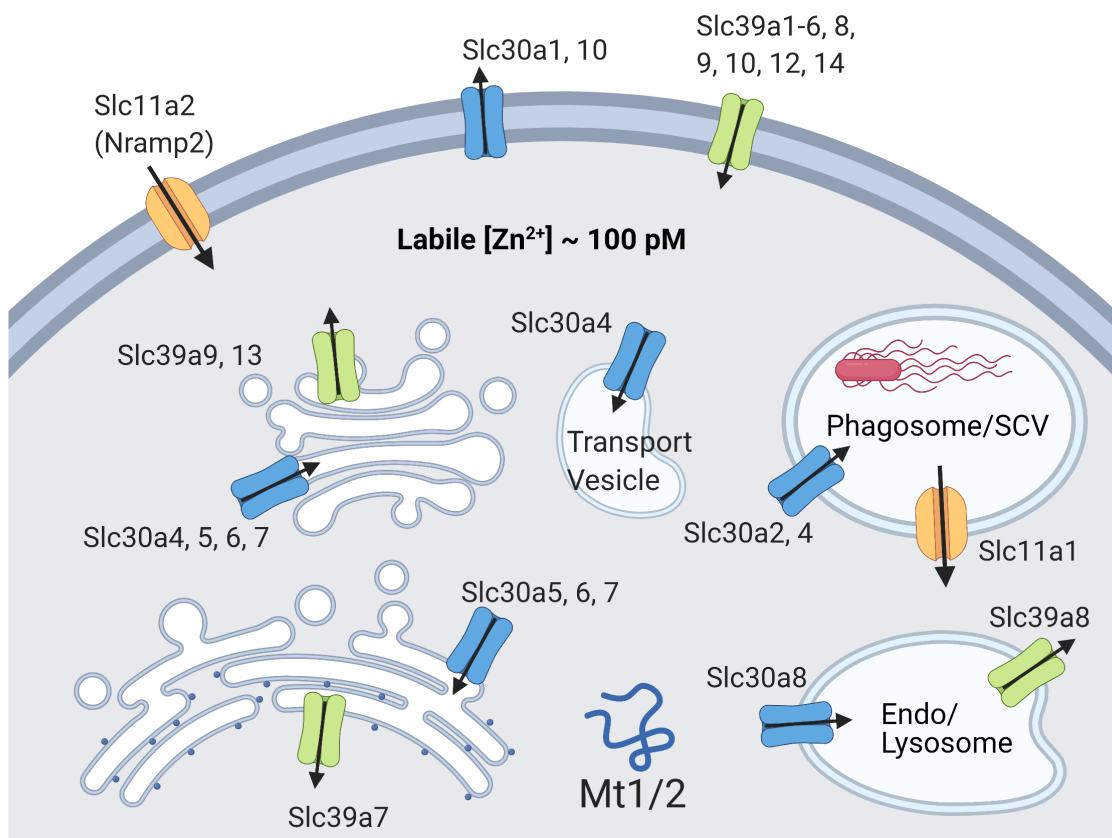


Figure 1.1: Zinc Transporter Localization. Zinc transporters localize to one or more cellular membranes, where they move Zn into (Zip/Slc39a) or out of (ZnT/Slc30a) the cytosol. While this is how they are defined, it is increasingly obvious that these transporters can have regulatory functions for the organelles they populate, including maintaining ER homeostasis and modulating cellular Zn export via the Golgi. Zip/ZnT regulation is not fully understood, though in humans all 24 appear capable of being regulated via phosphorylation, and some plasma membrane transporters are known to be regulated by endocytosis. Zips/Znts are fairly conserved and therefore presumed to be structurally similar to their bacterial homologs, for which there are a few crystal structures. Data suggest that, like their homologs, Zips have 8 transmembrane domains while ZnTs have 6, with most species functioning as homodimers. As secondary active transporters, Zip/ZnTs employ an alternating access mechanism to harness electrochemical energy from moving a non-Zn particle down its gradient. Figure created using Biorender.

the driving force for cytosolic Zn export via an alternating access mechanism[39]. This means that the transporter cycles between conformations that are ‘open’ to the inward facing cytosolic and then the outward facing periplasmic sides of the membrane, alternating the transport of protons and Zn. ZnTs are predicted to follow the same general structural and functional plan, and the alternating access transport of protons is especially suited to ZnT2-4,8 as they localize to acidic compartments, allowing the protons to move down their concentration gradient. Zips are predicted to have 8 transmembrane domains which form intramembranous binuclear metal centers, and to function as homodimers with extracellular termini[37]. The BbZip homolog is hypothesized to transport Zn by an electrodiffusional channel, where transported ions diffuse down their electrical and concentration gradients[40]. Though the transport mechanism of Zips has not been clarified, symport with bicarbonate ions has been suggested but not confirmed[41].

The residues along the intramembranous Zn binding sites provide metal specificity in Zips and ZnTs, and while many appear Zn specific, others have the capacity to transport multiple metals. ZnT10 is the only Zn exporter known to have residues allowing it to transport Mn as well as Zn. However, ZnT9 functions as a nuclear estrogen receptor and may lack Zn transporting function[37], while ZnT6 has hydrophobic amino acids in what should be its Zn binding channel, abolishing its transport capacity[42]. Instead ZnT6 functions as a secondary protomer in heterodimers with ZnT5. Zn importers Zip8 and Zip14 are capable of transporting Fe and Mn in addition to Zn, while Zip9 is a high affinity androgen receptor in addition to its Zn transport capacity, allowing for cooperative steroid and Zn signaling pathways.

Regulation of Zn transporters has not been fully clarified, though in humans all 24 transporters are predicted to be capable of regulation via phosphorylation[43]. Additionally, cell membrane Zip transporters are predicted to include cytosolic Zn sensing domains that induce endocytosis of the transporter in the presence of excess Zn, a condition that also induces ZnT1 transcription via MTF1. During Zn deficiency the extracellular domains of some Zips, including Zip4, are cleaved, which may influence transporter function or localization[44]. However, the mechanism for this process is unknown. ZnT regulation is less well studied, though data from pancreatic cells suggests that ZnT8

functions may be highly tunable based on the lipid composition of the membrane it resides in[45]. Additionally, many Zn transporters can localize to multiple membranes, and transfer between sites is likely a form of transporter regulation.

The 3 phylogenetic groups of ZnT proteins are based on sequence similarity and differ in localization[37]. ZnT1/10 are on the plasma membrane (PM), though in human macrophages ZnT1 has been found localized to the phagosome and actively increasing Zn stress on engulfed *E. coli*[46]. ZnT2-4 are all on intracellular secretory vesicles and are frequently specific to different professional secretory cells, while only ZnT4 is also found on endosomes, lysosomes and trans Golgi membranes. ZnT5-7 localize to the ER and Golgi, and are fundamental to the early secretory pathway. Not only do they control the Zn supply to nascent proteins and resident chaperones, the luminal domains of ZnT5 and 7 activate various ectoenzymes, including alkaline phosphatases.

The Zip proteins have 4 phylogenetic subfamilies, and clustering correlates with differing Zn coordination[37]. Zip1-3 homologs are tissue specific and contain hydrophobic residues which indicate a lack of binuclear metal centers, implying a different Zn coordination structure than that of other Zips[47]. Zip11 is its own family and is likely ancient, as it has an archaeal homolog. It, too, requires alternative Zn coordination, as it almost completely lacks cystine and histidine residues. Zip9 also has its own category, acting as both a Zn transporter and high affinity androgen receptor that induces cell signaling[48]. The remaining Zips engage in the conserved tetramer Zn coordination, as well as possessing a possible metalloprotease motif. Additionally, Zip8 and 14 can transport Fe and Mn in addition to Zn, likely because of glutamic acid in place of histidine in the metal binding domain. Zip7 and 13 may have altered metal specificity and their localization to the ER and Golgi gives them a role in Zn signaling and the homeostatic maintenance of the secretory pathway. Additionally, Zip7 upregulated by the unfolded protein response (UPR), and like ZnT5 and 7, its loss is disruptive to the ER.

1.1.4 Zinc Buffering

Zn buffering in cells is maintained by metallothioneins (Mt), small cytosolic proteins with multiple cysteine residues which coordinate and bind up to 7 Zn ions. Studies done on human Mt and Zn²⁺ in solution indicate that the first four Zn ions bind to Mt with dissociation constants in the picomolar range, while the fifth, sixth and seventh Zn ions bind with increasing KD values in the nanomolar range[49]. Together, these binding sites have dissociation constants that span 4 orders of magnitude, which allows for finely tuned Zn buffering, and is consistent with findings that labile Zn concentrations in cells are in the hundreds of picomolar[24]. In humans, there are 4 Mts, and Mt1 has 9 subtypes. Mice have Mt1-4, with Mt1 and 2 ubiquitously expressed, Mt3 expressed primarily in the brain, and Mt4 found in stratified epithelia[50, 51].

Zn buffering studies have introduced the concept of ‘zincosomes’[52, 53], defined as small vesicles possessing both Zn import and export capacity that store Zn with the potential for release of the vesicular Zn pool into the cytosol. It has been suggested that zincosomes could function as a Zn buffering pool with a faster reaction time than the synthesis or degradation of Mt proteins[53]. Data collected from *Saccharomyces cerevisiae*, using the small molecule Zn probe Zinquin as well as zinc-selenium autometallography, suggests the existence of zincosomes distinct from the yeast vacuole, and capable of buffering Zn even in the absence of endocytosis. These zincosomes accumulate Zn when it is supplied in excess and appear capable of its subsequent release under some low Zn conditions[52], but a mechanism for release was not suggested. Additionally, putative zincosomes have been isolated from RAW264.7 cells and subjected to X-ray absorption spectroscopy to study the Zn ligand environment within these compartments. Zn appeared to be complexed with sulfur, nitrogen and oxygen, which may differ from Zn binding in other cellular compartments[53]. However, the potential for Zn release from these vesicles was not studied, nor were differences between zincosomes and secretory vesicles. Thus far, cohesive evidence for these Zn vesicles seems lacking, while Mt proteins appear to be sufficient for Zn buffering[34].

1.1.5 Zinc Responsive Transcription

While Mts do not have the storage capacity of metal buffering proteins like ferritin, which can store 4500 Fe ions, they do appear to be the primary storage and buffering protein for Zn. This is due in part to the ubiquitous metal-dependent transcription factor (Mtf1), which is sensitive to rising Zn levels in the cytosol. Upon binding excess Zn, Mtf1 translocates to the nucleus and upregulates the expression of Mt genes, the translation of which lowers cytosolic Zn levels. This response is robust enough to protect cells from fluctuations in environmental Zn[54]. Consequently, increased Mt mRNA expression is often used as a proxy for increased cytosolic Zn concentrations. However, it should be noted that other transcription factors can act on Mt genes, including activation by Fos and Fra-1 and suppression by Pz120[55]. In addition to Zn, Mtf1 is also responsive to heavy metals, hypoxia, and oxidative stress[56]. Under these conditions, increasing the expression of Mts can lead to scavenging of heavy metal and ROS. Additionally, Mtf1 can induce expression of other target proteins including the putative antioxidant Sepw1 and cadmium response protein Csrp1[57]. Zn related targets of Mtf1 include upregulation of Mt genes and the plasma membrane Zn exporter Slc30a1[58], and downregulation of Slc39a10[57]. A knockdown study conducted to identify additional Zn related Mtf1 target genes showed that knockdown of Mtf1 decreased the zinc-induced transcriptional response of only some zinc responsive genes, while other genes became newly responsive to changes in Zn under knockdown of Mtf1[58]. This led to the hypothesis that Mtf1 is at the top of a hierarchy of Zn gene responses, but the other regulators remain to be determined.

Currently there are no known mammalian proteins that are responsive to low Zn conditions. However, in *C. elegans* low zinc activation (LZA) motifs have been identified in the promoter region of multiple Zn responsive genes[59]. Expression of slc39a (Zip) cytosolic Zn importer genes in HEK293T cells was also studied under low Zn conditions, and putative LZA motifs were identified in the promoter regions of Slc39a2 and Slc39a13. Additionally, reporter plasmids with promoter regions containing the *C. elegans* LZA were also responsive to low Zn conditions in HEK293T cells.

These data suggest conserved transcription functionality[59]. The transcription factor ELT-2 binds to the *C. elegans* LZA, but mammalian transcription factor involvement is still unclear.

1.2 Measuring zinc in cells

Total zinc within mammalian cells can be measured by a variety of elemental analysis techniques, including laser ablation inductively coupled plasma mass spectrometry and X-ray absorption spectroscopy[60], and tends to be in the micromolar range[61]. However, much of this zinc is bound to proteins, rendering it unavailable for kinetically favorable ligand exchange. Zinc that is loosely bound to proteins or small molecules, and therefore readily exchangeable, is termed the labile zinc pool and is available for metabolic or signaling processes. Measurement of this labile zinc pool and its fluctuations during infection are most relevant to my work, and this is achieved via fluorescent sensors which are broadly split into genetically encoded protein sensors and small molecule sensors.

Fluorescent sensors consist of at least one fluorophore attached to a Zn binding domain. This domain must be able to alter the fluorescent output of the fluorophore, typically by changing its physical or electronic configuration[61]. Zn sensors are most effective in compartments where the Zn levels are expected to be near the apparent dissociation constant of the sensor, that is, the concentration at which it is half saturated. An appropriate sensor should also have the highest dynamic range achievable in the conditions being measured. Dynamic range refers to the difference in fluorescence between unbound and saturated states, and a larger range affords better accuracy and sensitivity to changes in Zn levels.

1.2.1 Genetically encoded sensors

Genetically encoded sensors typically consist of one or two fluorescent proteins (FP) tethered to a naturally occurring Zn binding domain which tunes the fluorescent output of the FPs. One major advantage to this type of sensor is that their expression levels within cells are regulated by promoter regions, and they can be targeted to various subcellular compartments via genetic localization domains. Additionally, they can be tethered to domains from membrane or luminal

proteins with desired localization, allowing for targeting to specific compartments[31]. Unfortunately, targeting of genetically encoded sensors is not always straightforward. FPs can be quenched by protonation in acidic compartments, and cysteine residues can be oxidized to disulfide bonds in oxidizing environments like the ER[29]. Additionally, genetically encoded sensors are relatively large, and may mis-localize, even when tethered to a protein or a localization signal. However, these sensors will not passively enter subcellular compartments, making them ideal for cytosolic Zn measurements.

Single FP sensors are constructed as a circularly permuted FP with metal binding domains on the N and C termini. Metal binding changes the environment of the FP such that fluorescent output is measurably altered. Measurements from single FP sensors are necessarily intensimetric, which can be useful when calculations of [Zn] are not necessary. Additionally, the single FP sensors GZnP1[62] and GZnP2[27] have dynamic ranges equal to or greater than that of dual FP sensors with the same Zn domains, which is maintained within mitochondria. However, data from single FP sensors can be confounded by non-Zn related changes in the cell, such as pH, which can alter the fluorescent output.

Dual FP sensors are frequently based on fluorescence resonance energy transfer (FRET) between the FPs, and the ratiometric measurements from these sensors can be used to make quantitative [Zn] measurements. Additionally, they are more robust in the face of confounding variables like pH, as both FPs will be affected to similar degrees, allowing the ratio between them to remain relatively constant. These sensors do suffer from lower dynamic range than single FP sensors, and this is compounded within subcellular compartments. However, with rigorous optimization and calibration, high quality and replicable FRET data has been gathered within mitochondria, Golgi and the ER using ZapCY based sensors [25, 29].

The Palmer lab has developed multiple Zn FRET sensors in the Zap family, which revolves around 2 Zn finger domains from the *S. cerevisiae* transcription factor Zap1[63]. These Zn fingers serve as the Zn binding domain that tethers together the sensor's pair of FPs, and when bound with Zn this domain undergoes a conformational change that pulls the FPs into the correct proximity

and alignment for FRET to occur. The Zap2 binding domain was developed by mutating one Cys to a His in each Zn finger, which altered its affinity for Zn. In the lab's best cytosolic Zn sensor, ZapCV2, the Zap2 linker tethers an enhanced Cyan Fluorescent Protein (CFP) donor to a circularly permuted Venus FP as the acceptor. ZapCV2 has a $K_D = 2.3$ nM in HEPES buffer, and a robust dynamic range of 2.1[64]. While this sensor's K_d is well above the average cytosolic [Zn], it is used in the current work because increases in [Zn] during infection are unlikely to saturate the sensor, allowing us to collect accurate data.

1.2.2 Small molecule sensors

Small molecule sensors generally combine an organic fluorophore and an electron rich Zn chelating group[61]. The fluorophore is quenched in the unbound state, and quenching is disrupted with Zn binding. While these sensors are intensimetric, they generally have high fluorescent turn-on and very low background fluorescence, yielding high dynamic ranges. These probes have been successfully used to study Zn dynamics, Zn transport, and Zn dyshomeostasis in cancer cells. However, their concentration and localization within cells are not readily controlled or measured. Additionally, instead of being quenched by pH, many of these sensors experience fluorescence turn-on in low pH compartments, which is a confounding factor. Changes in charge can also alter their membrane permeability, causing them to become trapped within intracellular compartments, though this can be leveraged for specific targeting.

FluoZin-3, a frequently used small molecule Zn sensor, has been rigorously tested in multiple cell types[24]. It was found to have varied localization and aggregation depending on cell type. For example, likely dye aggregates were seen in the Golgi of HeLa cells, but the dye partially colocalizes with Vamp2 in neurons. When used to observe $[Zn^{2+}]$, the percent saturation of FluoZin-3 varied from 15-41% across a HeLa cell population. Additionally, the percent saturation decreased as [dye] levels increased, which indicates that the sensor is depleting the Zn pool in the system it is being used to measure[24]. Despite its drawbacks, much of the nutritional immunity literature relies on it or sensors like it to observe Zn during infection.

Another small molecule sensor of particular note is SpiroZin-2, which is unperturbed by pH from pH 3-7, has a strong dynamic range, and which readily reports Zn levels in lysosomes[30, 65]. This could prove valuable in the measurement of Zn in the *Salmonella* containing vacuole (SCV), as the bacteria allow partial fusion between the SCV and lysosomes in order to both acidify the compartment and obtain nutrients and molecular building blocks[66].

1.3 Nutritional immunity

In intracellular nutritional immunity the localization of metal ions is manipulated to limit the viability of engulfed pathogens, but this is now handled with metal specific mechanisms. Macrophages sequester many pathogens in a phagosomal compartment which helps the cell to direct its killing mechanisms, including nutritional immunity effectors.

1.3.1 Extracellular nutritional immunity

Transition metal ions, including iron (Fe), copper (Cu), zinc (Zn) and manganese (Mn), are essential protein cofactors for all kingdoms of life. However, all but zinc are redox active and all are toxic at high concentrations. To sustain growth and maintain pathogenicity, infectious organisms must acquire these essential micronutrients from within their hosts, while hosts exploit both the toxicity and necessity of these ions to suppress infection. This is the essence of nutritional immunity, and it occurs on an organismal and cellular level, with both hosts and pathogens having evolved varied mechanisms to outmaneuver one another.

Systemically organisms engage in metal sequestration upon infection, evident as a sharp decrease of free metal ions in serum[67], which is at least partially mediated by high expression of Mt proteins in the liver[68]. This sequestration is essential, as unfettered access can allow for exponential growth of an invasive microbe population[69]. The necessity for effective sequestration has been demonstrated for multiple metals. For example, when iron replete children are given iron supplementation, sequestration is taxed during infection, resulting in increased morbidity and mortality[70, 71]. Excess Zn in a mouse model induced disruption of the gut microbiome in response

to antibiotics, which allowed infection by the zinc tolerant pathogen *Clostridium difficile*[72]. Once *C. difficile* had colonized the gut excess zinc was again deleterious, as it promoted virulence and systemic infection through unknown mechanisms[72]. Additionally, excess dietary Mn in a mouse model enhanced the bacterial load and virulence of cardiac *Staphylococcus aureus* infection[73] since Mn is a cofactor for virulence factors as well as superoxide dismutase enzymes, which neutralize reactive oxygen species. These studies exhibit the repercussions of overwhelming a host's metal sequestration capacity.

1.3.2 Fe Starvation

A key player in Fe based nutritional immunity is the metal transporter Slc11a1, or Nramp1, the natural resistance-associated macrophage protein. Slc11a1 serves to starve the pathogen, and when this gene is knocked out of mouse strains it renders them immune compromised[74]. When this protein is intact it localizes to the phagosome during infection and engages in proton coupled metal transport, acidifying the compartment while removing Mn, Mg, Cu, Zn, and Fe divalent cations from the pathogen's immediate vicinity[75, 76, 77]. Additionally, in C57BL/6 mice infected with *Salmonella* Typhimurium, the macrophage Fe exporter ferroportin (Slc40a1) is upregulated in an NO dependent manner, further reducing the Fe availability within the macrophage[78].

Pathogens employ multiple methods to acquire Fe within a host, most of which occur in the bloodstream. These include high affinity uptake transporters for free Fe, extraction of Fe from heme, and expressing receptors for the mammalian Fe transporter transferrin, from which they can strip the Fe[69, 79]. Pathogens also express siderophores, molecules with an Fe affinity capable of stripping the ion from host proteins like transferrin[75, 79]. Complex energy dependent siderophore-Fe uptake systems are in place in Gram negative bacteria, attesting to the resources expended to acquire Fe[69]. While host proteins cannot compete with siderophores directly for Fe, siderocalin is a host expressed protein that binds siderophores, preventing their uptake by bacteria[79]. This evolutionary tug-of-war has multiple layers, including the production of siderophores that resist binding by siderocalin, as in *Bacillus anthracis*[80].

1.3.3 Cu Toxicity

Copper ions (Cu) are directly bactericidal and are imported into the cell via Slc31a1 (Ctr1) and into the phagosome via the ATPase Atp7a transporters[81]. In mouse tissues Slc31a1 has also been found localized to intracellular compartments, and may serve a roll in releasing Cu from intracellular stores[82]. Oxygen or nitrogen-based radicals are directed into the phagosome at early and late stages of infection, respectively. When Cu is released into the lumen with these factors it potentiates redox cycling of the radicals, depleting bacterial antioxidants. Alone, excess Cu mismetallates Fe containing proteins, including Fe-S clusters used in bacterial metabolism, effectively crippling the bacteria[82, 83, 84].

Many studies have been conducted to describe the variety of efflux transporters used by pathogens to protect against cytosolic Cu poisoning[84], which do not necessarily have redundant functions. For example, *Salmonella* Typhimurium tolerates the double knockout of *copA/golT* Cu efflux transporter genes in one mouse study[81] with no obvious decrease in *Salmonella* burden in the liver or spleen. However, in a second mouse study *Salmonella* did not exhibit a reduced bacterial load until deprived of the *cueO* gene[85]. Additional transporters are encoded to specifically protect the bacterial periplasm from Cu overload, including the *cus* operon in *E. coli*. Pathogens express other categories of protective proteins as well. These include detoxification enzymes like Cu oxidases (coproporphyrinogen(III) oxidase in *N. gonorrhoeae*), which cycle Cu(I) to the less toxic Cu(II), and chelators like bacterial metallothioneins (MymT in mycobacterium[68]) which bind Cu as well as Zn.

1.3.4 Zn Manipulation

As with other metals, Zn is sequestered extracellularly during infection, which includes uptake by liver cells as well as the production of calprotectin, a calcium and Zn chelator, by neutrophils. Calprotectin is present in pathogen traps created by neutrophil degranulation and is secreted by neutrophils into the gut upon infection. That said, the role of Zn in nutritional immunity within

macrophages is more nuanced than that of Fe or Cu, as it can be used either to poison or starve a pathogen[69]. This seems to depend largely on the pathogen encountered.

While Zn is not redox active, it is still toxic in excess. This is because in the Irving-Williams series zinc's avidity as a ligand is second only to copper[86]. Therefore, excess zinc can displace iron and manganese ions bound to proteins, causing protein mismetallation and loss of function[87]. When used against internalized *S. pneumoniae*, Zn competitively inhibits Mn by binding irreversibly to Mn uptake transporter PsaA, effectively starving the pathogen of Mn. In *S. pyogenes* glycolytic enzymes, including phosphofructokinase, are inhibited by Zn [69, 68], forcing the bacterium to modify its metabolism. Zn exporters have also proven to be necessary for full virulence by both of these pathogens. *M. tb* within human macrophages also experiences Zn toxicity, requiring the upregulation of heavy metal efflux ATPase transporters for virulence. Treatment with FluoZin3 suggested a buildup of Zn in the *M. tb* phagosome[88]. Studies of *E. coli* within human and mouse macrophages suggest that the bacterium is capable of Zn detoxification as well as evasion of Zn containing compartments. Slc30a1, which typically localizes to the plasma membrane, increases Zn stress by relocalizing to the phagosome during *E. coli* infection[89, 46]. Additionally, *H. pylori* expresses 3 Zn efflux ATP transporter systems, and loss of any of them decreases its viability within macrophages[90]. Conversely, challenge with *Histoplasma capsulatum* induces macrophages to sequester Zn and increase ROS production to counter the infection[91].

Zn starvation appears to be less prevalent within macrophages, though it appears to be an effective strategy against the fungal pathogen *H. capsulatum*. This fungus expresses several Zn uptake transporters, and its virulence is decreased within mice when these transporters are knocked out[92]. Extracellularly, it has been suggested that some siderophores are promiscuous in their metal binding, allowing them to function as 'zincophores'[93] for bacteria. Interestingly this is not necessary for some pathogens including *Salmonella* Typhimurium, which thrives in Zn deficient conditions extracellularly.

These processes are shown in Figure 1.2.

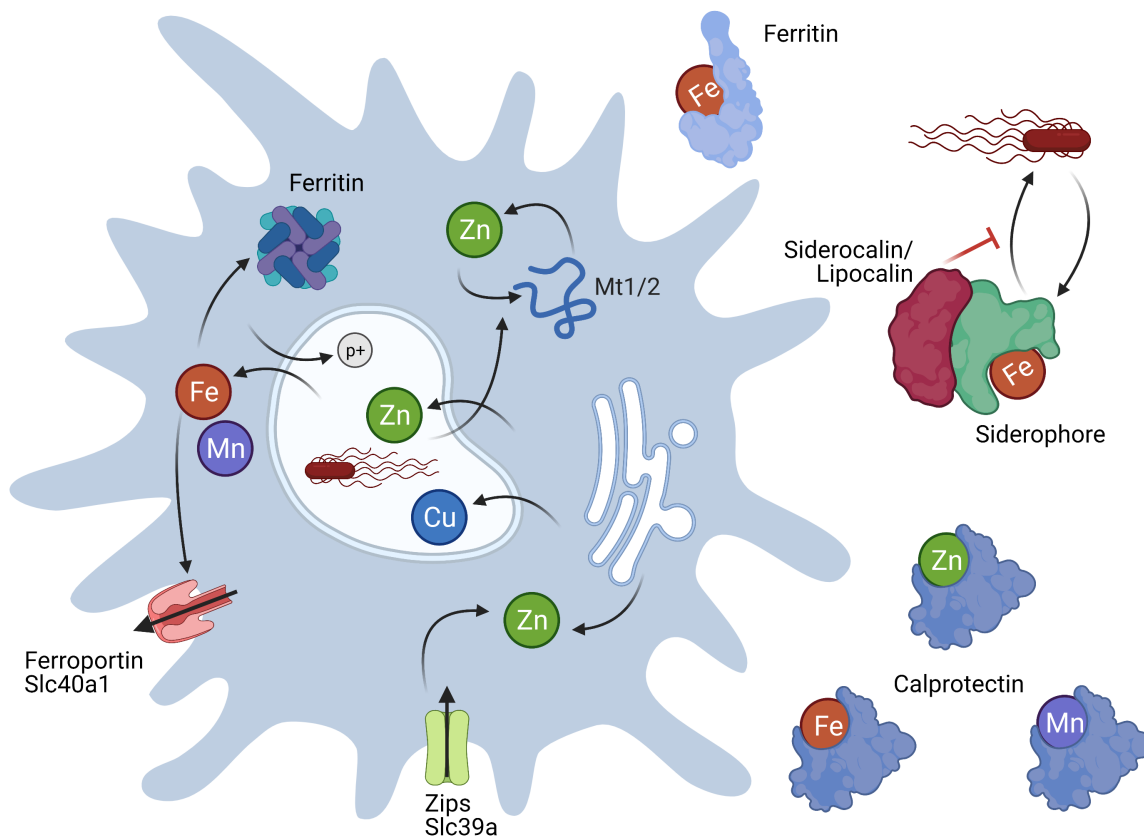


Figure 1.2: **Basic Intra- and Extracellular Nutritional Immunity Mechanisms.** Nutritional immunity is an innate immune function in which the host exploits both the necessity and toxicity of metal cation nutrients (Fe, Zn, Mn, Cu, Mg) to reduce pathogen load. The evolution of these tactics has given rise to the evolution of counter-measures in pathogens, resulting in a nutrient tug-of-war during infection. For example, hosts use chelators like calprotectin and transferrin to sequester metal ions, but pathogens developed high affinity siderophores to scavenge metals away from host proteins. In the case of iron, hosts have developed siderophore binding molecules, to prevent their delivery of Fe to the pathogen. Intracellularly pathogens are frequently contained in phagosomal vacuoles, an environment that host and pathogen attempt to control. Pathogens are starved of Fe and Mn, but overloaded with toxic Cu. Zn can be used to starve or poison a pathogen. Despite its lack of redox activity, Zn readily mismetallates proteins, disrupting their function. Figure created with Biorender.

1.4 Innate immune functions in macrophages

Macrophages are white blood cells involved in innate immunity and are referred to as ‘professional phagocytes’, as one of their primary functions is to engulf and digest pathogens as well as cellular debris and other ‘non-self’ particles. Most macrophages are released from the bone marrow as monocytes, which are incompletely differentiated and circulate in the bloodstream. In response to chemoattractant signals indicating tissue damage or infection, monocytes adhere to blood vessel walls and enter the affected tissue via extravasation. Here they differentiate to ameboid macrophages and follow chemotactic gradients to the site at which they are needed. These gradients can consist of cytokines, pathogens, or cellular debris, among others. These signals and others from the macrophages’ cellular milieu direct changes in gene expression and subsequent phenotype, which is referred to as macrophage activation or polarization. Once activated, macrophages can secrete dozens of pro- and anti-inflammatory mediators, thus playing a role in inflammation, the immune response, and tissue homeostasis[15].

Macrophages also possess more diverse functions beyond phagocytosis of pathogens. For example, macrophages play a role in antigen presentation and induction of adaptive immunity[94]. However, these functions are beyond the scope of this work and won’t be discussed further. Additionally, some macrophages are found as tissue residents, which can be specifically adapted to that tissue, as in the cases of brain glia and epidermal Langerhan cells. However, tissue resident macrophages frequently demonstrate self-renewal independent of the bone marrow[95], indicating a stem-like quality not seen in bone marrow derived macrophages[96]. Additionally, fate mapping indicates that many tissue macrophages have their origins in the fetal liver, and are seeded into tissues before birth[96]. While these cells are fascinating, they are not discussed further in this work.

1.4.1 Polarization

Although monocyte-derived macrophages are differentiated cells, their gene expression and metabolism remain plastic and are readily altered based on the tissue environment infiltrated and the immune-related signals received[15]. For example, a site of infection will likely require macrophages to contend with hypoxia and altered nutrient availability while maintaining the high energy production required for phagocytosis and cytokine production[15]. Alternatively, if this state is maintained after the infection is cleared the macrophage would be a liability to the host, inducing damaging inflammation and possibly contributing to auto-immune responses. To allow for plasticity, activated macrophages can exhibit a continuum of phenotypes, from pro-inflammatory and cytotoxic (termed M1 polarization) to anti-inflammatory and wound healing (M2 polarization). *In vitro* these two extremes are frequently induced by the introduction of a few activating proteins. Examples include lipopolysaccharide (LPS) and Ifng used separately or together to induce M1 activation, and Il-4 used to induce M2 activation. However, *in vivo* these states are more fluid, and activation can be heterogeneous across a population based on the multiple and conflicting polarizing factors typically present in a given environment[15, 97, 98]. Additionally, multiple M2 phenotypes are recognized as being induced by different pro- and anti-inflammatory factors, both endogenously and exogenously. Because of this, referring to a population of macrophages as simply M1 or M2 can be confounding, making comparisons between studies difficult. To help define experimental standards Murray et al[99] have proposed nomenclature conventions for specifying the protein species used for macrophage activation, for example (IL10)M2 or (LPS)M1.

Polarized macrophages have distinct metabolic requirements. M1 macrophages use glycolysis for their acute energy needs and bypass steps in the Krebs cycle, diverting intermediates to produce antimicrobial species (itaconic acid) or NO enhancing species (malate, citrate)[100, 101, 102]. Citrate also contributes to the activation of Hypoxia-inducing factor 1-alpha (Hif1a) genes and a pro-inflammatory cascade involving IL-1b[101]. In fact, hypoxia promotes glycolytic over oxidative metabolism, which in turn maintains M1 polarization[15]. In contrast, M2 macrophages rely

on fatty acid metabolism and the use of an intact Krebs cycle, which can be sustained for longer periods[15, 103, 104]. This is consistent with the less acute functions of M2 macrophages, including angiogenesis and extracellular matrix remodeling. Metabolic adaptation is therefore key to macrophage polarization (see Figure 1.3).

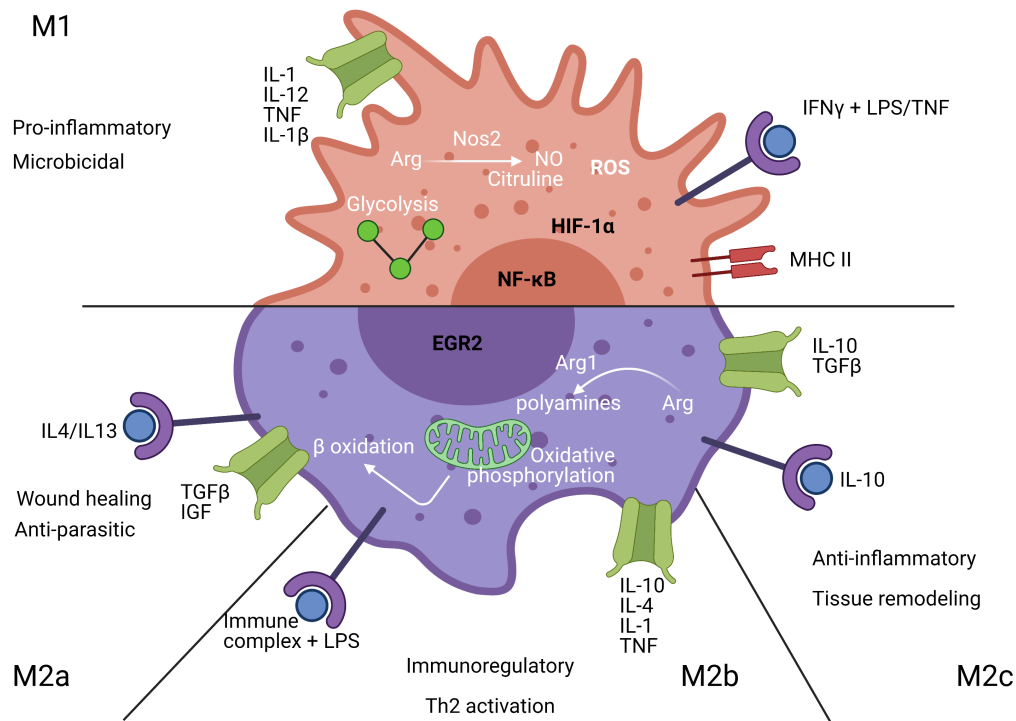


Figure 1.3: Mouse Macrophage Polarization. Macrophages are activated by polarizing signals in their surroundings, which can include cellular debris, pathogens, and cytokines. *In vivo* these signals can be complex and conflicting, resulting in macrophages with mixed pro- and anti-inflammatory phenotypes. However, *in vitro* polarization can be induced with specific factors, resulting in 4 fairly discrete phenotypes, as seen above. Polarized phenotypes can be flexible, and somewhat responsive to changes in their surroundings, though M1 cells are often refractory to M2 signals. Importantly, metabolism is a major factor in polarization. M1 cells have high energy demands and can be hypoxic, and therefore use glycolysis for energy production and interrupt the Krebs cycle, removing intermediates for antimicrobial functions. M2 cells instead upregulate fatty acid metabolism and oxidative phosphorylation for their less acute energy needs. In mice the metabolism of L-arginine is a delineating factor between M1 and M2 states, though this is not the case in human macrophages. Mouse M1 cells use Nos2 to make the toxic radical NO from L-arginine while M2 cells use Arg1 to produce polyamines for tissue repair from L-arginine. Human macrophages produce little to no Nos2 or Arg1 enzymes. Figure created with Biorender.

1.4.2 Immune competent mouse model

Critical comparison of Zn at the host-pathogen interface may be confounded by the differences in the macrophage models used across studies. Both Balb/c and C57BL/6 mice lack a functional Slc11a1 (Nramp-1), a phagosomal transporter for magnesium (Mg), Fe, Mn, and Zn[105]. Macrophages from these mice are more susceptible to infection and have reduced capacity to clear intracellular pathogens[106]. RAW264.7 cells, a popular mouse macrophage cell line used to study intracellular pathogens, are derived from C57BL/6 mice and therefore equally impaired. The lack of functional Slc11a1 compromises the host response to infection with respect to metal regulation, making it difficult to define the nutritional immunity landscape in an immune competent model system. To address this limitation, the current work uses macrophages from 129S6/SvEvTac mice which express functional Slc11a1. *In vivo* systemic *Salmonella* infection of these mice demonstrate their immune competence, as these mice experience enlarged lymph nodes and spleens but otherwise remained asymptomatic[106].

1.5 Overall project description

1.5.1 Research questions

How does the transcriptional program of immune competent macrophages change upon infection with *Salmonella*, and what are the impacts of bacterial status (alive versus heat killed) and time?

Given the lack of consensus in the literature regarding intra-macrophage zinc-based nutritional immunity against *Salmonella*, I chose to investigate the mRNA expression changes induced by *Salmonella* infection. Further, I wanted to explore how the transcriptional landscape is altered when the *Salmonella* are heat-killed, and unable to modify macrophage responses via protein expression changes. While lipopolysaccharide (LPS) treatment is the most common negative control used in *Salmonella* experiments, I felt that it was not sufficient for my purposes, as expression differences between live and heat-killed *Salmonella* exposure were likely to be subtle. LPS is a major component

of the *Salmonella* protein coat and it binds the toll like receptor 4 (Tlr4) in the host-cell to activate an immune response. But, LPS is not the only *Salmonella* antigen to effect an immune response. Flagellin proteins and peptidoglycans[107] are adjuvants, bound by macrophage Tlr5 and Tlr2, respectively[107]. Interestingly, flagellin are down-regulated by live *Salmonella* during infection, which somewhat attenuates the immune response[108]. While the activation pathways downstream of Tlr2/4/5 have redundancies, I felt it was important to have all of these factors present in my heat-killed condition. Use of heat-killed bacteria also allows direct comparison of RNAseq data with infection imaging data, which would use fluorescently-tagged heat-killed *Salmonella*. Additionally, macrophages demonstrate an early acute phase and late phases of infection, much of which is based on transcriptional alterations. Because of this I investigated the interaction of this variable with that of *Salmonella* status by collecting RNA at two time points, 2 Hrs and 18 Hrs, post infection.

Are there defined patterns of changes in transcription of metal regulatory genes across time or in response to live vs heat killed *Salmonella*? What does this imply about nutritional immunity and other immune functions?

As noted previously, 129S6 macrophages are immune competent because of the metal transporter Slc11a1, which localizes to the phagosome during infection. I chose these macrophages as my model system to evaluate if there was evidence of differential metal handling during *Salmonella* exposure, either across time or between live and heat-killed *Salmonella* exposure, based on changes in metal regulatory genes. Additionally I investigated differences between my RNASeq data and already published data collected under similar conditions in immune compromised mouse macrophages[109]. Primarily, I asked if my cells showed the same metal handling and polarization at 18 Hrs as was demonstrated in the compromised macrophages. My secondary question asked if the upregulated genes in these two studies showed disparate GSEA or DAVID annotation, and what functional inferences could be made from these.

Since Zn handling is a facet of immune function, can I demonstrate that altered Zn availability affects infection outcomes? Do either high or low Zn levels give host or pathogen a clear advantage?

If Zn is a specific factor in *Salmonella* infected macrophages, then alterations of zinc availability during infection should affect the outcome. That is, bacterial replication vs bacterial clearance should differ across conditions of Zn availability. Using *Salmonella* expressing a fluorescence dilution plasmid, I asked if altering zinc concentrations in media after bacterial internalization by macrophages would tip the balance in favor of host or pathogen. This was investigated at 4 time points: 2, 10, 18 and 24 Hrs post infection. This also allowed us to indirectly examine the Zn stress experienced by *Salmonella* in 129S6 macrophages, in lieu of a fluorescent sensor localized to the phagosome.

1.5.2 Novelty and relevance

While multiple studies have carried out RNASeq in *Salmonella*-infected macrophages, I found none with the combination of variables that I used: immune competent macrophages, heat-killed *Salmonella* instead of LPS, and a time course post infection. Additionally, I look specifically and comprehensively at metal handling and metal responsive genes, which is novel in the literature, especially in this macrophage cell type. Further, I paired this dataset with ratiometric measurements of free zinc concentrations within macrophage cytosol measured with ZapCV2, a zinc FRET sensor with fewer confounding variables and lower variability than is found with small molecule sensors. This [Zn] data was collected from 2 to 24 Hrs post infection in live macrophages and can therefore be correlated with both my sequencing results and my longitudinal Zn dependent infection outcome experiment. This data is relevant to both the nutritional immunity and macrophage polarization literature.

Chapter 2

Infection of immune competent macrophages expressing Functional Slc11a1 alters global gene expression, regulation of metal ions, and infection outcomes

2.1 Publication status

All of this chapter was submitted for review to PLOS Pathogens in February 2021 as Lara N Janiszewski, Michael Minson, Mary A Allen, Robin D Dowell, Amy E Palmer, Infection of immune competent macrophages expressing Functional Slc11a1 alters global gene expression, regulation of metal ions, and infection outcomes. All raw next-generation sequencing data files and processed data files used to draw conclusions are available at the Gene Expression Omnibus, data series GSE166642. Financial support was provided by the following sources: National Institutes of Health - NIH Pioneer Award (DP1 GM114863 to AEP), MIRA (R35 GM139644 to AEP), RO1GM125871 (RDD), and R01HL156475 (ML). LJ was supported by a National Science Foundation GRF. None of the funders played any role in study design, data collection, decision to publish, or preparation of the manuscript.

2.2 Introduction

Pathogenic organisms must acquire essential micronutrients such as iron, zinc, and manganese to sustain growth and maintain pathogenicity. To protect itself, a host organism in turn attempts to sequester these nutrients, as unfettered access can allow for the exponential growth of an invasive microbe population[69]. Metal ion sequestration occurs on a systemic level, evidenced by the sharp decrease of free metal ions in serum upon infection[67]. Additionally, phagocytic immune cells manipulate the intracellular localization of metal ions to limit the viability of engulfed pathogens,

but this process is more complex than unilateral sequestration. Within macrophages, iron (Fe) ions are bound by cytosolic storage proteins and transported out of phagosomal compartments[75], while these same compartments are flooded with bactericidal copper (Cu) ions[83, 84]. The role of zinc (Zn) in nutritional immunity in macrophages is more nuanced than that of Fe or Cu, as it can be used either to poison or starve a pathogen[69]. Some microbes have developed strategies to counter these tactics, including siderophores to scavenge Fe ions, oxidases to detoxify Cu, exporters to expunge excess metals, and high-affinity importers to overcome metal limitation[69][67, 79]. There is a growing body of work suggesting that both the pathogen and the host have mechanisms to regulate Zn accessibility[69, 8], however the overall picture of Zn regulation during infection is not well understood.

Zn is an essential micronutrient required for growth, proliferation, and several fundamental biological processes. In mammals, Zn is a requisite cofactor either structurally or catalytically for approximately 10% of the proteome[9], including many transcription factors and enzymes. As with other metal ions, excess Zn can be toxic, and cells tightly regulate its availability. Mammalian cells contain hundreds of micromolar total Zn but most of this is bound to proteins, enzymes and other ligands such that labile (or exchangeable) Zn, as measured by fluorescent sensors, is typically in the hundreds of picomolar range in the cytosol[23, 24, 25]. There are fewer tools for, and hence less consensus on, the concentration of labile Zn in organelles. However, multiple different fluorescent sensor platforms have suggested that labile Zn distribution in organelles is heterogeneous[25, 110, 111, 29, 61]. Zn is regulated by membrane-specific Zn transporters, including Slc30a1-10 (also referred to as ZnT1-10) that transport zinc out of the cytosol, and Slc39a1-14 (also referred to as Zip1-14) that transport Zn (as well as Fe and manganese, Mn) into the cytosol[14]. Cells also contain metallothioneins (Mt), which serve to bind and buffer Zn ions, and a metal-dependent transcription factor (Mtf1) that translocates to the nucleus upon binding excess Zn to regulate the expression of genes that lower cytosolic Zn levels. One major role of Mtf1 is regulating the expression of Mt genes in response to cytosolic Zn levels, protecting cells from fluctuations in environmental Zn[54]. Consequently, increased Mt expression is often used as a proxy for increased

cytosolic Zn.

How macrophages use Zn to fight infection seems to depend on the pathogen it encounters, as well as the nature of the host cell. Macrophages poison *M. tb*, *S. pneumoniae*, *E. coli*, and *H. pylori* by transporting toxic levels of Zn into pathogen-containing phagosomes[90, 88, 89, 112]. Conversely, challenge with *Histoplasma capsulatum* induces macrophages to sequester Zn and increase ROS production to counter the infection[91]. There does not appear to be consensus regarding Zn manipulation upon infection with *Salmonella* Typhimurium. *Salmonella* possess genes that aid in surviving Zn toxicity and starvation[113, 114, 115, 116], and studies done in different types of macrophage have suggested that Zn can both facilitate and impair infection. In a study of macrophages derived from primary human monocytes and the human monocyte THP-1 cell line, infection induces Zn to accumulate in punctate vesicular compartments, though *Salmonella* managed to avoid these toxic Zn compartments via an SPI-1-dependent mechanism[117]. In contrast, *Salmonella* infection of the mouse RAW264.7 macrophage cell line induced Zn mobilization, and increased Zn correlated with impaired bacterial clearance[116]. On the other hand, multiple studies have revealed that the high-affinity ZnuABC zinc uptake system and associated accessory proteins are critical virulence factors in *Salmonella*, suggesting that *Salmonella* experience Zn starvation inside the host[113, 114, 118]. Critical comparison of Zn at the host-pathogen interface may be confounded by the differences in the macrophage models used across studies. For example, both Balb/c and C57BL/6 mice lack a functional Slc11a1 (Nramp-1), a phagosomal transporter for magnesium (Mg), Fe, Mn, and Zn[105]. Macrophages from these mice are more susceptible to infection and have a reduced capacity to clear intracellular pathogens[106]. RAW264.7 cells, a popular mouse macrophage cell line used to study intracellular pathogens, are derived from C57BL/6 mice and therefore equally impaired. The lack of functional Slc11a1 is also likely to compromise the host response to infection with respect to metal regulation, making it difficult to define the nutritional immunity landscape in an immune-competent model system.

In this study, I carried out global RNA sequencing upon infection of macrophages from 129S6 mice with *Salmonella* Typhimurium and examined the changes in gene expression via clustering,

and gene set enrichment analysis (GSEA). I deliberately used the 129S6/SvEvTac (hereafter referred to as 129S6) mouse because it contains a functional Slc11a1 protein and has been used as a model system for chronic systemic infection[106]. We examined changes in metal-regulatory and metal-dependent genes and compared my results to published data on infection of C57BL/6 mice. While some changes in metal regulatory genes were similar between the two different model systems, suggesting common mechanisms of altering metals at the host-pathogen interface, there were also notable differences, indicating that functional Slc11a1 does alter the nutritional immunity landscape within the host. We also found that cytosolic Zn levels increased over the course of infection and that Zn availability alters infection outcome. Specifically, we found that Zn supports increased replication of intracellular bacteria, but also facilitates clearance of bacteria from macrophages. My results indicate that functional Slc11a1 significantly affects changes in gene expression, including the immune response, metal regulation in response to infection, and infection outcomes.

2.3 Results

2.3.1 Infection induces widespread changes in gene expression

To study metal homeostasis during infection, we used bone marrow derived macrophages (BMDMs) from 129S6 mice containing functional Slc11a1. Slc11a1 plays a critical role in regulating metal homeostasis and is important for allowing macrophages to mount an effective immune response to bacterial pathogens[105, 106]. To distinguish changes in macrophage gene expression in response to *Salmonella* infection from gene expression changes due to bacterial exposure, macrophages were treated with live or heat-killed *Salmonella enterica* serovar Typhimurium (hereafter referred to as *Salmonella*). Macrophages that were subjected to media changes but not exposed to *Salmonella* served as a control. To examine both early and late immune responses, macrophages were lysed at 2 or 18 hours post bacterial exposure and subjected to global RNA sequencing (Figure 2.1A). Principal component analysis shows that samples clustered predominantly by time post infection and status of bacteria (alive versus heat killed, Figure 2.1B).

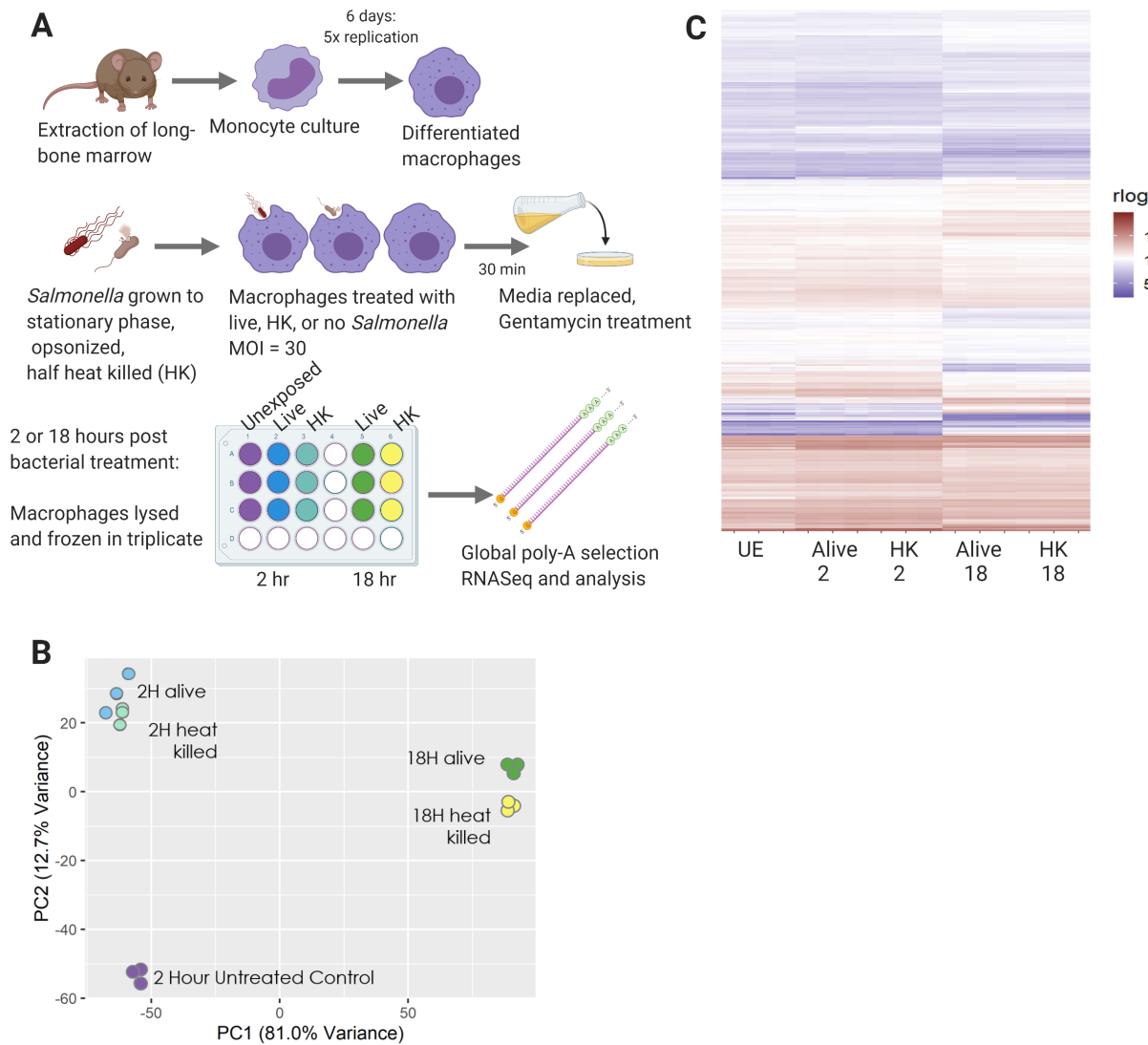


Figure 2.1: *Salmonella* treatment of macrophages induces global RNA expression changes across two primary axes: time post exposure and *Salmonella* status (live vs. heat killed) **A**) Schematic of infection experimental design for 129S6 BMDMs exposed to live or heat killed *Salmonella* Typhimurium SL1344. **B**) Global principal component analysis (PCA) with x-axis showing differential expression correlated with time post exposure and y-axis showing differential expression correlated with *Salmonella* status (live, heat killed (HK) or unexposed (UE)). **C**) Heatmap of the 7600 differentially expressed genes in this data set (log ratio test data $p_{adj} < 0.01$). Figure created with Biorender.

We identified 7766 genes that were differentially expressed and performed hierarchical clustering to examine the main patterns of gene expression changes. We limited analysis to genes with significant differential expression (adjusted p-value (p_{adj}) < 0.01), as determined by a DESeq2 log ratio test. An expression level cutoff was also applied (see Methods). An unsupervised algorithm (degPatterns function in DEGreport R package) was used to cluster genes based on similar expression profiles across all conditions. Twenty groups, each with at least 15 genes, emerged. Some groups showed time dependent expression, with little change between bacterial conditions, while others showed significant differences in expression upon treatment with alive versus heat-killed bacteria. Additionally, some groups were different based primarily on expression levels in control cells.

In Figure 2.2 we highlight the four different expression patterns that encompass the largest gene groups. The remaining groups are presented in Supplementary Figures 2.10 through 2.13 on pages 63 through 66 and the genes associated with each group are presented in Supplementary Dataset 1. We used DAVID Bioinformatics Resources 6.8 to annotate molecular functions and biological processes associated with the different gene expression clusters. Figure 2.2A presents group 1, which consists of genes with time-dependent increases in expression. These genes respond to the presence of *Salmonella* regardless of its live or heat-killed (HK) status, and are enriched for mitochondrial function (e.g. oxidative phosphorylation, ATP production), ER-Golgi transport and protein folding, immune response, sugar metabolism, and protein degradation (including proteasome and unfolded protein response genes). Specific genes that are characteristic of the M2 anti-inflammatory immune response[119] such as *il4r α* , *arg1*, *timp1*, and *fcgr2b* are present in this group, along with master regulators of the lipopolysaccharide (LPS) immune response *ift1*, *stat2*, and *irf7*. Finally, genes involved in pH and redox homeostasis such as *sod1*, *nos2*, *hif1 α* , carbonic anhydrases *car2/4/13*, as well as metal regulatory *slc11a1*, iron sequestering *lcn2*, and ferritin iron storage *fth1* are found in this group. Finally, *s100a8*, a metal-binding protein that is a component of calprotectin and plays a prominent role in nutritional immunity exhibited a similar expression pattern, with low expression at 2 Hrs and a significant increase at 18 Hrs (Supplementary Figure 2.10D on page 63). These results indicate that the M2 anti-inflammatory response along with many

metal associated genes are upregulated over time in response to infection, regardless of whether the bacteria are alive or HK.

The genes in group 2 (Figure 2.2B) are upregulated at 2 Hrs, with higher expression in alive compared to HK conditions, and are subsequently suppressed below baseline at 18 Hrs. This group is enriched in proinflammatory M1 immune genes[119], including *tnf*, the inflammasome component *nlrp3*, and *irf1* responsible for activating cytokine production. This group also contains multiple genes involved in membrane transport of zinc (*slc30a4*, *slc39a6/a8/a10*). Another hallmark proinflammatory M1 marker *tlr2* and metal regulatory genes (the zinc-dependent transcription factor *mtf1* and iron storage ferritin light chain *ftl1*) are present in group 3 (Supplementary Figure 2.10A on page 63, which is similar to group 2 across time but differs in alive vs HK expression at 2 Hrs. Combined, these two groups indicate that in macrophages with functional *slc11a1*, much of the pro-inflammatory response is activated at early time points and then suppressed later in infection.

Figure 2.2C (group 8) shows genes expressed in the absence of bacterial exposure and distinctly downregulated upon infection over time. This group is notable for its relatively small number of GO annotations, which are focused on cell cycle, cell motility, zinc-binding and transport, and transcription. Noteworthy genes in group 8 include cytosolic zinc exporters *slc30a1/a5* and iron exporter *slc40a1*. Finally, Figure 2.2D demonstrates group 10 in which genes are suppressed at 2 Hrs post-infection and upregulated above untreated cells at 18 Hrs. This group is enriched for metabolism, protein export, and transcription. Specifically, these genes are involved in ER and Golgi trafficking, respiration, lysosomal activity, zinc transport (*slc39a3/a7*), iron-dependent functions (cytochrome *bs*, glutaredoxin2, NADH dehydrogenase), mRNA and phospholipid transport, and autophagy. Approximately 10% of these genes are involved in transcription, and half of these transcription factors bind zinc. Also in this cluster are key inflammation-related genes *tlr4* which binds lipopolysaccharide (LPS) and *irf2/3/10* which mediate the Type I IFN response. Combined, these gene expression patterns reveal remodeling of metal homeostasis, metabolism and transcription during infection.

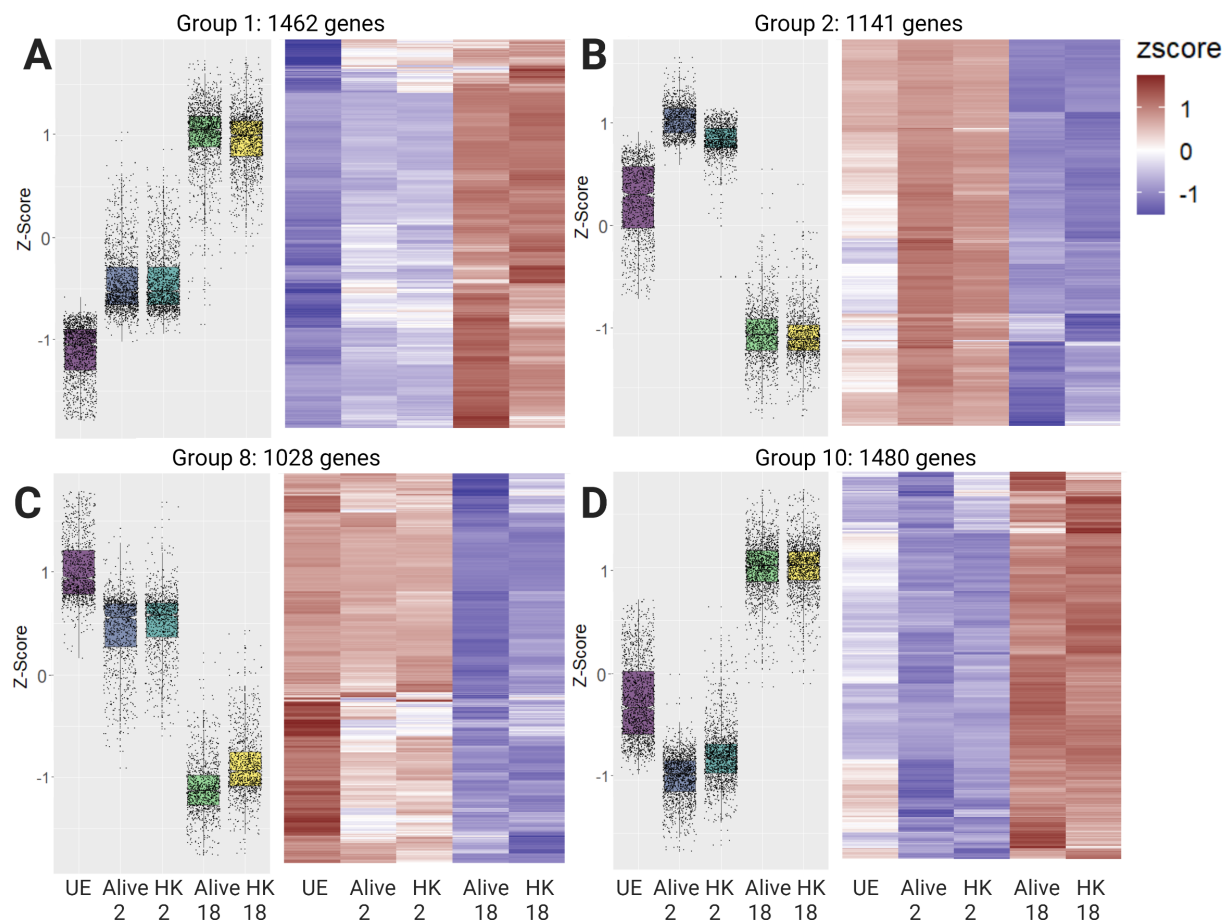


Figure 2.2: **Clustered data exposes multiple distinct expression trends in global data**
 Four of the twenty groups that emerged from clustering analysis are presented as a box and whisker plot of gene expression levels as Z-scores (normalized across all DE genes) and a hierarchically clustered heat map of gene expression as rlog-scaled DESeq2 normalized counts. **A)** Group 1 contains 1462 genes that increase in expression at 2 Hrs and increase further at 18 Hrs, without significant differences between the Alive and HK conditions. **B)** Group 2 contains 1141 genes that increase in expression at 2 Hrs and then decrease below baseline at 18 Hrs. **C)** Group 8 contains 1028 genes which are expressed in unexposed cells, but then decrease as a function of time post infection. **D)** Group 10 contains 1480 genes that decrease in expression at 2 Hrs and increase at 18 Hrs. UE: unexposed control cells; HK: stimulation with heat killed bacteria

2.3.2 GSEA reveals pathways differentially affected by live versus heat-killed bacteria

In analyzing global transcription patterns, I found that some groups contain differences in gene expression between live and heat killed bacterial treatments (see groups 4, 5, 7 and 16 as examples), revealing genes that respond differently to a generalized LPS trigger (HK bacteria) vs *Salmonella* with active virulence mechanisms. To identify biological processes or signaling pathways underlying these differences, GSEA[120] was performed on differentially expressed ranked gene list from Alive vs HK at 2 hours, and Alive vs HK at 18 hours. Several significant gene sets were enriched in macrophages treated with live versus HK *Salmonella*, as defined by a false discovery rate of $q < 0.05$. When using the Hallmark Gene Set from the Molecular Signatures Database[121], I found 47 gene sets enriched at 2 Hrs, and 14 gene sets enriched at 18 Hrs for live versus HK treatment (Supplementary Dataset S2). One gene set that is significantly enriched in live *Salmonella* vs HK exposure at both time points is hypoxia (Figures 2.3A, 2.3B). Hypoxia is an important aspect of the *in vivo* immune response to infection as hypoxia accompanies inflammation, and a hypoxic environment may affect macrophage M1/M2 polarization[119, 122]. Hypoxia is also accompanied by decreased glucose, increased lactate, and decreased pH, and as discussed above, I observed an increase in *hif1a*, carbonic anhydrases, and *nos2*. Multiple studies have shown activation of hypoxia induced factors upon infection of macrophages, and hypoxia is generally associated with macrophage stress as well as defense against bacterial replication[122, 123, 15]. However, prolonged hypoxia is associated with tissue damage, so the severity and duration of hypoxia is an important factor in infection.

The complement gene set is activated more strongly in macrophages infected with live *Salmonella*. The complement system is part of the innate immune response and mediates a host responses such as opsonization, inflammation and direct bacterial lysis[124]. Complement systems respond to bacterial coat components[125] and were therefore expected to respond similarly to live and HK *Salmonella*. Instead, many of these genes showed upregulation in live vs HK conditions (Figures 2.3C, 2.3D).

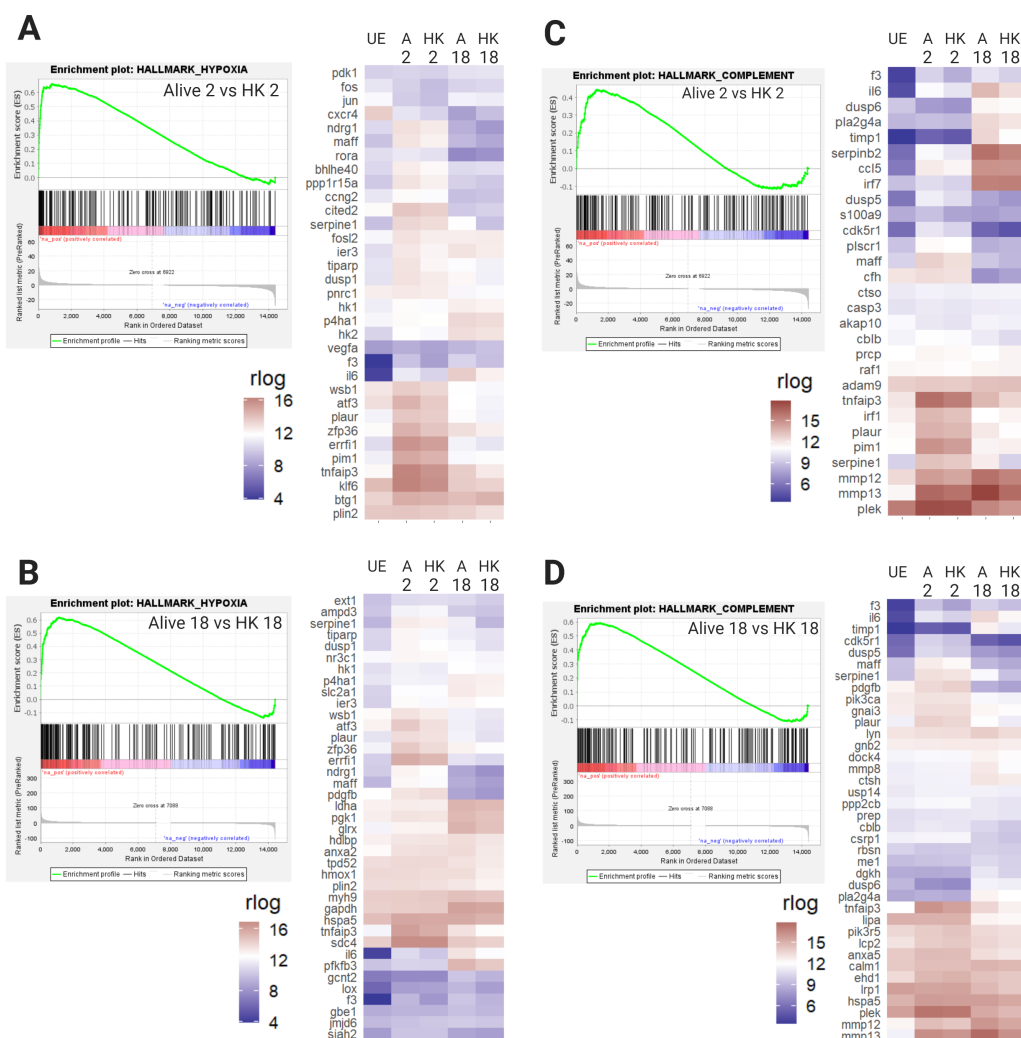


Figure 2.3: GSEA reveals enrichment of the hypoxia and complement Hallmark gene sets in BMDMs infected with live *Salmonella* compared to treatment with heat killed bacteria. Each panel shows a GSEA enrichment plot for a Hallmark gene set and a hierarchically clustered expression heat map of the leading edge genes from that GSEA plot. In GSEA plots each gene is represented by a vertical black line, and leading edge genes are on the positive end of the spectrum, up to the point of maximum Enrichment Score. **A)** GSEA and heat map of leading edge genes for the Hallmark hypoxia gene set enriched in the 2 Hr Alive condition compared to 2 Hr HK ($q = 0.000$, NES = 2.12). **B)** GSEA and heat map of leading edge genes for the Hallmark hypoxia gene set enriched in the 18 Hr Alive condition compared to 18 Hr HK. At 18 Hrs, analysis of the hypoxia gene set shows 50 leading edge genes vs. 36 at 2 Hrs. Only 20 of these genes are in the leading edge at both time points. ($q = 0.024$, NES = 1.65). **C)** GSEA and heat map of leading edge genes for the Hallmark complement gene set enriched in the 2 Hr Alive condition vs. 2 Hr HK ($q = 0.062$, NES = 1.44). **D)** GSEA and heat map of leading edge genes for the Hallmark complement gene set enriched in the 18 Hr Alive condition vs. 18 Hr HK ($q = 0.042$, NES = 1.57). 42 complement genes appear in the leading edge, compared to 36 at 2 Hrs. While there is a core set of 16 genes upregulated at both time points, the remaining genes are unique. UE: unexposed control; HK: heat killed; q : false discovery rate; NES: Normalized Enrichment Score from GSEA. Figure created with Biorender.

At two Hrs post infection, the complement leading edge is enriched for zymogens, enzymes, and secreted proteins, while at 18 Hrs there are more chemokine- and Fc-signaling related genes. At both timepoints, live conditions show upregulation of matrix metalloproteinases *mmp12* and *mmp13* and their inhibitor *timp1*. Additionally, this gene set includes members of the coagulation pathway (*plaur*, *serpin*, *f3*) which overlaps and interacts with complement to trap and kill microbes. Bacteria co-evolved with the complement system, and many bacteria, including *Salmonella*, possess arsenals of anti-complement proteins. Frequently anti-complement proteins work directly against host proteins, but my data suggest live *Salmonella* affect complement gene transcription.

TNF α signaling via NF-KB is also more strongly activated by live *Salmonella*. During infection multiple signaling cascades activate the transcription factor NF-KB, including the proinflammatory cytokine TNF α (TNF in mice). NF-KB is a master regulator and specifically responds to TNF activation with pro-inflammatory and anti-apoptotic signaling. At both 2 Hrs and 18 Hrs, live infected samples were enriched for pro-inflammatory genes, while each time point was enriched in a different set of anti-apoptotic genes (Supplementary Figure 2.14 on page 67). At two Hrs *btg2*, *egr3*, *jun*, *vegfa*, *klf4* and *nr4a* were enriched in alive conditions compared to HK, while at 18 Hrs *bcl6*, *smad3*, *stat5a*, *plaur* and *socs3* were upregulated in alive versus HK. Most genes present in the leading edge for both time points were more highly expressed at 2 Hrs, reinforcing the trend of macrophages moving toward an M2-like state later in infection.

I also observed gene sets that were enriched only at 2 Hrs or 18 Hrs. For example, the Hallmark Apoptosis gene set was enriched at 2 hours, and Hallmark Unfolded Protein Response (UPR) was enriched at 18 hours (Figure 2.4). Late log phase growth induces maximal expression of *Salmonella* Pathogenicity Island 1 (SPI1) genes which allow *Salmonella* to be highly invasive and frequently induce apoptosis in macrophages[126]. To promote longer term infections, the *Salmonella* in this experiment were grown to stationary phase before infection, which reduces their expression of SPI1 genes. However, several pro-apoptosis genes are upregulated in Alive exposure at 2 Hrs including the cAMP-dependent transcription factor *atf3*, *jun*, and *pmaip1*. The fact that the apoptotic pathway is not enriched at 18 Hrs suggests that the macrophages manage this response. While UPR and

apoptosis are both possible responses to metabolic and ER stress, the upregulation of UPR at 18 Hrs could represent an attempt to restore cellular homeostasis. The transition from apoptosis genes at 2 Hrs to UPR genes at 18 Hrs correlates with a shift in macrophage polarization and may imply decreased ER stress over time.

2.3.3 There is significant remodeling of metal homeostasis in response to infection

One of my primary goals in carrying out RNAseq upon infection of 129S6 BMDMs was to define infection-related changes in transition metal regulatory and dependent genes in a model system with functional Slc11a1 (NRAMP1). This allows me to inform my understanding of nutritional immunity in an immune competent model system. Figure 2.5A shows several major metal regulatory proteins in macrophages. This includes Slc39a1-14 (Zip) transporters that facilitate entry of Zn, as well as Mn and Fe for some Slc39a members, into the cytosol, Slc30a1-10 (Znt) transporters that remove Zn from the cytosol, the Fe exporter Ferroportin (Slc40a1), and Cu transporters Atp7a and Ctr1/2 (Slc31a1/2). Also shown are metallothioneins which store and buffer cytosolic Zn, and the Fe storage protein ferritin (Fth1 – ferritin heavy chain and Ftl1– ferritin light chain), which is protective against Fe-induced oxidative stress in macrophages.

Infection of 129S6 BMDMs leads to broad changes in genes that control metal transport (Figure 2.5B, Supplementary Dataset S3). There is a significant increase in *slc11a1* upon infection, particularly at 18 Hrs. Slc11a1 localizes to the phagosomal membrane where it exports divalent metal cations (Fe, Zn, Mn) while simultaneously acidifying the compartment. The other member of this family, Slc11a2, imports metal ions across the plasma membrane, and is significantly upregulated at 2 Hrs. This may indicate an acute phase emphasis on importing metals into the cell, and a late phase emphasis on exporting metals from the phagosome. At 18 Hrs *slc11a1* is more highly expressed in response to live versus HK *Salmonella*, suggesting that macrophages actively upregulate this gene to help combat live infection.

There are also significant changes in transporters dedicated to import, export, and distribution of Fe, Cu and Zn (Figure 2.5B). There is a downregulation of the transferrin (*trf*) Fe import

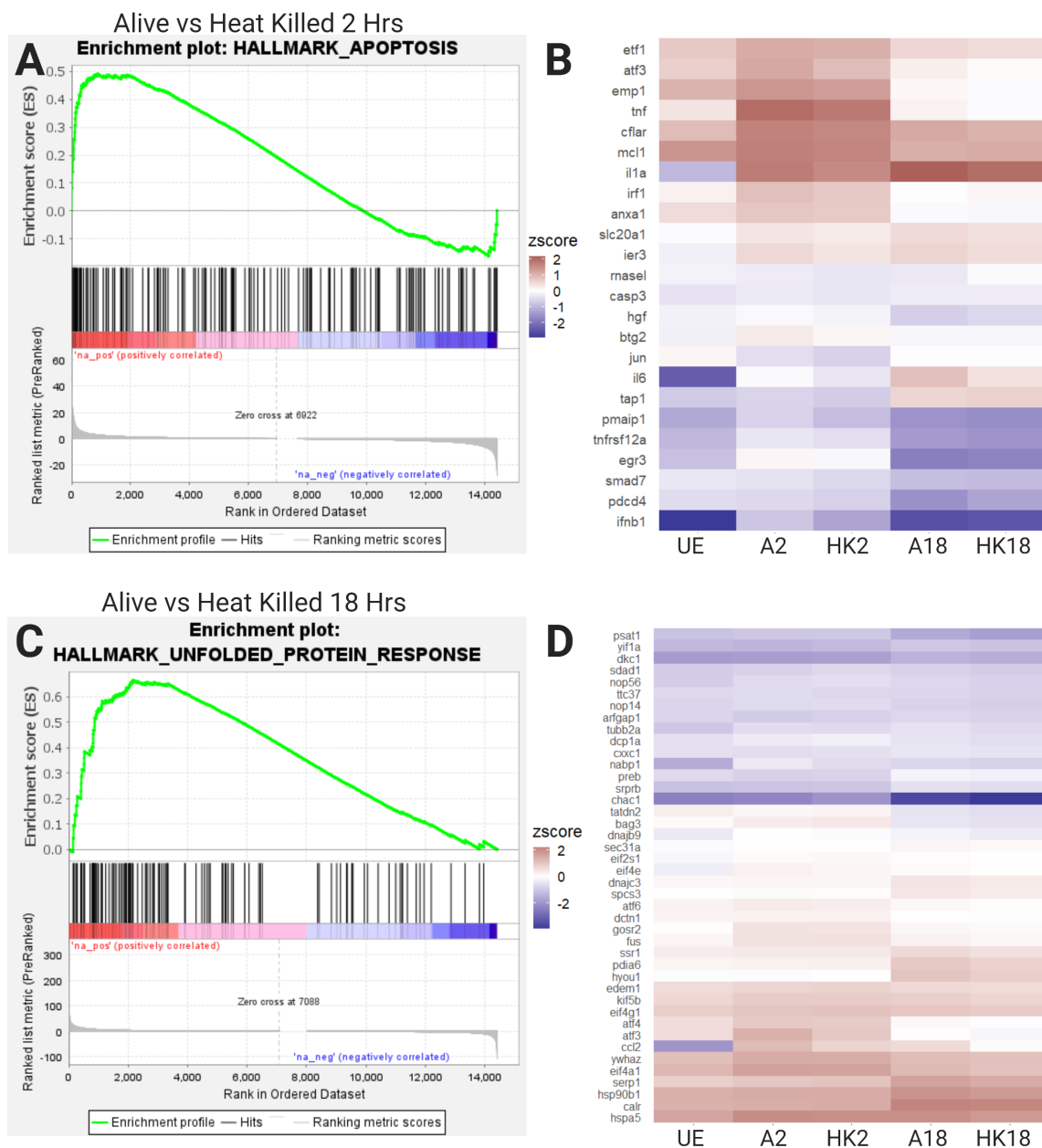


Figure 2.4: GSEA reveals enrichment of the apoptosis Hallmark gene set at 2 Hrs and the UPR gene set at 18 Hrs in BMDMs treated with live versus heat killed *Salmonella*. **A**) GSEA curve of the Hallmark apoptosis gene set, showing enrichment in the 2 Hr alive condition vs. the 2 Hr HK condition ($q = 0.023$, NES = 1.58). **B**) Heatmap of 25 leading edge apoptosis genes. **C**) GSEA curve of the Hallmark UPR gene set, showing enrichment in the 18 Hr Alive condition vs. the 18 Hr HK condition ($q = 0.021$, NES = 1.69). **D**) Heatmap of the 47 leading edge UPR genes. UE: unexposed control; HK: heat killed; q : false discovery rate; NES: Normalized Enrichment Score from GSEA.

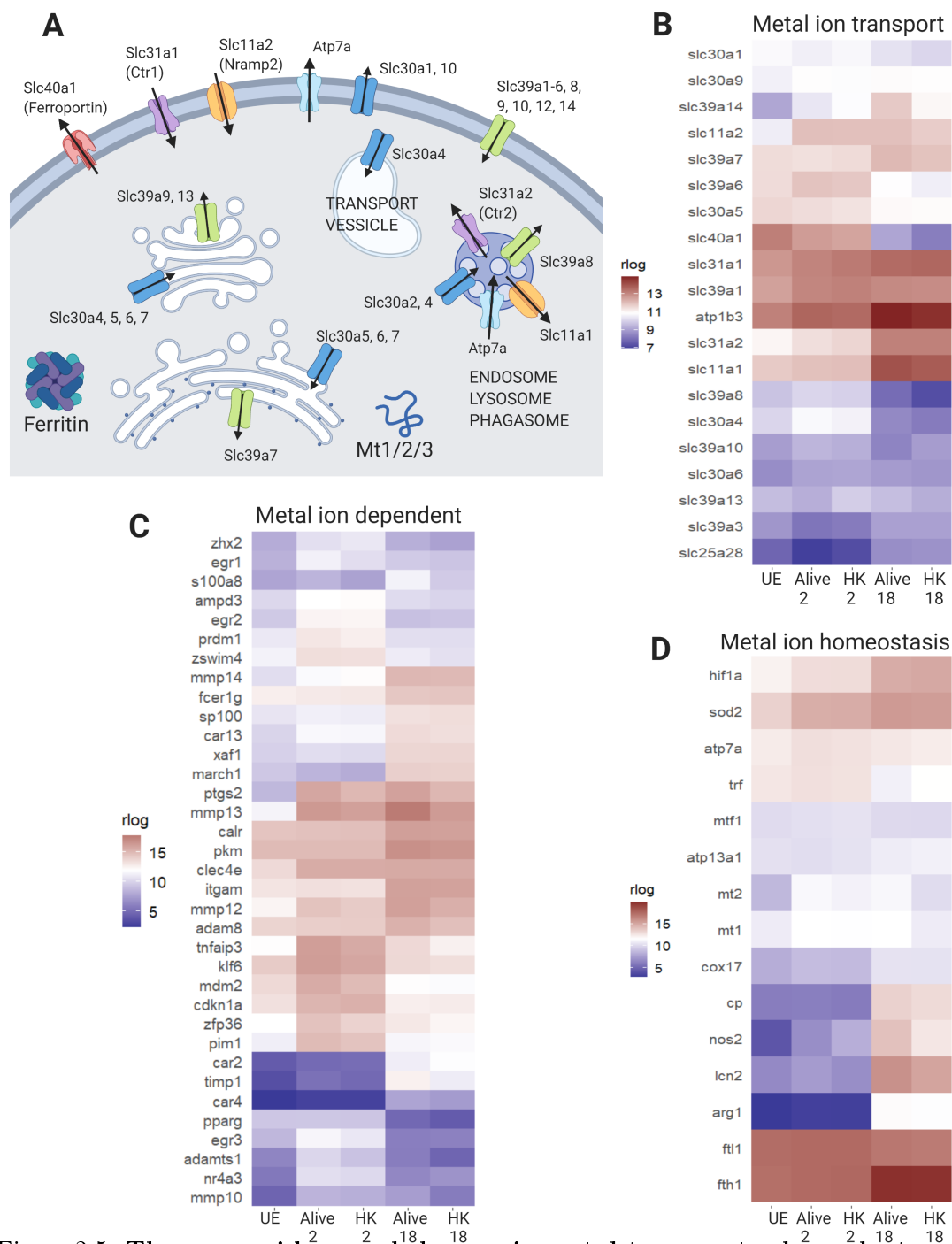


Figure 2.5: **There are widespread changes in metal-transport, -dependent and homeostasis genes.** **A)** Schematic of major metal ion transporters and buffering proteins in macrophages. Slc30a1-10 are also referred to as ZnT1-10. Slc39a1-14 are also referred to as Zip1-14. **B-D)** Heatmaps of subsets of metal-transport, -dependent, and -homeostasis genes that are highly expressed and differentially expressed in my data set (log ratio test $q < 0.01$, mean normalized counts > 100). These gene sets are curated to focus on nutritional immunity metals, including Fe, Zn, Cu, and Mn. Genes that fit in multiple categories are only listed once. **B)** Metal ion transporters. **C)** Metal-dependent and -responsive genes. **D)** Metal ion homeostasis genes. UE: unexposed control cells; HK: heat killed bacteria exposure. Figure created with Biorender.

pathway and the Fe exporter *slc40a1*, indicating restriction of Fe. The Cu transporters *slc31a1* (plasma membrane) and *slc31a2* (endosome) are significantly increased in expression at 18 Hrs. These changes in gene expression would increase Cu influx into the cytosol, while the upregulation of *atp7a* (endosome) at 2 Hrs suggests an active effort by the macrophages to kill the internalized bacteria. Changes in Zn transporters include upregulation of *slc30a4*, *slc39a14*, *slc39a1*, *slc39a7* and downregulation of *slc30a5*. The significant increase in expression of plasma membrane importer *slc39a14* is especially strong at 18 Hrs, and could result in an increase in cytosolic Zn. Decreased expression of Golgi importer *slc30a5* and increased expression of ER exporter *slc39a7* suggest diminished Zn in the secretory pathway, perhaps to deprive the pathogen of Zn. *Slc30a4*, which transports Zn into the phagosome and secretory vesicles, is upregulated at 2 Hrs and downregulated below control at 18 Hrs, indicating restriction of Zn at late stages of infection. Combined, there are widespread changes in metal transport that indicate limitation of Fe, accumulation of Cu, and redistribution of Zn.

In addition to metal transport, there are significant changes in genes that are metal dependent (Figure 2.5C) and genes related to metal homeostasis (Figure 2.5D). There is an increase in intracellular storage capacity for Fe at 18 Hrs; *fth1* increases while *ftl1* drops in expression, reflecting the fact that during infection, heavy chains polymerize together to the exclusion of light chains[127]. Similarly, Zn buffering capacity in the form of cytosolic metallothioneins (*mt1/2*) is increased early in infection and maintained with expression at 18 Hrs higher in macrophages treated with live versus HK *Salmonella*. These changes in metallothionein would be consistent with increased cytosolic Zn late in infection. There is also a significant increase in expression of Zn-dependent carbonic anhydrases that regulate pH, Zn-dependent proteases (*mmp10*, *12*, *13*, *14*, *timp1*, *adamts1*, *adam8*), the ferroxidase ceruloplasmin (Figure 2.5C). Additionally, there is an increase in expression of lipocalin, a protein involved in innate immunity by binding Fe-bound siderophores and depriving pathogens of Fe. Finally, there are significant increases in genes involved in metal homeostasis and oxidative stress, particularly at late stages of infection. These include: *hif1a*, Cu/Zn-dependent *sod2* and *sod3*, Mn-dependent *arg1*, and Zn-dependent *nos2*. These changes indicate that remodeling metal

transport is accompanied by significant changes in the expression of metal-dependent enzymes and metal storage.

2.3.4 Cytosolic labile Zn increases at late stages of infection

The widespread changes in Zn transporter expression upon infection suggest remodeling of Zn homeostasis, and would be expected to lead to an increase in cytosolic Zn and decreased Zn in the secretory pathway. Previous studies in different model systems have suggested different changes in intracellular labile Zn pools in response to infection[117, 128]. However, all previous studies have used small molecule indicators such as FluoZin3 or Zinpyr-1, which often exhibit variable and unpredictable localization within a cell and can confound measurement of Zn in a defined location. For example, FluoZin3-AM has been shown to localize to the cytosol, Golgi, lysosomes and vesicles, and localizations differ among cell types[24, 129, 130]. Previous studies in Slc11a1 defective Raw264.7 cells used FluoZin3 to determine that there was an increase in labile Zn upon infection via FACS. Unfortunately, the absence of fluorescence images precluded evaluation of where the Zn increase occurred. In human monocyte-derived macrophages FluoZin3 appears to be in vesicles or early endosomes[117], and reported an increase in Zn in these compartments upon infection. Of the studies that have attempted to measure Zn inside activated or infected macrophage, none have unambiguously addressed whether there are changes in cytosolic Zn.

To directly measure cytosolic Zn in 129S6 BMDMs at various time points post-infection, Michael Minson used the genetically encoded zinc sensor NES-ZapCV2[64, 7]. This sensor uses the ratio of YFP emission to CFP emission upon CFP excitation (Forster Resonance Energy Transfer, FRET, ratio) to measure labile Zn in cells. The advantage of the genetically encoded sensor is that localization of this sensor is restricted to the cytosol. Briefly, cells were nucleofected with a plasmid encoding NES-ZapCV2 15 hours prior to infection with *Salmonella*. At select time points post-infection cells were imaged on a widefield fluorescence microscope to measure the resting FRET ratio (Figure 2.6A). Cells were subsequently subjected to an *in situ* calibration to determine the minimum and maximum FRET ratio in each cell (Figure 2.6B) and the calibration parameters were

used to calculate the fractional saturation of each cell under resting conditions and the concentration of labile cytosolic Zn (see Methods for details, Figure 2.6C). Uninfected cells have a mean fractional saturation of 0.30 which corresponds to a Zn concentration of 80 pM. At 12 Hrs and beyond, the fractional saturation increased to 0.5 which corresponds to 2.9 nM Zn. My data show that labile Zn in the cytosol does indeed increase later in the infection (36-fold), consistent with the observed increase in expression of mt1 and mt2.

2.3.5 Zn promotes bacterial clearance as well as bacterial replication

Having established that Zn regulation and Zn availability in the cytosol are altered upon infection, I, in collaboration with Mike Minson, evaluated the influence of Zn availability on infection outcome. While a previous study examined increases and decreases in Zn on *Salmonella* infection of Raw264.7 cells[116], we explore the impact of Zn on infection outcome in immune competent macrophages with functional Slc11a1. To examine infection outcomes, we incorporated the pDiGc plasmid (Figure 2.7A) into *Salmonella*, which encodes two fluorescent proteins. DsRed is expressed under an arabinose inducible promoter while GFP is constitutively expressed[131]. This plasmid allows tracking of infected cells (green signal) and bacterial replication (dilution of the red signal upon cell division). Arabinose induction of DsRed is halted upon macrophage infection, such that any bacterial division occurring within the macrophage leads to dilution of the red fluorescent signal. Comparison of green and red signals across time yields a picture of bacterial division vs macrophage clearance of bacteria.

To alter Zn availability, we manipulated Zn levels in the macrophage media after *Salmonella* had been internalized. Four media conditions were used in this study to span the range from Zn replete to Zn deficient. The four conditions were: standard macrophage growth media (DMEM + 20% FBS) containing 25 μM Zn (Figure 2.7B), or media prepared with Chelex-100-treated FBS to deplete metal ions (4 μM Zn, Figure 2.7B), which was then further depleted of Zn (Chelex media + 3 μM ZX1, 0 μM Zn) or reconstituted with replete Zn (Chelex media + 30 μM Zn, 34 μM Zn total).

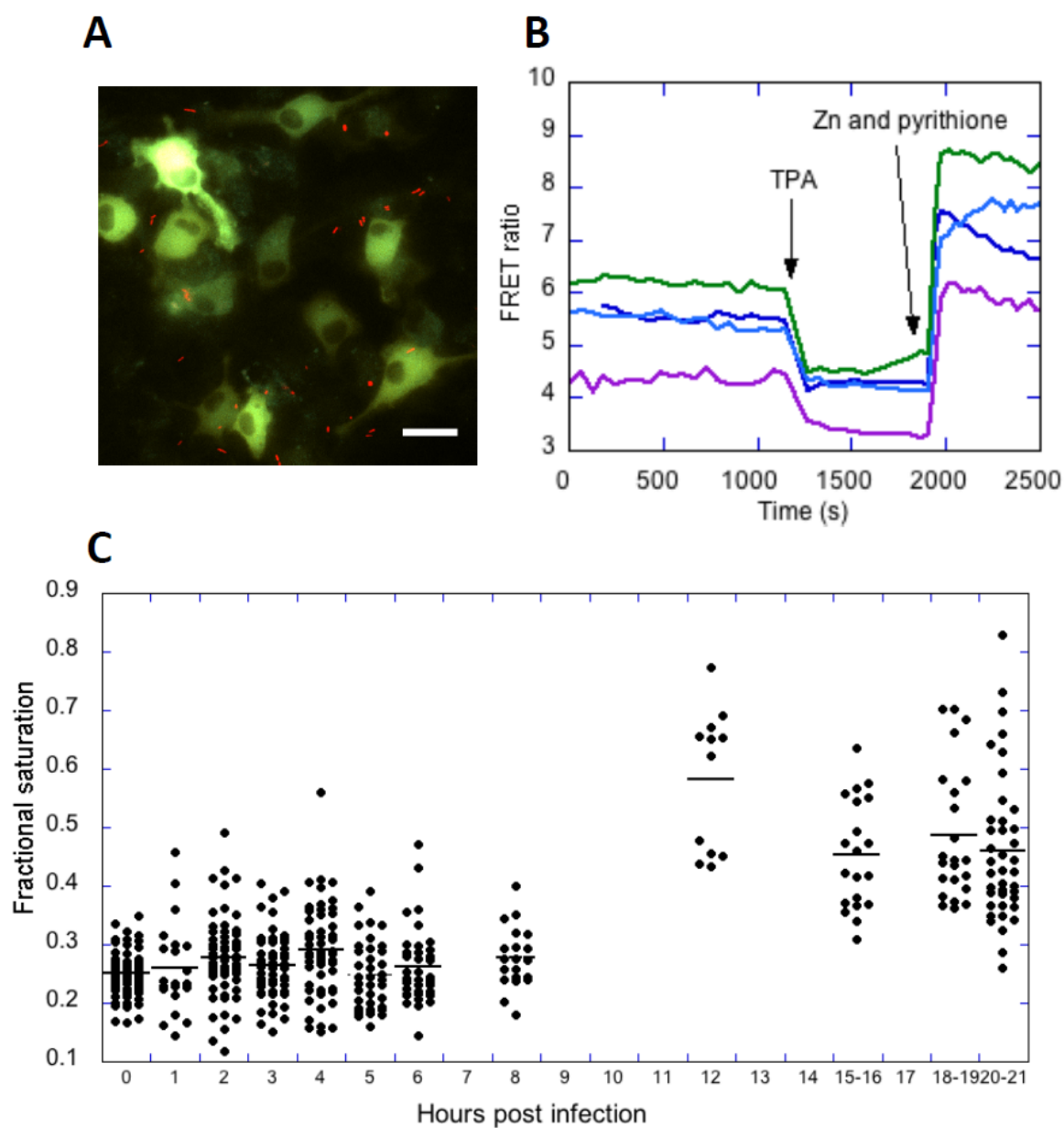


Figure 2.6: **Changes in labile cytosolic Zn in 129S6 BMDMs upon infection with *Salmonella*.** **A)** Representative image of BMDMs expressing the NES-ZapCV2 fluorescent Zn sensor (green) treated with *Salmonella* constitutively expressing mCherry (red). Scale bar = 20 μm . **B)** Representative *in situ* calibration of the NES-ZapCV2 sensor showing the FRET ratio (R, background corrected FRET channel divided by the background corrected CFP channel) over time. The R_{min} is obtained upon addition of 50 μM TPA and the R_{max} is obtained upon addition of 23.8 nM buffered Zn, 0.001% saponin and 0.75 μM pyrithione. Each trace represents a single cell. **C)** Fractional saturation of the NES-ZapCV2 sensor at different time points post infection. Each dot represents an individual cell. Data represent at least two independent experiments per time point. Figure credit Amy Palmer, data credit Michael Minson.

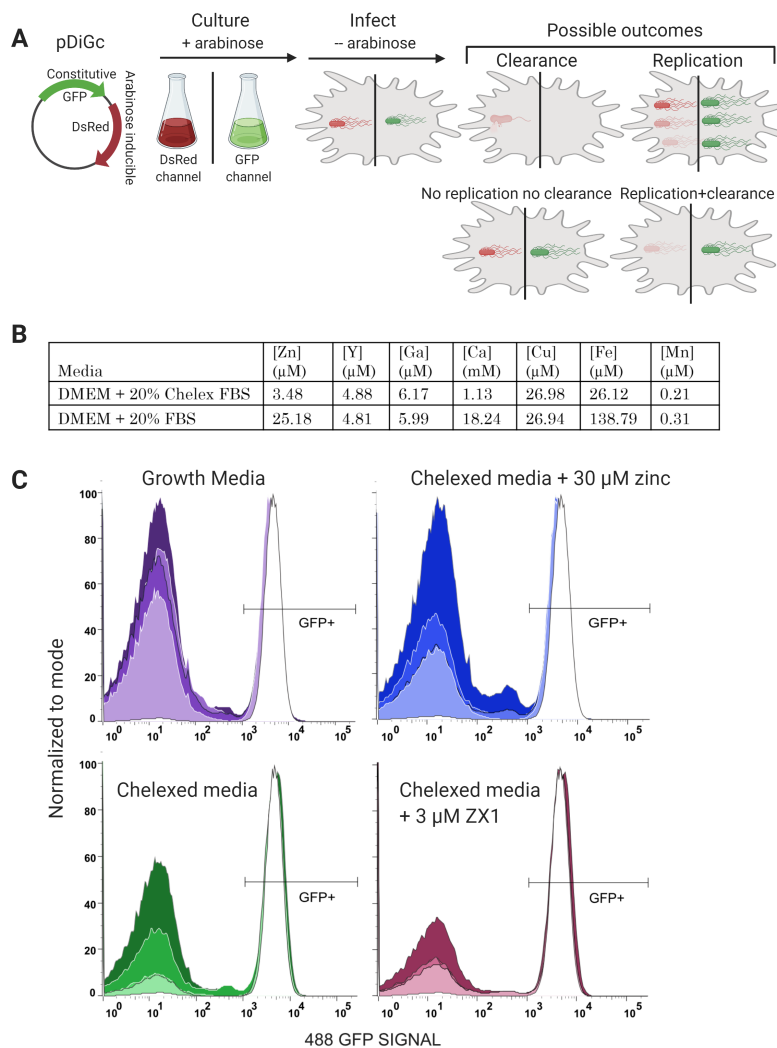


Figure 2.7: Bacterial clearance as a function of time and Zn availability. **A)** Schematic of the experimental protocol. *Salmonella* expressing the pDiGc plasmid expresses GFP constitutively and DsRed under arabinose induction. Bacteria are cultured with arabinose and aeration to the stationary phase, at which point they express both fluorescent proteins. Arabinose is removed at infection, and infected macrophages are fluorescent in both red and green channels by flow cytometry. As infection proceeds the green to red fluorescent ratio ‘tracks’ the bacteria. **B)** Metal content of normal growth media and media containing Chelex-treated FBS, as determined by inductively coupled plasma mass spectrometry (ICP-MS). **C)** Histograms of the GFP signal in macrophages expressing pDiGc in 4 different medias and at 4 time points. Each experimental condition was done in triplicate, and 10,000 cells were measured per sample. Replicates were essentially identical, so data for the replicates was concatenated. Increasing color saturation indicates time post *Salmonella* exposure (2, 10, 18 or 24 hours). The right peak in each graph corresponds to the GFP+ macrophages, indicating infection. As *Salmonella* are cleared the macrophages become GFP- and shift to the left peak on each graph. At the initial inoculation (white curve in each panel), macrophages show almost 100% infection rate. Normal macrophage growth media and Chelexed media supplemented with 30 μM Zn (replete Zn conditions) show almost 100% bacterial clearance at 24 hours. Chelexed media (low Zn) shows decreased bacterial clearance while Chelexed media with 3 μM extracellular zinc chelator ZX1, (essentially no Zn) shows poor bacterial clearance. Figure created with Biorender.

Macrophages were infected with *Salmonella* expressing pDiGc in macrophage growth media and infection proceeded for 45 minutes before experimental media conditions were introduced. This avoided the confounding variable of Zn's effect on the phagocytosis of bacteria. Infected macrophages in each media condition were fixed at four time points: 2, 10, 18 and 24 Hrs post inoculation and subjected to flow cytometry. A control sample was fixed immediately after the 45 min infection and verifies that 91% of macrophages contained GFP-positive bacteria at the beginning of the experiment. Figure 2.7C demonstrates the loss of GFP signal in macrophages in each growth media as a function of time. The increase in the fraction of cells with no GFP is indicative of bacterial clearance. In each panel, the white curve is from the initial infection, and increased color saturation indicates time post-infection. In normal growth media, clearance of bacteria is strong at 2 Hrs, with 70% of initially infected cells having lost all GFP signal. Clearance further increases over time, with 76%, 74%, and 85% clearance at 10, 18 and 24 Hrs. Control and Zn replete media contained similar Zn levels but different amounts of Ca and Fe due to Chelex treatment. At early time points (2, 10 and 18 Hrs) there is 56%, 64% and 59% bacterial clearance in the Zn replete media compared to the control, likely due to either depleted Ca or Fe. By 24 Hrs, Zn replete samples reached a similar level of infection clearance, with 87% clearance. In contrast, macrophages in Chelexed media with low Zn and ZX1-treated media with effectively no Zn show significantly impaired bacterial clearance. At 24 Hrs Chelex and Zx1 conditions had achieved 73% and 53% clearance, respectively. Direct comparison of the different media conditions at each time point are presented in the Supplementary Figure 2.15 on page 68. These results confirm that 129S6 macrophages are competent at clearing *Salmonella* throughout infection and that Zn availability positively correlates with the effectiveness of bacterial clearance.

In addition to measuring bacterial clearance, the pDiGc plasmid can also be used to measure bacterial replication, as the DsRed signal is diluted with every cell division. I compared the DsRed signal versus GFP signal as a function of time and different media conditions (Figure 2.8). In standard macrophage growth media (top row), the DsRed signal decreases over time in 23% of the GFP+ cells, indicative of bacterial replication. It is important to note that although 129S6

macrophage are efficient at clearing the *Salmonella* infection, here we are looking at the small portion of the macrophage population that remains infected (GFP+). The Zn replete media (2nd row) shows bacterial replication comparable to standard growth media, with 23% of GFP+ macrophages showing diluted DsRed signal at 24 Hrs. In contrast, in Chelexed media with depleted Zn and Chelexed media containing ZX1 (no Zn) there is weaker bacterial replication (11% and 7%, respectively), as indicated by the lack of a fluorescent “tail” at lower DsRed intensity. Interestingly, this result suggests that while Zn facilitates host clearance of bacteria, it also helps bacteria to replicate in cells that do not clear the infection. This may suggest that bacterial clearance occurs more easily in dividing bacteria as persistent infections are mainly non-replicating.

2.3.6 Macrophages from 129S6 and C57BL/6 differ in nutritional immune response to infection

Because the Slc11a1 transporter specifically aids in depriving pathogens of metal ions, I hypothesized that expression of genes related to metal handling in my cells would differ significantly from macrophages derived from Slc11a1 non-functional mice (BALB/c, C57BL/6, and the Raw264.7 cell line). Therefore, I performed a comprehensive analysis of changes in expression in 129S6 macrophages (this study) and macrophages derived from C57BL/6 mice (RNAseq study by Staples et al[109]) at 18 hours post infection. Specifically, I compared my unexposed control (UE), 18 Hr Alive and 18 Hr HK conditions against uninfected macrophages (UI), those containing growing *Salmonella* (G), and bystander macrophages not containing *Salmonella* at 18 Hrs (BY) from Staples et al. All data were analyzed on the same pipeline and normalized together within DESeq2 to make the data as comparable as possible (Supplementary Dataset S4).

To evaluate potential differences in genes involved in nutritional immunity between the two datasets, I examined all genes with UNIPROT keywords for iron, zinc, or copper transport or homeostasis. Figure 2.9 presents heat maps for Fe, Cu, Zn transport and Ze-dependent genes. There are a number of similarities in regulation of metal-transport, -homeostasis, and -dependent genes, indicating that there are common mechanisms for managing metal ions at the host-pathogen

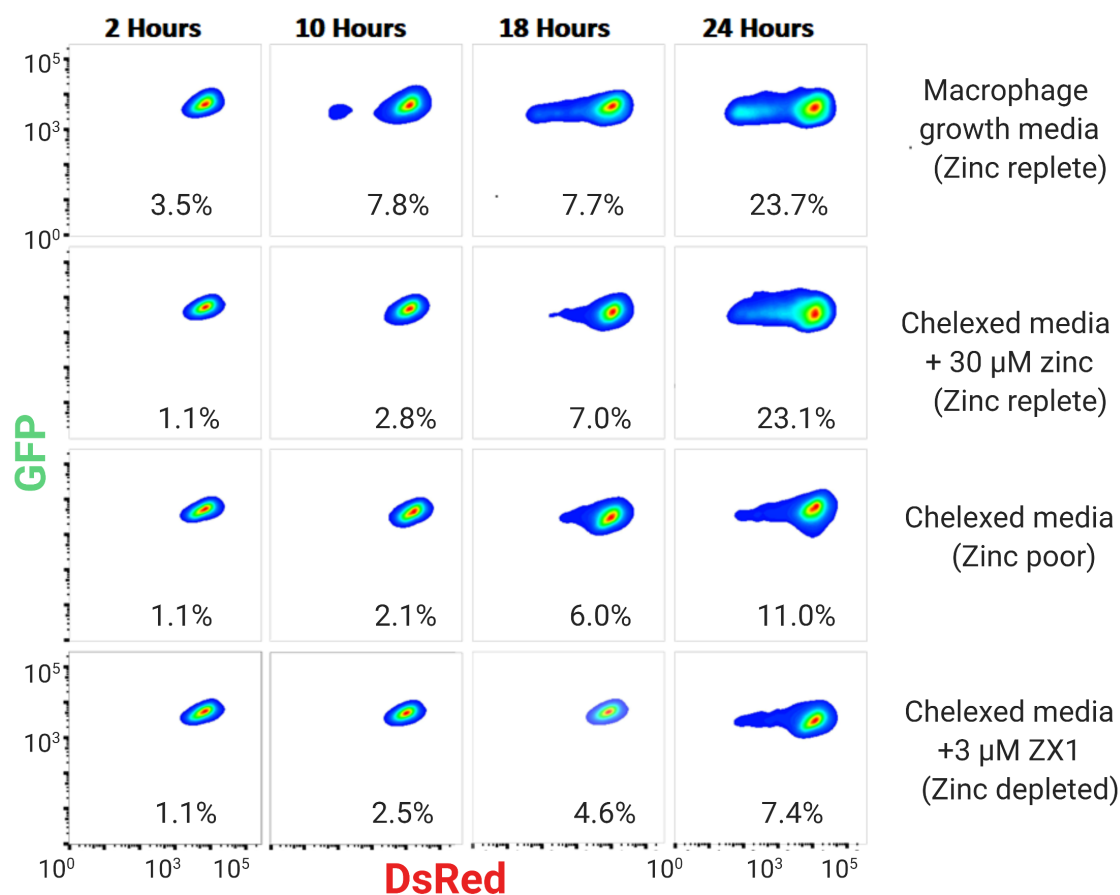


Figure 2.8: **Bacterial replication as a function of time and Zn availability.** 129S6 BMDMs were infected with *Salmonella* expressing pDiGc. The GFP and DsRed signals in BMDMs were measured by flow cytometry and plotted against one another. These density graphs show only macrophages containing GFP+ *Salmonella*, which indicates active infection. Percentages on each plot indicate the number of macrophages with diluted DsRed signal, an indicator of *Salmonella* division. Dilution of DsRed is a function of time and zinc availability, with all media conditions showing an increase in bacterial division over time, but control and zinc replete conditions (first and second rows) show much more robust division.

interface, even when there are differences in the host. In particular, there is a significant decrease in Fe import (*trf*), export (*slc40a1*), and an increase in ferritin storage (*fth1*) in both studies (Figure 2.9A). Similarly, both studies show upregulation of plasma membrane copper transporter *slc31a1* indicating Cu uptake from the extracellular space (Figure 2.9B). With respect to Zn regulation, both studies show upregulation of plasma membrane Zn importer *slc39a14*, downregulation of the Golgi importer *slc30a5*, and an increase in expression of Zn buffers *mt1* and *mt2* (Figure 2.9B, 2.9C). Combined these results suggest a general pattern of limiting the availability of Fe, increasing exposure to Cu, and increasing cytosolic Zn.

Despite these similarities, there are also notable differences that suggest the presence of functional *slc11a1* alters metal regulation at the host-pathogen interface. With respect to Fe, lactoferrin (*ltf*), a major Fe binding factor with bactericidal properties, *steap3*, which encodes a ferrireductase that reduces ferric Fe released from transferrin in the endosome, and *mmgt1*, which encodes a Mg transporter that ferries multiple metal ions across membranes are all downregulated in infected 129S6, but do not respond to infection in C57BL/6 cells. There are also notable differences in key Cu regulatory genes. The Cu importer *slc31a2* is upregulated in 129S6, while there is no change in C57BL/6. Copper chaperones play an important role in distributing Cu and loading it into enzymes; the copper chaperone *atox1* is upregulated in 129S6, but downregulated in C57BL/6; *cox17* is upregulated in 129S6, but not C57BL/6 ($q > 0.06$). Finally, *sco1* is upregulated in C57BL/6 but not 129S6. There are also differences in the magnitude of gene expression changes, with more marked changes in 129S6, including for ferroportin (*Slc40a1*), multi-copper enzyme ceruloplasmin (*cp*), and *lcn2*, which reduces bacterial replication by sequestering Fe bound to microbial siderophores. *Lcn2* is also intimately involved in regulating the expression of pro-apoptotic *bcl2l11*, which is strongly downregulated in 129S6 but is unaffected in C57BL/6 cells, suggesting these two cell types have disparate apoptotic tendencies at 18 Hrs post infection.

There are also notable differences in infection-induced expression changes in genes encoding Zn transporters and Zn-dependent proteins between the two systems (Figure 2.9C, 2.9D). Specifically, upregulation of *slc39a7* and downregulation of *slc30a4* in 129S6 but not C57BL/6 suggest

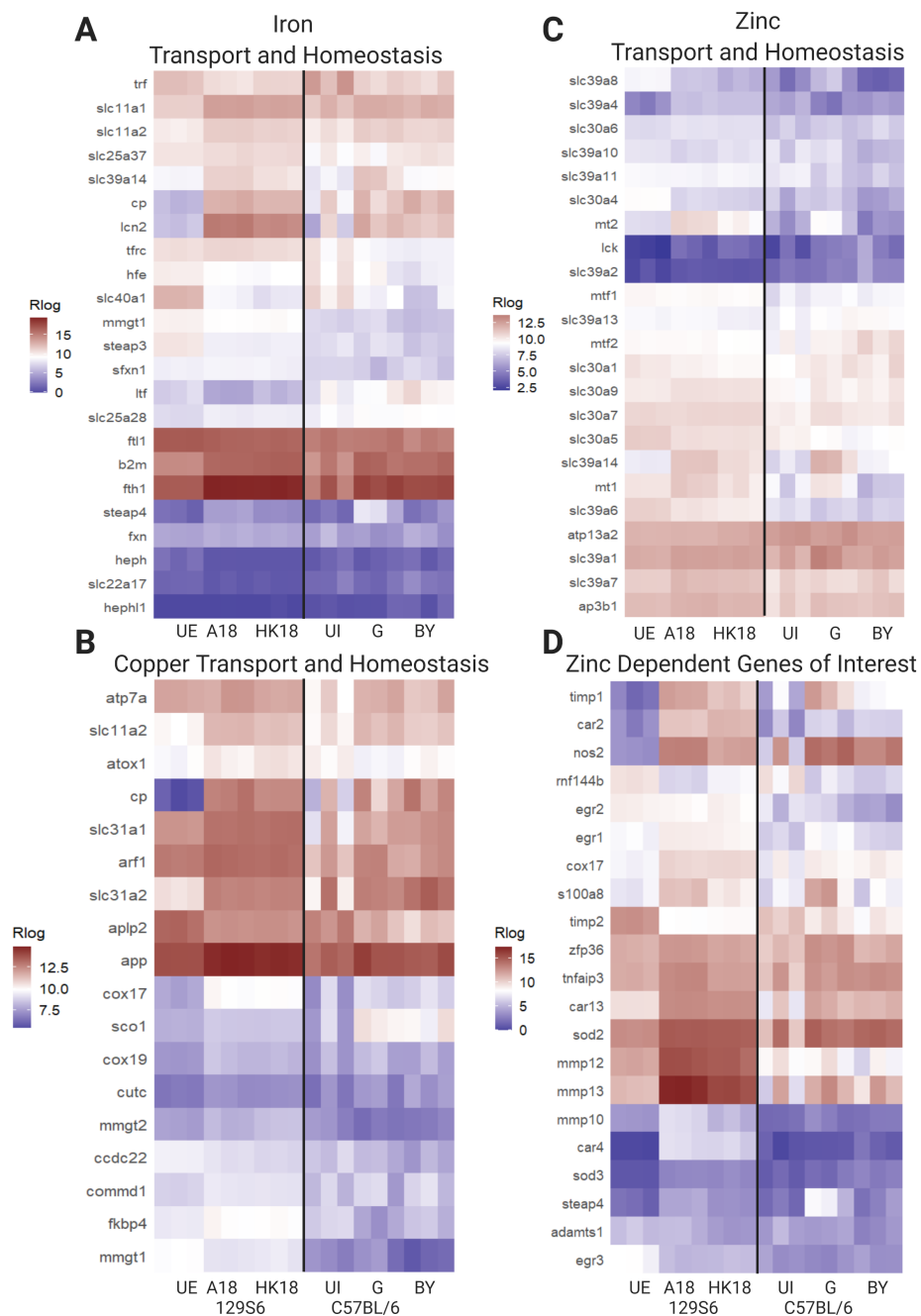


Figure 2.9: **Changes in metal-transport and -homeostasis genes reveal differences in metal regulation in BMDMs derived from *Slc11a1*-functional mice compared to non-functional mice.** RNAseq data from this study are compared to data from Stapels et al, GEO Accession GSE104785. Data from both studies were processed through the same pipeline and normalized together. Gene lists were compiled using Uniprot keywords and the mouse genome, and filtered for mean normalized *count* > 5 in at least one data set. **A)** Genes involved in Fe transport and homeostasis. **B)** Genes involved in Cu transport and homeostasis. **C)** Genes involved in Zn transport and homeostasis. **D)** Zn dependent genes of interest. UE: 129S6 BMDMs unexposed to *Salmonella*; HK: heat killed *Salmonella* treatment; UI: uninfected C57BL/6 BMDMs; G: C57BL/6 BMDMs containing growing *Salmonella*; BY: bystander C57BL/6 BMDMs.

limitation of Zn in the secretory pathway and phago-lysosomal compartment in response to infection in 129S6 BMDMs. Additionally, *slc39a8* is downregulated in 129S6 but upregulated in C57BL/6. In primary human lung macrophages, the Zn importer *slc39a8* is upregulated in response to LPS and negatively regulates proinflammatory responses[132]. Zn-dependent proteins such as proteases (*mmp9/10/12/13*) and carbonic anhydrases (*car 4/11*), are upregulated in 129S6 but not C57BL/6. Finally, there are notable differences in the magnitude of gene expression changes, including *car2*, *car4*, and *nos2*. These differences suggest changes in Zn distribution between the two model systems and altered regulation of Zn-dependent enzymes.

A comparison between A18 vs UE and G vs UI revealed global expression differences as well. 1991 genes are differentially expressed ($p_{adj} < 0.01$) between G and UI that were not differential ($p_{adj} > 0.03$) between A18 and UE. Further, 2723 genes were significantly different between A18 and UE, but not in G versus UI. When these gene lists were scrutinized using DAVID annotation clustering, the genes differential in 129S6 were enriched for cell cycle functions, and the majority are down regulated. Interestingly, the genes differentially expressed in C57BL/6 were enriched for apoptosis, and almost all of these genes were upregulated. These data suggest that these two cell types are moving toward different fates by 18 Hrs post *Salmonella* exposure, with 129S6 cells entering quiescence but C57BL/6 cells experiencing apoptosis. This observation is consistent with the fact that *Slc11a1* knockout macrophages are models for acute infection and are more susceptible to killing by *Salmonella*.

2.4 Discussion

This work presents a systematic analysis of changes in global gene expression, as well as a more targeted analysis of changes in genes related to transition metal ions in 129S6 macrophages infected with *Salmonella*. The 129S6 model system was chosen because these mice contain functional *Slc11a1* (*Nramp1*), a divalent metal ion transporter that localizes to phagosomes and regulates metal availability to the intracellular pathogen. *Slc11a1* confers resistance to intracellular pathogens and the 129S6 mouse has been used to model long-term chronic infection by *Salmonella*, as the mice

don't succumb to initial acute infection the way C57BL/6 or BALB/c mice do[106, 77, 133]. A recent study examined the *Salmonella* proteome upon infection of mice homozygous or heterozygous for functional versus nonfunctional Slc11a1 and found an abundance of Mg, Zn, Fe and Mn uptake systems expressed in *Salmonella* in resistant mice but not *Salmonella* that colonized susceptible BALB/c mice[77]. This study indicates that Slc11a1 plays a major role in affecting metal ion availability for uptake by *Salmonella*. However, how metal regulation in the host differs in the presence and absence of functional Slc11a1 has not been explored. Given that metal manipulation is a key component of nutritional immunity, I sought to define how genes encoding metal transporters, metal-dependent proteins, and metal-regulatory proteins were affected by treatment with live or heat killed *Salmonella* at early (2 Hrs post infection) and late (18 Hrs post infection) time points.

I observed widespread changes in metal transport, metal-dependent, and metal homeostasis genes, suggesting remodeling of Fe, Cu, and Zn availability by host cells. There is significant up-regulation of slc11a1, especially at late stages of infection, consistent with the host cell limiting Fe, Mg, Mn and Zn in the phagosome. Further changes in gene expression are consistent with decreased Fe uptake (trf), export (slc40a1) and increased storage (fth1); increased Cu uptake (slc31a1), import into the phagosome (atp7a) and altered distribution (Cu chaperones atox1, sco1, cox17) and increased transport of Zn into the cytosol (slc39a1, slc39a14) coupled with decreased transport into the secretory pathway and endo-lysosomal system (slc39a7, slc30a4, slc30a5). Increased expression of mt1 and mt2 genes, which encode Zn buffering proteins, further suggests an increase in cytosolic Zn. I also observed numerous changes in metal-dependent proteins and enzymes, many of which play an important role in nutritional immunity (lcn2, ltf, cp, steap3, sod2, arg1, nos2, mmp, car, s100a8). Some of these changes have been seen in a variety of mouse model systems in response to diverse intracellular pathogens, suggesting widespread or universal strategies for the host to combat infection. In particular, the changes in gene expression to limit Fe[79, 134] and accumulate Cu appear to be common strategies for nutritional immunity[83]. Indeed, the changes in expression of trf, slc40a1, fth1, slc31a1, lcn2 and cp were also observed in analysis of RNAseq data from infection of macrophages from C57BL/6 mice at 18Hrs post infection. However, it is notable that many of

the changes are significantly more pronounced (larger fold change) in the 129S6 model system, indicating a more robust nutritional immunity response in macrophages with functional *Slc11a1*. This observation is consistent with the findings of Cunrath and Bumann, which found that only in infection of mice with functional *Slc11a1* were bacterial metal uptake systems induced[77], suggesting that functional *Slc11a1* is necessary to activate nutritional immunity mechanisms. Interestingly, the changes I observed in expression in *slc11a1*, as well as key Fe and Cu regulatory genes were comparable in macrophages infected with live bacteria or treated with HK bacteria. This suggests that the host response is driven not only by active pathogen virulence factors, but also pathogen-associated cues, such as LPS.

As noted previously, there does not appear to be a universal strategy for host manipulation of Zn at the host-pathogen interface, with examples of host mechanisms to both starve and poison an intracellular pathogen[67, 84, 91]. Cellular regulation of Zn is more complex than Fe or Cu, with 24 Zn transporters that control transport into and out of the cytosol as well as intracellular organelles. Indeed, pathogens and immune system modulators have been shown to have different effects on Zn transporter expression[8] including upregulation of *slc39a8*[132] in response to LPS and $\text{TNF}\alpha$, upregulation of *slc30a4* and *slc30a7* upon stimulation with GM-CSF[135], and upregulation of *slc39a14* in response to LPS[136]. Previous studies have suggested that *Salmonella* experiences Zn starvation inside the host as the high affinity bacterial Zn uptake system *ZnuABC*[113] and associated accessory protein *ZinT*[114] and low affinity uptake system *ZupT*[137] contribute to virulence in mice. But the concept of Zn starvation is hard to reconcile with reports of Zn accumulation in puncta[117] and the suggestion that *Salmonella* induce Zn elevation to evade bacterial clearance[116]. To provide a more complete picture of Zn modulation within the host, I analyzed changes in the expression of Zn regulatory genes, measured labile Zn levels in the cytosol at different times post infection, and examined the effect of Zn availability (based on manipulation of Zn levels in media) on infection outcomes: bacterial clearance and bacterial replication. I was particularly interested in comparing how the host cell remodels Zn availability in macrophages with functional *Slc11a1*, and hence a robust nutritional immunity response.

The changes in Zn transporters and homeostasis genes predict an increase in cytosolic Zn and a decrease in Zn in the ER / Golgi / phagosome. Specifically, I observed significant upregulation of *slc39a1*, *slc39a14*, *mt1* and *mt2*, with more pronounced changes at late stages of infection (18 Hrs). Slc39a1 and a14 are plasma membrane transporters that mediate entry of Zn into the cytosol, while Mt1 and Mt2 are Zn buffering proteins that are frequently used as proxies for cytosolic Zn, as increased Zn leads to increased *mt1/2* expression via the Zn-dependent transcription factor Mtf1. Using a genetically encoded Zn sensor explicitly targeted to the cytosol, Michael Minson measured an increase in Zn from 80 pM to 2 nM at 12 Hrs post infection that remained elevated through the last measurement time (21 Hrs post infection). Intriguingly, *mt1*, *mt2*, and *slc39a14* are more highly upregulated upon infection with live *Salmonella* compared with heat killed bacteria, suggesting an active recognition of and response to live bacteria. I speculate that the host cell increases cytosolic Zn to support metabolic and transcriptional proteins that fight infection. This is consistent with my observation that a large fraction of differentially expressed genes has DAVID annotations that include “Zn binding”. When we manipulated Zn availability in the media, we found that Zn replete conditions led to robust clearance of infected bacteria, suggesting that the host may use elevated cytosolic Zn to fight infection.

I also observed an increase in *slc39a7* which encodes the transporter that moves Zn out of the ER and secretory pathway, a decrease in *slc30a5* which encodes the transporter that moves Zn into the Golgi and vesicular compartments, and a decrease in *slc30a4* which encodes a transporter which moves Zn into the phagosome. All three of these changes were comparable in macrophages treated with live *Salmonella* versus heat HK bacteria, suggesting a general host response to the pathogen and pathogen-associated cues (for example LPS). Further, all three of these changes in expression would lead to Zn limitation in the secretory / phago/lyoso-somal pathway and hence Zn restriction for the pathogen. This finding is consistent with previous observations that *Salmonella* upregulate bacterial Zn uptake mechanisms, especially in the presence of functional Slc11a1. Manipulation of Zn in the media revealed that zinc availability strongly correlated with bacterial replication, where Zn limitation blocked replication and Zn elevation enabled replication. Combined, my results

indicate that manipulation of Zn at the host-pathogen interface is more nuanced than Fe or Cu, where the host leverages its intricate means of manipulating Zn availability and distribution to limit the ability of the pathogen to access Zn while simultaneously ensuring sufficient Zn to support the immune response.

In addition to representing a distinct model system for studying nutritional immunity, I anticipated that the presence of functional *Slc11a1* would affect the global immune response to infection, since *Slc11a1* profoundly affects infection outcomes, namely resistance versus susceptibility. To critically compare infection-induced changes in the transcriptome, I identified an RNAseq study that was carried out in macrophages from C57BL/6 mice[109], with strong parallels to my conditions, and reanalyzed the data along with ours in an identical pipeline. I found that 4500 genes were differentially expressed in one study but not the other, with differences in expression at baseline as well as in response to infection. This is consistent with studies of mouse lines possessing one or two functional *slc11a1* alleles on a C57BL/6 background[106, 77]. These mice experienced lower infection loads but still ultimately succumbed to *Salmonella* infection, implying differences between C57BL/6 mice and 129S6 mice that extend beyond *Slc11a1*. However, the magnitude of differential expression was unexpected, as it involved more than a third of all genes differentially expressed in my data. Annotation analysis of this differential gene list indicates that these cell types tend toward different fates in response to the stress of *Salmonella* infection, with 129S6 cells showing suppression of cell cycle genes but C57BL/6 cells showing upregulation of apoptotic genes.

In assessing the GSEA and GO term enrichment present in my data I find recurring themes of inflammation, hypoxia, apoptosis and the unfolded protein response (UPR), which are inextricably linked[15, 103]. Both intracellular hypoxia and *Salmonella*-induced inflammation can result in apoptosis or the UPR, which is an attempt to regain cellular homeostasis under stress. When comparing live vs HK *Salmonella* conditions across time, I see enrichment of hypoxia-related genes along with enrichment of apoptosis 2 Hrs, which transitions to enrichment of UPR at 18 Hrs. This apparent transition in the cellular stress response over time demonstrates the ability of 129S6 macrophages to withstand *Salmonella* infection. In contrast, infection of C57BL/6 macrophages showed marked

enrichment of apoptosis genes at 18 Hrs. This finding is supported by multiple previous studies which found that *Salmonella* induces apoptosis in Slc11a1 nonfunctional macrophages[126, 138].

Macrophages experience a range of phenotypes, from inflammatory and cytotoxic (termed M1 polarization) to anti-inflammatory and wound healing (M2 polarization), depending on their milieu. These states are fluid, differing in gene expression and metabolism, and are heterogeneous across *in vivo* cell populations[15]. The bactericidal mechanisms available to M1 macrophages enable them to kill internalized pathogens efficiently. The lack of these mechanisms in M2-like macrophages make them a more permissive niche for facultative intracellular bacteria like *Salmonella*. Although a number of previous studies have tried to identify individual genes that distinguish M1 and M2, for example: *arg1* vs *nos2*[139] or *egr2* vs *CD38*[140], the increasing availability of whole transcriptome sequencing makes it possible to define a more comprehensive genetic signature of M1 and M2. Single cell RNAseq by Saliba et al[119] enabled identification of gene clusters related to M1 and M2 and how these gene clusters correlated with infection (naïve macrophages, bystanders, macrophages with growing bacteria and macrophages with non-growing bacteria). Dual RNAseq of both the pathogen and host by Stapels et al[109] further enables correlation of the M1 and M2 gene clusters within the host with expression of *Salmonella* virulence genes. Indeed, this analysis revealed that in C57BL/6 macrophages, the M2 polarization correlates with increased SPI2 expression, suggesting that *Salmonella* activates virulence mechanisms in this niche.

Examination of M1 and M2 gene clusters further reinforces that 129S6 macrophages represent a distinct intracellular niche with respect to immune response to infection. As shown in Figure 2.2, polarization genes follow a temporal pattern of expression, with the majority of M1 related genes strongly upregulated 2 Hrs post infection but sharply downregulated by 18 Hrs. On the other hand I see slower time-dependent activation of M2 related genes. This observation is supported at 2 Hrs by enrichment in glycolysis, the metabolic state of inflammatory or hypoxic macrophages, and at 18 Hrs by enrichment in oxidative phosphorylation and fatty acid metabolism, which are the metabolic markers of M2 macrophages[15, 103]. Importantly, at each time point I see little difference in M1/M2 associated genes between live and HK *Salmonella* conditions, especially when

normalized to C57BL/6 data (Supplementary Figure 2.16 on page 69). This is in contrast to findings in *Slc11a1* non-functional macrophages which indicate that dividing *Salmonella* may actively induce M2 polarization to enhance bacterial survival, and that macrophages exposed to but not infected by *Salmonella* maintain an M1 phenotype late in infection[119, 109]. While my work is at a population level and therefore contains macrophage and *Salmonella* heterogeneity, exposure to HK *Salmonella* does not lead to retention of an M1 phenotype at 18 Hrs, nor does it seem that 129S6 cells are induced to M2 by live *Salmonella*.

My study recapitulates the ability of 129S6 macrophages to fight infection at all time points, which intriguingly occurs regardless of the expression profile of M1 or M2 genes. At 2 Hrs, 70% of initially infected macrophages had cleared the infection, which correlated with the transcriptional induction of M1 polarization. However, despite the shift toward an M2-like transcriptional profile at 18 Hrs, the rate of bacterial clearance increased slightly over time to 74%. Concurrently the proportion of infected macrophages showing evidence of bacterial replication also increased over time, from 8% at 10 and 18 Hrs to 24% by 24 Hrs. This high clearance rate and relatively low replication rate resulted in only 3% of initially infected macrophages harboring dividing bacteria at 24 Hrs (Supplementary Dataset S5). This is in contrast to studies of *Nramp1*^{+/+} 129X1 mice[141] and *Slc11a1* nonfunctional macrophages which report that replicating *Salmonella* are preferentially found in M2 cells[119, 123, 109]. It is also notable that 129S6 macrophages surviving to 24 Hrs while harboring dividing *Salmonella* are not allowing high division rates, as indicated by only modest decreases in the inducible fluorescent signal (Figure 2.9), whereas *Slc11a1* nonfunctional macrophages experience high levels of *Salmonella* division at 24 Hrs[123, 131]. It is important to note that Zn was a key factor in both clearance and bacterial replication processes, as reduced zinc availability correlated with attenuation of both.

This study reveals that 129S6 macrophages differs significantly from other model systems of *Salmonella* infection which possess a nonfunctional *Slc11a1*. First, 129S6 macrophages show a robust remodeling of metal homeostasis and expression of metal-dependent enzymes, that indicate the nutritional immunity response within the host differs in the presence of functional *Slc11a1*.

Second, remodeling of Zn regulatory proteins leads to an increase in cytosolic Zn and a likely restriction of Zn for the pathogen. This multi-pronged approach ensures sufficient cytosolic Zn to fight infection and promote bacterial clearance, while still limiting Zn availability to fight against bacterial replication. Third, transcription of M2-related genes doesn't correlate exclusively with live *Salmonella* exposure or with a lack of bactericidal capacity, suggesting that in this model system the M2 polarization does not promote bacterial survival. Rather, activation of M1-related genes early and M2-related genes at later time points correlates with the switch from expression of apoptosis genes to UPR genes and suggests a choreographed response to fight infection without killing the host cell. Together, these imply that 129S6 macrophages do not conform well to the M1/M2 expression dichotomy derived largely from Nramp1 nonfunctional macrophages and mice. Instead, they appear to present a mixed phenotype that effectively uses zinc to quell *Salmonella* infection.

2.5 Methods

2.5.1 Monocyte extraction from bone marrow

Animal work followed protocol 2547, approved by University of Colorado IACUC. 8-12 week-old 129S6 female mice (Taconic Laboratories) were euthanized by CO₂ inhalation according to IACUC guidelines, followed by cervical dislocation. Femur, tibia and humerus bones were extracted, then scraped and flushed with ice cold phosphate buffered saline (PBS). Approximately 1 mL of PBS was used per bone. PBS with marrow cells was passed through a 70 micron nylon mesh Falcon™ Cell Strainer (Corning™ 352350), then overlaid onto an equal volume of Histopaque-1083 (Sigma-Aldrich) in centrifuge tubes. Tubes were centrifuged at 500 x G for 30 min and allowed to slow with no brake. Monocytes appear as a fuzzy layer at the fluid interface. These were removed to clean tubes and washed twice with 14 mL PBS. After the final wash monocytes were resuspended in a small amount of macrophage growth media and counted with a hemocytometer. Growth media consisted of DMEM (Sigma-Aldrich) supplemented with 20% fetal bovine serum (FBS), 2 mM L-glutamine, 1 mM sodium pyruvate, penicillin/streptomycin (50 IU/mL penicillin and 50 µg/mL

streptomycin) and 10 pg/ μ L recombinant murine macrophage colony stimulating factor (PeproTech, Inc.).

2.5.2 Primary cell culture and infection

Monocytes were plated into 12-well plates at a density of 200,000 cells per well. 2 mL macrophage growth media was added to each well and plates were incubated at 37°C and 5% CO₂ for 6 days. Media was refreshed 3 days after plating. Wild type *Salmonella* Typhimurium SL1344 was cultured to stationary phase in LB with [antibiotics] at 37°C with aeration. Bacteria were washed with PBS and opsonized for 30 minutes at room temperature in a 1:1 solution of mouse serum (Sigma) and cell culture media (Gibco). Bacteria were then pelleted at 13,000 x G for 1 minute and resuspended in PBS. Half of the bacteria was heat killed at 60° C for 3 minutes, then placed on ice. One well of macrophages was scraped and counted, and bacteria were diluted in macrophage media without antibiotics to an MOI of 30. Plated macrophages were washed 3 times with PBS, then treated with antibiotic free macrophage media containing live, heat killed, or no bacteria. 30 minutes later bacterial media was removed, cells were washed 3x with PBS, and macrophage media containing 100 g/mL gentamicin was added. 90 minutes later media was again removed. RNEasy lysis buffer was added directly to wells designated as 2 Hr samples. Macrophage media with 10 μ g/mL gentamicin was added to wells designated as 18 Hr samples. Lysed samples were collected and frozen at -20 °C. 18 Hrs post *Salmonella* exposure media was removed from remaining wells, lysis buffer was added, and cell lysates were frozen at -20 °C. To examine both early and late immune responses, macrophages were lysed at 2 or 18 hours post bacterial exposure. Control samples were lysed at the two-hour timepoint.

2.5.3 RNA extraction and sequencing

RNA extraction was done on all samples at once, after one freeze-thaw cycle. An RNEasy kit (Qiagen) was used, and DNase I treatment was done on the column. RNA integrity was checked via Tape Station, and library prep was done with an Illumina TruSeq LT kit which included polyA

selection. Paired end 75 base sequencing was done on a NextSeq 2.1.0 Illumina machine. Tape station run, library prep and sequencing were performed by the JSCBB sequencing core.

2.5.4 Data analysis pipeline

R 3.3.0 on the JSCBB computing core was used for analysis of raw data. Data quality was assessed with fastqc (0.11.2) and the first 10 bases were trimmed with Trimmomatic (0.36). Reads were mapped with TopHat(2.0.6)/Samtools (0.1.18)/bowtie2 (2.0.2) using `-b2-very-sensitive, fr-firststrand` settings. Read counting was completed with EdgeR Subread featureCounts (1.6.0) using the mm10 gtf file from UCSC (July 2015 version). MetaFeature mapping was paired end, with both ends mapped, and no MultiOverlap allowed. R 4.0.2 was used for all remaining analysis. A principal component analysis (PCA) of global RNA expression was performed using EdgeR. Analysis of differential expression was done with DESeq2 (1.18.1) but the nature of this dataset violates the DESeq2 assumption that most genes do not change expression between conditions. Therefore, all genes with differential expression $p_{adj} < 0.05$ in binary comparisons were compiled and excluded from the final dds normalization using the controlGenes parameter. A log ratio test on the correctly normalized DESeq dataset matrix (dds) with the following function: `DESeq(dds, test="LRT", reduced = 1)`, and resulted in a list of globally differentially expressed genes. This dataset ($p < 0.01$) was further filtered with two Transcripts Per Million (TPM) requirements. Inclusion in the final analysis indicates that a gene has an overall mean $TPM > 5$, and at least one condition with a mean $TPM > 10$. The 7766 genes meeting these criteria were fed into DEGReport R package(1.24.1) for rlog transformation, which produced normalized counts, and expression clustering, which produced Z-scores. Expression clustering was done with the following function: `degPatterns(cluster_rlog, metadata = metadata, time = "Treatment").Heatmap` gene dendrograms were constructed using hierarchical clustering package hclust and gg dendro (0.1.22), and this gene order was used to construct global and cluster heatmaps with ggplot (Tidyverse R package 1.3.0). The median value for each plot was set as white. DAVID annotation enrichment categories were used to assess the makeup of DEGReport clusters. This analysis included functional

categories, Gene Ontology, Biocarta and Kegg pathways, and protein domains.

In brief, DESeq2 binary comparisons between conditions were fed into GSEA[142] to validate GO term enrichment and assess transcription targets. More specifically, adjusted p-value ranked lists were created from DESeq2 differential expression data sets comparing 2A vs. 2HK or 18A vs. 18HK. For each gene in a given data set, a rank was determined from the padj value (false discovery rate) and the direction of fold change value (up or down regulation). Rank = $-\log(\text{padj}) * \text{sign}(\text{fold change})$. All genes with a valid padj value were included. GSEA was used to compare these ranked lists to validated gene sets. These were: Canonical Pathways, Hallmark gene sets, GO_Biological Processes, GO_Molecular Functions, and Transcription Factor Targets. Because GSEA's default is human gene sets, the mouse genome was collapsed and remapped using the Mouse Gene Symbol Remapping Human Orthologs MsigDB.v7.2.chip. Gene set permutations were used in this analysis, which is a less stringent assessment of significance, and produces more false positive results. Therefore, a cutoff of $q < 0.05$ was applied to gene set results.

2.5.5 Comparison of current study with Staples et al, Science, 2018

FASTQ files (GEO accession GSE104785) were downloaded and run through the above pipeline with the following alterations: Trimmomatic was used to remove Illumina adaptors, and alterations were made to mapping and counting based on the unstranded nature of the data. This differs from the pipeline of Staples et al. in that their data was mapped to the *Salmonella* genome prior to the mouse mm10 genome. Additionally, their read counts were performed with HTSeq (version 0.6.1) instead of FeatureCounts. To normalize my data with this previously published dataset, DESeq2 was run on the combined data with the experimental design Treatment, and normalized counts were calculated. PCA and dendrogram of the Staples dataset were created and compared with their published heatmap to generally validate my sequencing results (Supplementary Figure 2.17 on page 70).

To assess differences in metal homeostasis genes as comprehensively as possible, mouse specific lists of genes involved in the transport and homeostasis of metal ions were compiled from the Uniprot

database. Separate lists were compiled for Zn, Fe, and Cu, and each list was compared against the normalized counts of the aggregated sequencing studies. Only genes expressed above background were used for further analysis.

2.5.6 Measurement of cytosolic Zn and Imaging analysis

For quantification of cytosolic labile Zn in primary macrophages, calibration experiments were performed at the indicated times post infection on a Nikon Ti-E widefield fluorescence microscope equipped with Nikon elements software, Ti-E perfect focus system, an iXon3 EMCCD camera (Andor), mercury arc lamp, and YFP FRET (434/16 excitation, 458 dichroic, 535/20 emission), CFP (434/16 excitation, 458 dichroic, 470/24 emission), and YFP (495/10 excitation, 515 dichroic, 535/20 emission) filter sets. External excitation and emission filter wheels were controlled by a Lambda 10-3 filter changer (Sutter Instruments), while dichroic mirrors were placed on cubes in the dichroic turret. Channel EM gain and exposure settings for both YFP FRET and CFP were set to be the same. Images were collected using a 60X oil objective (NA 1.40), 200 ms exposure time, EM gain 1 MHz at 16-bit readout mode with an EM gain multiplier of 200, and a neutral density filter with 25% light transmission. Sensor expression level was controlled by selecting cells with YFP intensities between 4,000-15,000 fluorescence units under these conditions. 8 fields of view were collected using multipoint acquisition mode and the Perfect Focus System (PFS) set to 'ON' in between points. Cells were maintained at 37°C and 5% CO₂ in a LiveCell™ environment chamber (Pathology Devices) during the experiments. Images were collected every minute during R_{Resting} and R_{min} calibration acquisition phases and every 30 seconds during the R_{max} calibration phase.

Fresh calibration solutions were prepared the day of the experiment and include a 2X solution of R_{min} buffer (50µM TPA in PO₄³⁻-free HHBSS) for minimum FRET ratio collection and a 2X solution of R_{max} buffer (0.001% saponin + 0.75 µM pyrithione + 23.8nM buffered Zn in PO₄³⁻-, Ca²⁺-, Mg²⁺-free HHBSS) for collecting the maximum FRET ratio. The resting FRET ratio of the sensor was collected for 10 mins prior to calibration to ensure a stable signal. After 10 min of

imaging 50 μM TPA was added to the dish to collect the minimum FRET ratio of the sensor. Once a stable signal had been achieved cells were then washed with phosphate, calcium, and magnesium-free HEPES-buffered HBSS, $\text{pH} = 7.4$ to remove the chelate and then treated with pyrithione and Zn with 0.001% (w/v) saponin.

All imaging data were analyzed in MATLAB (Mathworks). Images were background corrected by subtracting a local background intensity from each pixel grouped in a certain region of the image. Regions of interest were generated by using a segmentation algorithm that segments the image based on the fluorescence intensity of the FRET ratio channel to obtain single cell traces. FRET ratios for each cell trace were calculated by dividing the background-corrected YFP FRET intensity by the background-corrected CFP intensity. The resting, minimum, and maximum FRET ratios for each cell were used to calculate the fractional saturation, the dynamic range, and the reported $[\text{Zn}]$ from the sensor in each cell. Resting $[\text{Zn}]$ is calculated by $[\text{Zn}^{2+}] = K_d * \left(\frac{R_{\text{Resting}} - R_{\text{min}}}{R_{\text{max}} - R_{\text{Resting}}}\right)^{1/\text{hill}}$ where the $K_d = 230\text{pM}$ and $\text{hill} = 0.53$ for NES-ZapCV2. The dynamic range of the sensor can be impacted by both over expression and under expression of the sensor which has a negative impact on the fidelity of the apparent $[\text{Zn}]$. For this reason, cells were excluded from the analysis if they fell outside of an acceptable dynamic range, 1.6 – 2.3 for the NES-ZapCV2 sensor.

2.5.7 Flow cytometry study of infection outcome with varied zinc availability

Four different media conditions were used for flow cytometry. Standard macrophage growth media (DMEM + 20% FBS) was found to contain 25 μM Zn by ICP-MS and was used as the baseline. The other three medias used chelex-100-treated FBS. Briefly, FBS was treated with Chelex 100 resin (Sigma-Aldrich, St. Louis, MO, USA) for 5 hours, stirring at 4°C, followed by sterile filtration using a 0.22 μm PES membrane filter. This chelex-treated FBS was used to prepare the baseline Chelex media, which contained DMEM + 20% FBS + L-glutamine (2 mM) + sodium pyruvate (1 mM). Zn replete media was made by adding 30 μM ZnCl_2 (Sigma-Aldrich, St. Louis, MO, USA) to Chelex media. Media with essentially no Zn was made by adding 3 μM 2-[Bis(2-pyridinylmethyl)amino]ethylaminobenzenesulfonic (ZX1, an extracellular Zn chelator[143])

(Strem Chemicals, Inc.) to Chelex media. ICP-MS measurements were carried out as described previously[144] to quantify the metal content of the media. While Chelex treatment depleted Zn, Ca, and Fe, the Zn replete, Chelexed media, and Zn deficient media are identical except for the amount of zinc present in the media (34 μ M, 4 μ M, no Zn, respectively).

For analysis of intracellular bacterial replication, monocytes from three mice were grown and differentiated to macrophages in 6 well plates. Six days later, *Salmonella* expressing pDiGc and induced with arabinose were grown to stationary phase with aeration. Macrophages were infected with *Salmonella* at a multiplicity of infection of 30, and infection proceeded for 45 min. At this point *Salmonella* media was removed, cells were washed 3x in PBS, and initial inoculum cells were collected by scraping with a nylon cell lifter (Corning™ C3008) and homogenized by pipetting gently with a P1000. Homogenized cells were fixed in a gentle fixative for preserving fluorescent protein fluorescence (1% PFA and 1% sucrose) for 15 min and then washed and resuspended in PBS and chilled at 4°C. Media in all other samples was changed to experimental conditions which included 10 μ g/mL gentamicin. Three wells were treated with each media, for each time point. At 2, 10, 18 and 24 Hrs post infection, cells were rinsed, lifted, fixed and chilled as above. Samples were analyzed on a BD FACSCelesta™ (BD Biosciences) collecting forward scatter area and width, side scatter area and width, 488 nm excitation 530/30 nm emission, and 561 nm excitation and 585/15 nm emission. Data were analyzed using FlowJo 10.5.3 software (FlowJo LLC).

The cell gating hierarchy was set as Single cells > GFP positive cells > Cells containing replicated bacteria. 25-30,000 single cells were collected per sample. Single cells were determined first by forward scatter area versus side scatter area then by side scatter width versus side scatter area. Non-fluorescent uninfected cells were used to set the gate for GFP positive cells. A ratio of the 488 nm channel to the 561 nm channel was taken by dividing 488 nm intensity by 561 nm intensity. Samples collected at 2 Hrs post infection were used as the “initial inoculum” to determine the fluorescence intensities for cells infected with bacteria that have not undergone replication. Cells containing replicated bacteria were gated as having a 488 nm:561 nm ratio above the initial inoculum.

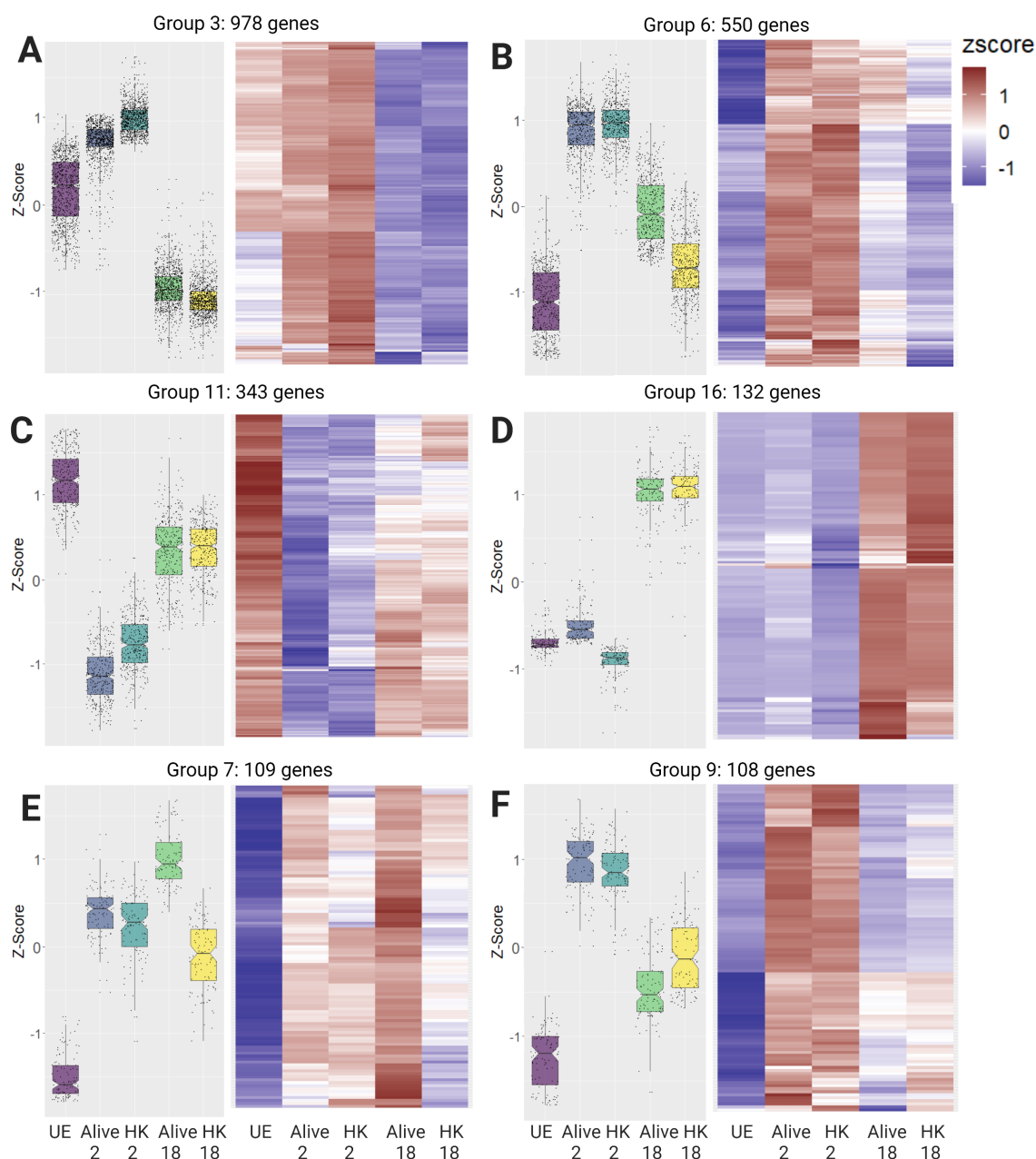


Figure 2.10: **Clustered data exposes multiple distinct trends in gene expression (groups 3, 16, 11, 16, 7, 9)**. A) Cluster 3 is enriched in genes involved in transcription and translation, cell adhesion, Zn binding (beyond transcription factors), cell cycle, and kinase signaling pathways. B) Cluster 6 is enriched for cell adhesion, actin binding, translation (preinitiation and initiation), immune responses to specific diseases, ATP binding, protein transport (secretion and retrograde transport), and heat shock. C) Cluster 11 is enriched for transcription, Zn binding, DNA repair and autophagy. Transcription and Zn overlap on 40/80 genes. D) Cluster 16 is enriched for mitochondrial transit peptides, ATPase/kinase function, Golgi proteins, immunity, and fatty acid metabolism. E) Cluster 7 is enriched for cell adhesion, ER protein processing, unfolded protein response, redox, and proteasome proteins. F) Cluster 9 is enriched for genes involved in TNF signaling and response to lipopolysaccharide (LPS), ER functions, and cytokines/inflammatory response.

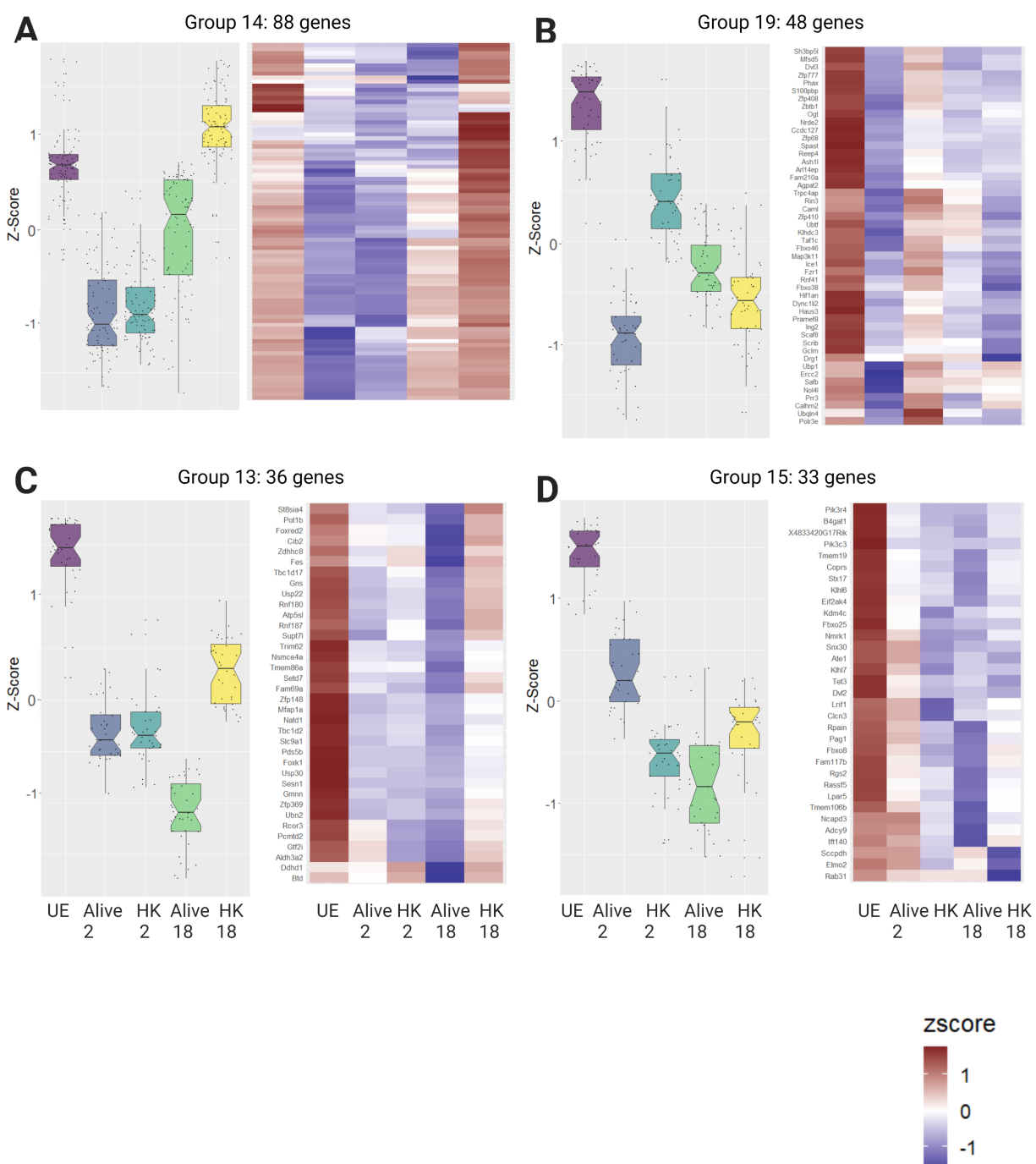


Figure 2.11: **Clustered data exposes multiple distinct trends in gene expression (groups 14, 19, 13, 16).** A) Cluster 14 is enriched for genes involved in innate immunity, Zn binding, and transcription. B) Cluster 19 is enriched for transcription and mitosis related genes, and Zn finger motifs. C) Cluster 13 is enriched for genes involved in transcription, Zn binding, ubiquitylation, redox, and Golgi transport. D) Cluster 15 is enriched for genes involved in endosome functioning, redox, Zn binding, and those with transmembrane domains.

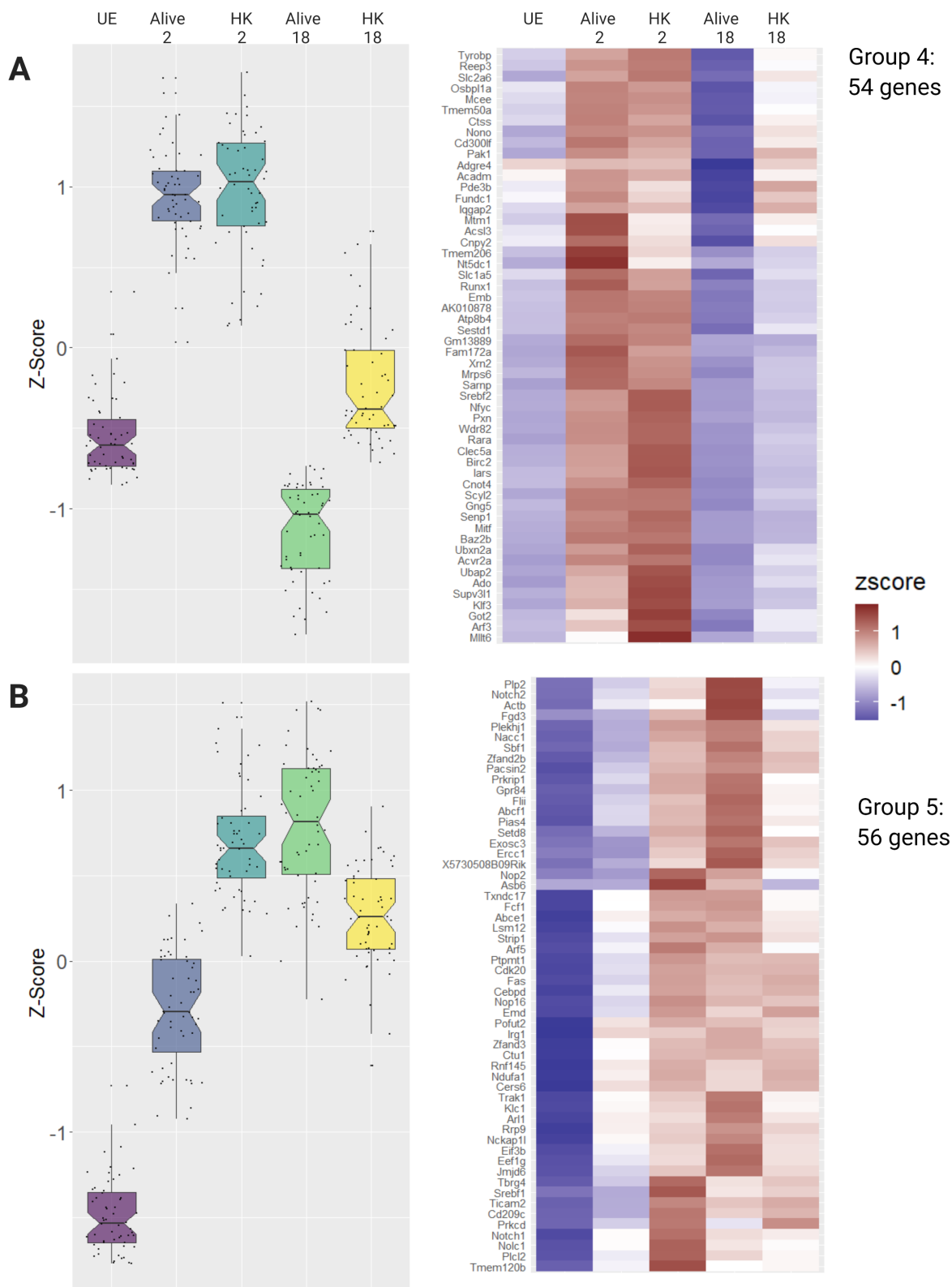


Figure 2.12: **Clustered data exposes multiple distinct trends in gene expression (groups 4 and 5).** A) Cluster 4 is enriched for apoptosis regulation and transcription/nuclear functions. B) Cluster 5 is enriched for RNA processing functions.

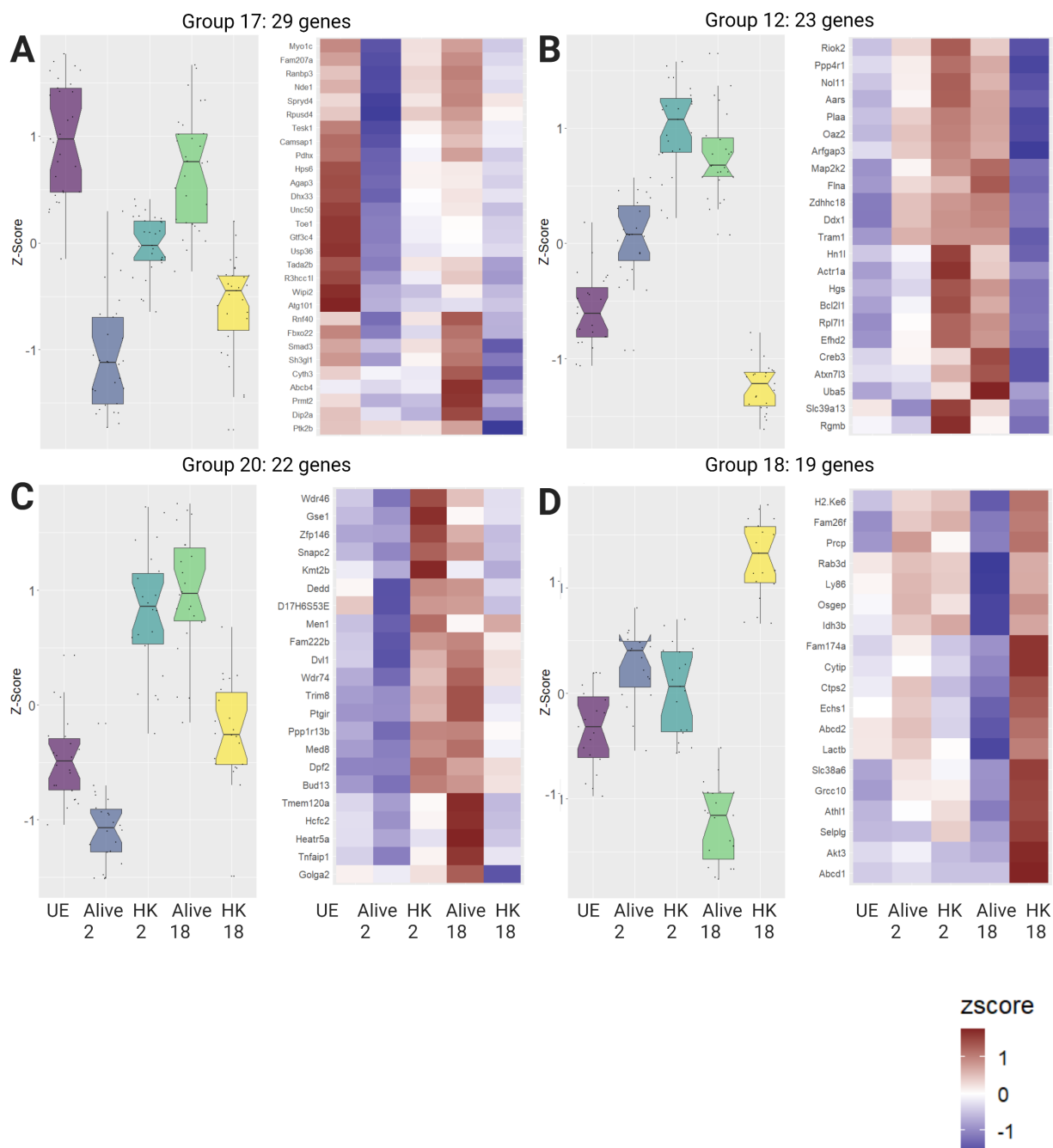


Figure 2.13: **Clustered data exposes multiple distinct trends in gene expression (groups 17, 12, 20, 18).** A) Cluster 17 is enriched for protein transporters and Zn binding. B) Cluster 12 is enriched for ATP binding, Zn and metal binding, transcription and protein transport. C) Cluster 20 is enriched for transcription, apoptosis, and Zn binding. D) Cluster 18 is enriched for ATP binding, glycoprotein/disulfide modifications, and membrane functions.

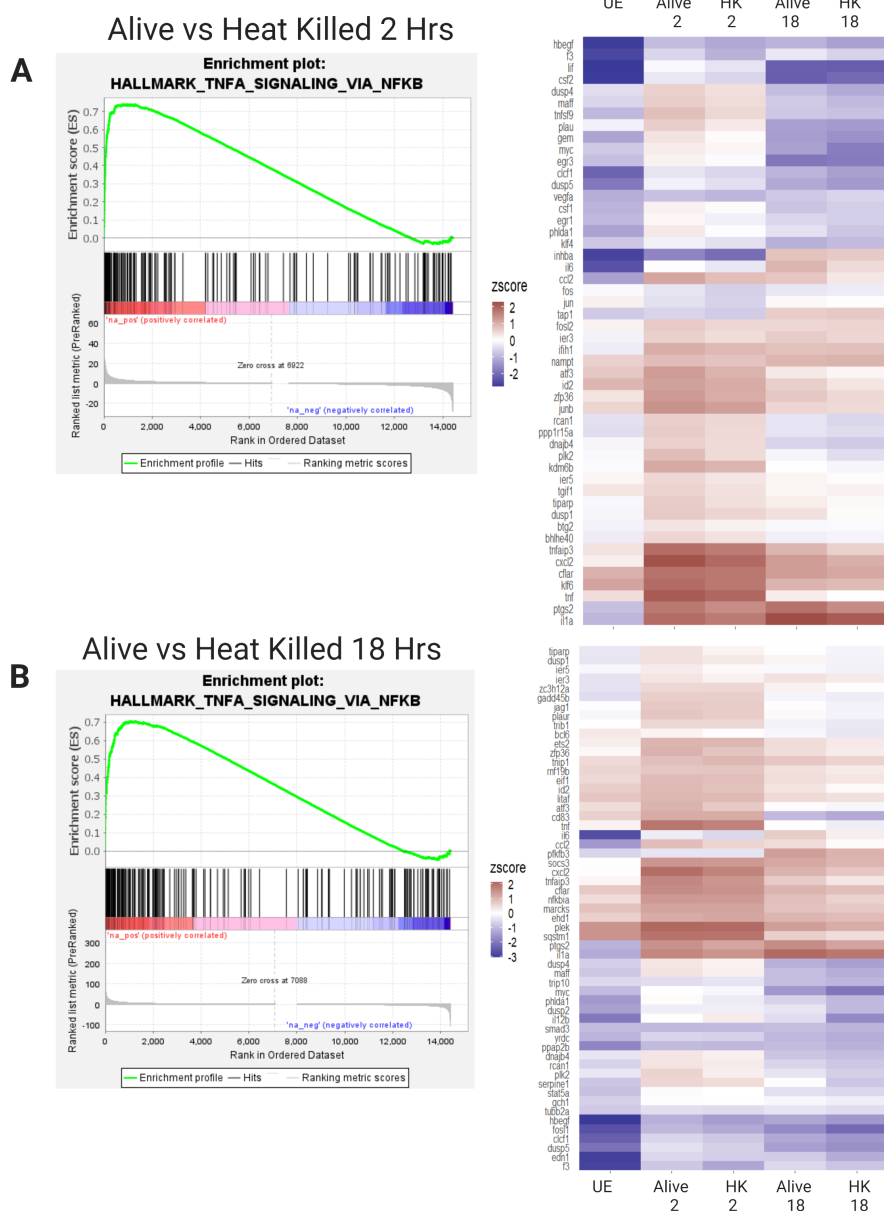


Figure 2.14: **GSEA analysis of Hallmark gene set TNF α signaling via NF- κ B.** Each panel shows a GSEA enrichment plot and a hierarchically clustered expression heat map of the leading edge genes from that GSEA plot. The leading edge genes are all vertical black lines on the positive end of the spectrum, down to the point of maximum Enrichment Score. Enrichment plots were constructed based on a ranked gene set of differential expression data (either A2 vs HK2 or A18 vs HK18). A) At 2 Hrs the TNF α signaling via NF- κ B gene set is strongly enriched in response to live vs HK *Salmonella*. ($q = 0.000$, NES = 2.42) B) At 18 Hrs the TNF α signaling gene set has been dampened somewhat, though it is still enriched in live vs HK conditions ($q = 0.002$, NES = 1.88), and while there is a core set of 32 genes upregulated at both time points, there are 15 fewer leading edge genes at 18 Hrs than at 2 Hrs. UE: unexposed control; HK: heat killed; q : false discovery rate; NES: Normalized Enrichment Score from GSEA.

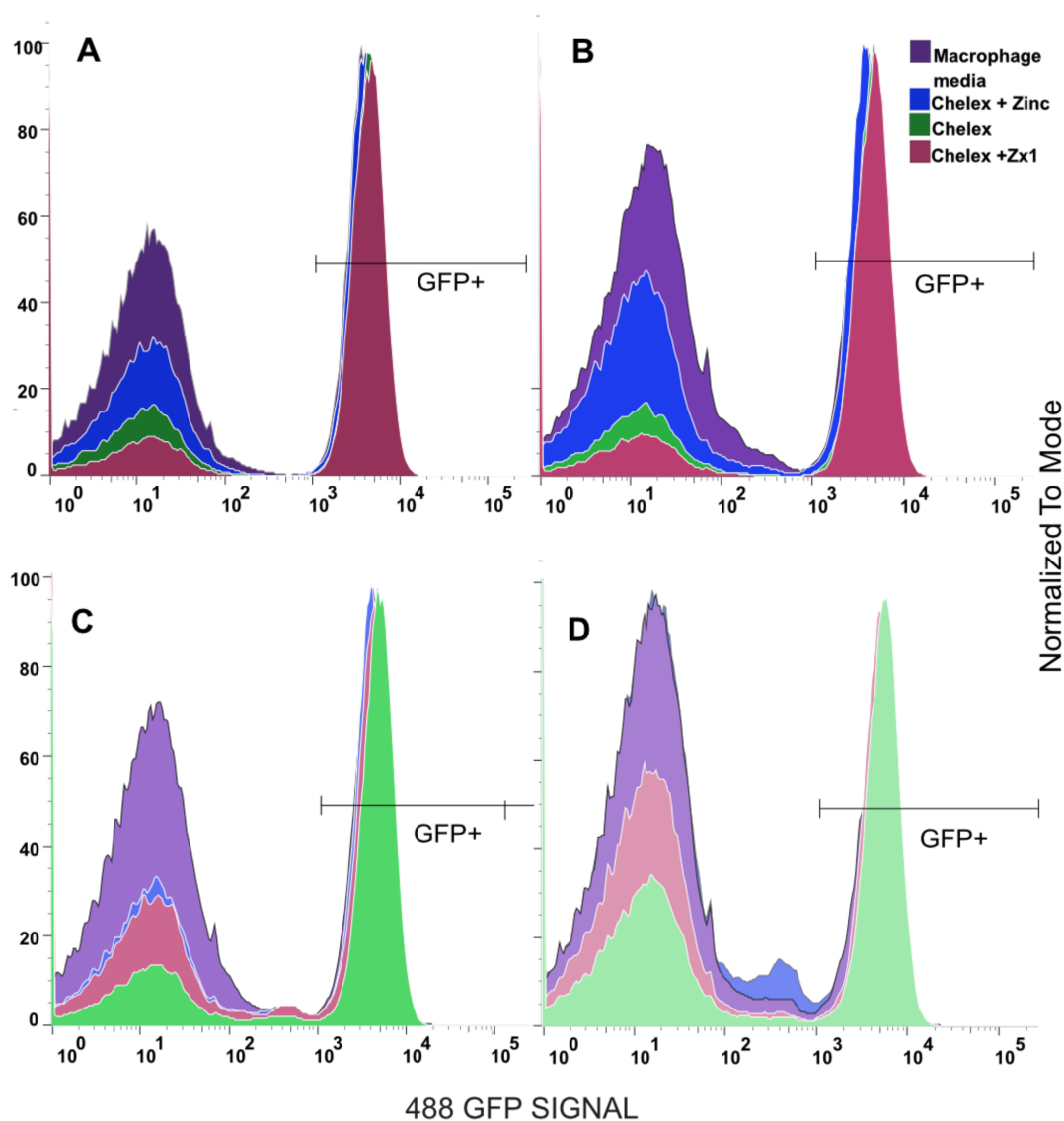


Figure 2.15: **FACS analysis of infected 129S6 BMDMs clustered by time post infection.** These histograms of flow cytometry data indicate the GFP signal from macrophages infected with *Salmonella* expressing pDiGc at 2, 10, 18 or 24 hours post infection. At each time point, Zn replete medias (normal macrophage growth media, serving as a positive control, and Media with Chelex-treated FBS + 30 μ M Zn) showed more robust bacterial clearance than Zn depleted media (Media with Chelex-treated FBS) or Zn deficient media (Media with Chelex-treated FBS + ZX1 extracellular Zn chelator). A) 2 Hrs post infection. B) 10 Hrs post infection. C) 18 Hrs post infection. D) 24 Hrs post infection. Blue 'chelex+zinc' curve is directly behind the purple macrophage media curve, both showing almost 100% bacterial clearance.

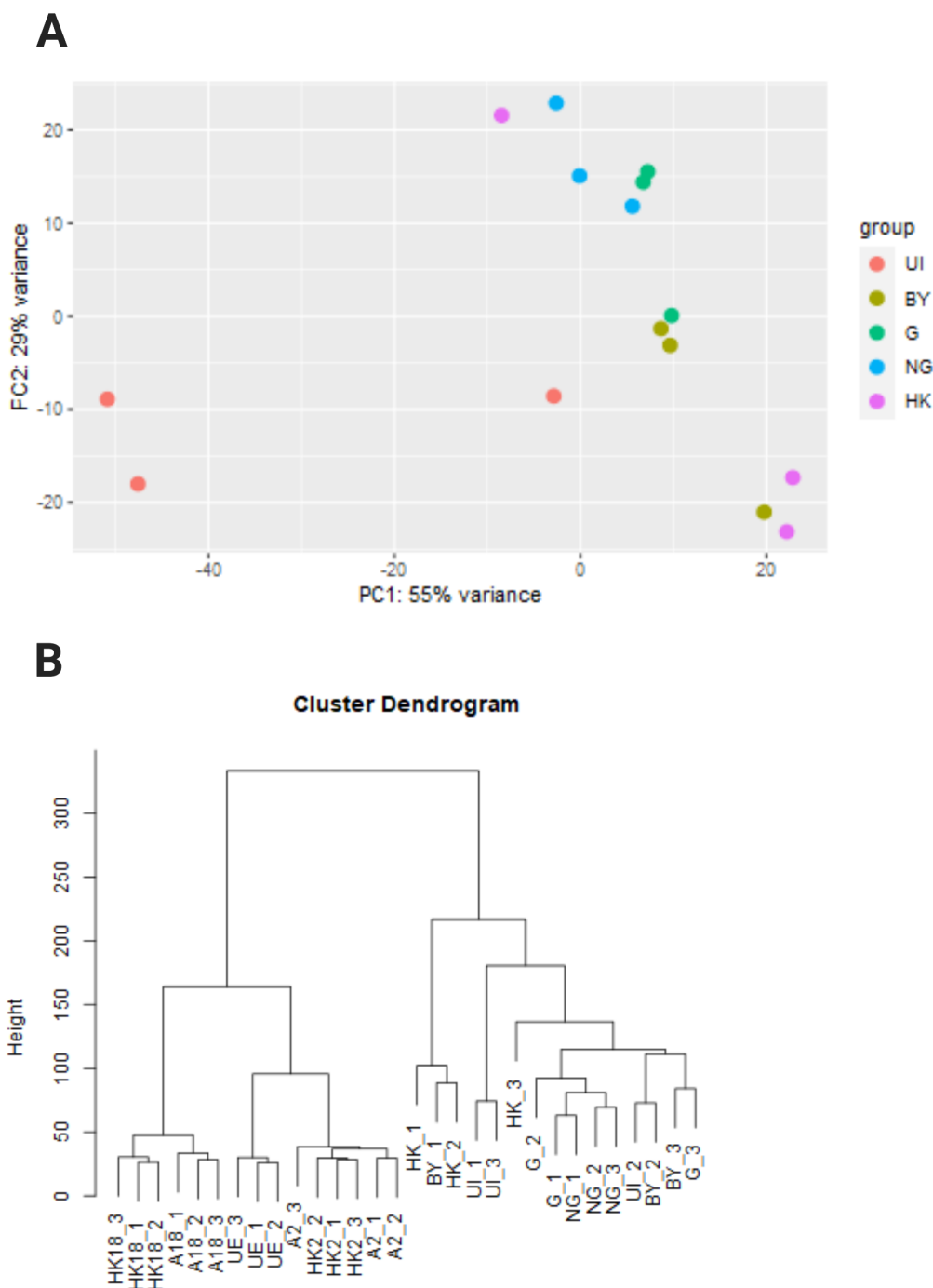


Figure 2.16: **Heatmaps of the gene clusters III and IV that were defined in Staples et al.** After processing Staples' data and normalizing it with my own, I mapped the expression values of the genes in Staples' cluster III (M1 in character) and IV (M2 in character). Genes in each cluster that were differentially expressed ($q < 0.01$) in binary comparisons of A18 vs HK18 or G vs BY and expressed above background are included here. Staples et al hypothesize that this differential expression indicates an M2 phenotype that is being induced by the presence of live, growing *Salmonella*. Overwhelmingly though, these genes are DE in Staples' data and not between my alive and HK conditions, supporting the idea that 129S6 macrophages represent a distinct model system.

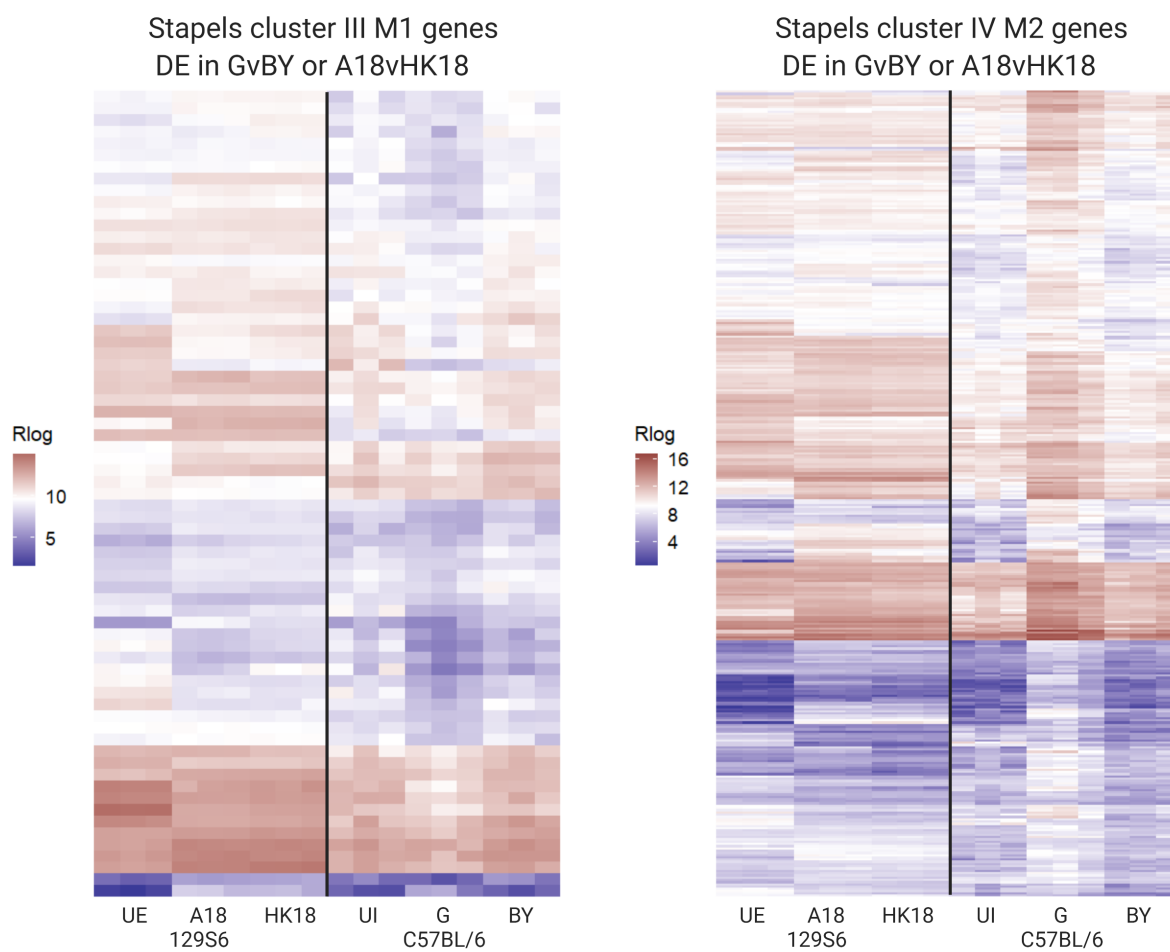


Figure 2.17: **PCA and dendrogram showing Stapels et al's data analyzed with my pipeline.** A) PCA of all 15 of Stapels' samples after their FASTQ files were trimmed, mapped and counted using my pipeline. PCA produced with EdgeR. B) Dendrogram demonstrating hierarchical clustering of Stapels' samples and ours, normalized together in DESeq2.

Chapter 3

Future Directions

3.1 Fluorescent imaging of macrophages under Zn manipulation conditions

Because Zn is essential to both macrophage immune function and survival of *Salmonella* within macrophages, I wanted to show that altered Zn availability during infection induced a measurable phenotypic change. In collaboration with Mike Minson, I altered the availability of Zn in the media during infection but after bacterial internalization. I wanted to know which, if either, of the contestants would profit or suffer from altered Zn, and the outcomes we measured were macrophage killing of *Salmonella* and *Salmonella* replication within macrophages. I reasoned that if macrophages were attempting to starve *Salmonella* of Zn then lowering its media availability might improve *Salmonella* clearance or suppress *Salmonella* division. On the other hand, if *Salmonella* were being poisoned with Zn and its availability was reduced, this might subdue clearance and/or improve replication.

In this study we infected Macrophages with *Salmonella* containing the pDiGc plasmid, which expresses GFP constitutively and DSRed when induced with arabinose. The initial ratio of expression between GFP and DSRed is set as 1:1, and as bacteria divide in the arabinose free macrophage phagosome, the GFP signal will remain constant between mother and daughter cells, while the DSRed signal will be divided equally between daughter cells. This means that the GFP:DSRed will decrease in each subsequent generation of *Salmonella* daughter cells produced, allowing us to track bacterial replication. Bacterial clearance is determined based on the loss of the GFP signal, which is quickly quenched upon bacterial death within macrophages[145]. The initial infection rate

is determined by the fraction of macrophages expressing GFP immediately after the infection time period, and this is compared to subsequent ratios of GFP+ : GFP-.

The group that developed this reporter plasmid[146] tested it in *Salmonella* grown in three conditions: broth, within RAW264.7 cells and within C57BL/6 primary mouse macrophages. They then conducted flow cytometry on individual bacteria, either removed from broth or collected and fixed after macrophage lysis. This provided single-*Salmonella* granularity regarding bacterial replication/DSRed dilution, which was the focus of their work. With all conditions they saw red dilution over time, and distinct populations were seen at each time point in broth and RAW264.7 grown *Salmonella*. While this validated the plasmid functionality, it did not preserve data on macrophage infection rates.

Our goal was to acquire data on infection clearance rates and intracellular *Salmonella* replication rates on the scale of single macrophages. At the conclusion of the infection, we gently lifted the macrophages, made a single cell suspension, and fixed them along with their internalized *Salmonella*. This provided data on the ratio of cells that remained infected, and therefore the infection clearance rate. However, DSRed signal was necessarily collected on a small population level, as all *Salmonella* within a given macrophage were interrogated for fluorescence together. While this does not give clear cut replication populations, it does show a 'tail' of DSRed signal loss indicative of replication. Taken together these data demonstrated what was occurring within macrophages which had not cleared the infection at each time point. That is, I could quantify how many macrophages contained undivided vs divided *Salmonella* for each condition.

Initially I had planned to use fluorescent imaging studies to expand and validate our flow data by imaging the fixed cells remaining after flow cytometry was completed. I hoped to visualize the populations we saw in the cytometry and gather some semi-quantitative data regarding the percent of cells infected, and the percent with replicating *Salmonella*. I also wanted to validate that the multiplicity of initial infection was similar across cells, as it appeared in the cytometry data. However, these cells were not flat and adherent like living macrophages during imaging, but were in solution and roughly spherical. It was very difficult to get more than a few cells in a given plane,

even after centrifugation and plate coating. I was also concerned that over time the fluorescent signals might degrade or otherwise produce artifacts, so this experiment was not pursued.

However, I would like to repeat the infection experiment we conducted with the sole aim of imaging. This would allow me to infect macrophages in imaging dishes and then fix them while they were still adhered, which would vastly improve the quality of data I could collect. I believe this is the next experiment that should be conducted in this project.

3.2 Long term live imaging of macrophages expressing ZapCV2 and treated with heat killed *Salmonella*.

My RNAseq data unexpectedly revealed that there were significant expression differences in specific Zn importers, as well as both *Mt* Zn buffering genes, between live and heat killed (HK) *Salmonella* conditions, and that these changed over time. These differences indicate that that macrophage Zn handling and cytosolic [Zn] concentrations may be partially dependent on *Salmonella* status. To corroborate this, fluorescent imaging of cytosolic Zn at multiple time points in macrophages treated with either live or HK *Salmonella* would be invaluable. I have this data for live *Salmonella* infection, and this future direction suggests completing the dataset with long term imaging of macrophages with HK *Salmonella*.

Collecting this data should be relatively straightforward, and would involve transfecting the cytosolic Zn FRET sensor ZapCV2 into macrophages, allowing them to recover, and treating them with HK *Salmonella* at an MOI of 10. A live *Salmonella* treated well will be imaged in tandem as a positive control. If I see differences in cytosolic [Zn] trends between live and HK conditions, then the few Zn transporters with significant differential expression between live and HK conditions might be worth scrutinizing. In my data *Slc39a13* (ER/Golgi) and *14* (plasma membrane (PM)) are more highly expressed in HK conditions at 2 Hrs. By 18 Hrs both of these genes are more highly expressed in alive conditions, as are *Slc39a6/8* (PM), while *Slc39a10* (PM) simultaneously shows lower expression. The data I propose to collect would help to dissect which of these expression changes might have the biggest effect during infection.

The *Mt* data is particularly interesting, since cytosolic Zn levels directly affect metallothionein (*Mt*) expression via the Zn sensing transcription factor MTF1. Because of this, *Mt* expression levels are often used as a proxy for cytosolic [Zn]. In my data, *Mt1* and *Mt2* expression increases dramatically and similarly in both live and HK conditions at 2 Hrs post infection. At 18 Hrs this expression level is maintained for live treated conditions, but levels in HK conditions have been suppressed significantly for both *Mts*, with *Mt1* back to baseline expression. Interestingly, the cytosolic [Zn] changes seen in imaging do not entirely match with the *Mt* expression seen. If this is also the case for HK *Salmonella* treatment, it will be an indication that *Mt* is being regulated in response to some other stressor, like oxidative stress. It will also point toward the conclusion that *Mt* gene expression is not a good marker of cytosolic [Zn] during infection in this system.

This experiment was planned but not fully carried out, after imaging of the treated macrophages showed that many *Salmonella* had survived the heat shock. Though the same temperatures and times were used for this as for heat killing in my RNAseq experiment, this time the *Salmonella* were heated and cooled while pelleted with little supernatant. It appears that dry heat is much less damaging to *Salmonella* than is wet heat[147].

3.3 SpiroZin2 to interrogate Zn levels within the *Salmonella* containing vacuole

Quantifying Zn within the phagosome would provide direct evidence as to whether *Salmonella* experiences Zn limitation during infection. Measurement of Zn in the cytosol corroborated my predictions from RNAseq, namely that increases in Zip14 and *Mt* expression are consistent with increases in cytosolic Zn. While my RNAseq data predict that Zn in the secretory pathway and phago-lysosomal compartment will decrease in infection, I did not directly measure this. Having a Zn FRET sensor able to maintain fluorescence within an acidified compartment would be ideal because ratiometric sensors are more robust than intensity-based sensors. In the absence of that, I would like to attempt phagosomal Zn sensing using SpiroZin2. This small molecule probe reliably localizes to acidified compartments[65] and the Palmer Lab lab has validated its ability to measure

[Zn] fluctuation in lysosomes[30]. While this measurement would not be ratiometric, with correct in situ calibration I think this sensor could be used to give us valuable information about relative Zn levels in phagosomes. This measurement would help establish whether *Salmonella* indeed experience Zn limitation and provide insight into the nuanced way that macrophages utilize Zn for nutritional immunity. As presented in Chapter 2, I have evidence that Zn availability during infection is important for the macrophage to clear the infection. But Zn also promotes *Salmonella* replication. Therefore, observing the extent and timing of [Zn] flux in the phagosome will be a valuable component of understanding this infection system.

While pH is a confounding factor for many small molecule Zn probes, SpiroZin2 is insensitive to fluctuations from pH 3 to pH 7. Phagosomal pH has been estimated as 4.99 – 7.55, depending on the activation state of the cell[148], which should not perturb SpiroZin2. This insensitivity to pH is likely due to SpiroZin2’s chemistry. Many small molecule fluorescent sensors are based on photoinducible electron transfer (PET), which quenches fluorescence unless bound by Zn, but can also be disrupted by protons. Instead, SpiroZin2 fluorescence is “turned on” by a chemical reaction. When Zn binds, spiobenzopyran is converted to fluorescent cyanine dye in a ring opening reaction, which is much less readily perturbed.

Another issue with small molecule dyes is that dye internalization between cells can be inconsistent, which causes apparent resting [Zn] to be inconsistent as well. Han et al. report a normalization technique which uses the dye’s apo state, after treatment with the Zn chelator TPA, to normalize the resting state fluorescence[30]. With this normalization SpiroZin2 fluorescence was consistent and uniform across several cell types.

Experimentally, I would validate the localization of SpiroZin2 with acidic compartments in 129S6 macrophages using colocalization studies with LysoTracker Green, and then perform Zn titrations to determine the dynamic range of the sensor in these cells. However, phagosomes will not acidify immediately upon bacterial engulfment and in fact pro-inflammatory macrophages demonstrate slower acidification and higher ultimate pH[148]. Because of this I will need to infect with GFP expressing *Salmonella* and optimize the timing of SpiroZin2 addition post infection to ensure

that the sensor localizes to the phagosome. Additional Zn titrations under infection conditions may also be necessary. If variations in phagosomal Zn are discernable during infection, I would repeat the experiment under varying levels of Zn availability, to parallel our flow cytometry fluorescence dilution study. Additionally, I would track phagosomal Zn after engulfment of FP tagged heat-killed (HK) *Salmonella*, to determine if phagosomal Zn levels have a relationship to the live vs HK status of the *Salmonella*.

Bibliography

- [1] Ananda S. Prasad, A. Jr Miale, Z. Farid, H. H. Sandstead, and A. R. Schulert. Zinc Metabolism in Patients with the Syndrome of Iron Deficiency Anemia, Hepatosplenomegaly, Dwarfism, and Hypogonadism. Journal of Laboratory and Clinical Medicine, 61(4):537–49, 1963.
- [2] Ananda S. Prasad. Zinc in Human Health: Effect of Zinc on Immune Cells. Molecular Medicine, 14(5):353–357, May 2008.
- [3] Rosalind S Gibson, Victor Raboy, and Janet C King. Implications of phytate in plant-based foods for iron and zinc bioavailability, setting dietary requirements, and formulating programs and policies. Nutrition Reviews, 76(11):793–804, November 2018.
- [4] Maria N Lo, Leah J Damon, Jian Wei Tay, Shang Jia, and Amy E Palmer. Single cell analysis reveals multiple requirements for zinc in the mammalian cell cycle. eLife, 9:e51107, February 2020.
- [5] Emily L. Que, Reiner Bleher, Francesca E. Duncan, Betty Y. Kong, Sophie C. Gleber, Stefan Vogt, Si Chen, Seth A. Garwin, Amanda R. Bayer, Vinayak P. Dravid, Teresa K. Woodruff, and Thomas V. O’Halloran. Quantitative mapping of zinc fluxes in the mammalian egg reveals the origin of fertilization-induced zinc sparks. Nature Chemistry, 7(2):130–139, February 2015.
- [6] Kisang Eom, Jung Ho Hyun, Dong-Gu Lee, Sooyun Kim, Hyeon-Ju Jeong, Jong-Sun Kang, Won-Kyung Ho, and Suk-Ho Lee. Intracellular Zn²⁺ Signaling Facilitates Mossy Fiber Input-Induced Heterosynaptic Potentiation of Direct Cortical Inputs in Hippocampal CA3 Pyramidal Cells. The Journal of Neuroscience: The Official Journal of the Society for Neuroscience, 39(20):3812–3831, May 2019.
- [7] Lynn Sanford and Amy E. Palmer. Dissociated Hippocampal Neurons Exhibit Distinct Zn²⁺ Dynamics in a Stimulation-Method-Dependent Manner. ACS Chemical Neuroscience, 11(4):508–514, February 2020.
- [8] Hong Gao, Wei Dai, Lu Zhao, Junxia Min, and Fudi Wang. The Role of Zinc and Zinc Homeostasis in Macrophage Function. Journal of Immunology Research, 2018, December 2018.
- [9] Claudia Andreini and Ivano Bertini. A bioinformatics view of zinc enzymes. Journal of Inorganic Biochemistry, 111:150–156, June 2012.

- [10] Cynthia Tallant, Aniebrys Marrero, and F. Xavier Gomis-Rüth. Matrix metalloproteinases: Fold and function of their catalytic domains. Biochimica et Biophysica Acta (BBA) - Molecular Cell Research, 1803(1):20–28, January 2010.
- [11] Sung Ryul Lee. Critical Role of Zinc as Either an Antioxidant or a Prooxidant in Cellular Systems. March 2018. Publication Title: Oxidative Medicine and Cellular Longevity Type: Review Article.
- [12] Saul R. Powell. The Antioxidant Properties of Zinc. The Journal of Nutrition, 130(5):1447S–1454S, May 2000.
- [13] Albert W. Girotti, James P. Thomas, and John E. Jordan. Inhibitory effect of zinc(II) on free radical lipid peroxidation in erythrocyte membranes. Journal of Free Radicals in Biology & Medicine, 1(5):395–401, January 1985.
- [14] David J. Eide. Zinc transporters and the cellular trafficking of zinc. Biochimica et Biophysica Acta (BBA) - Molecular Cell Research, 1763(7):711–722, July 2006.
- [15] Paula Díaz-Bulnes, María Laura Saiz, Carlos López-Larrea, and Ramón M. Rodríguez. Crosstalk Between Hypoxia and ER Stress Response: A Key Regulator of Macrophage Polarization. Frontiers in Immunology, 10, 2020.
- [16] Namrata Chaudhari, Priti Talwar, Avinash Parimisetty, Christian Lefebvre d’Hellencourt, and Palaniyandi Ramanan. A molecular web: endoplasmic reticulum stress, inflammation, and oxidative stress. Frontiers in Cellular Neuroscience, 8:213, 2014.
- [17] V. Frazzini, E. Rockabrand, E. Mocchegiani, and S. L. Sensi. Oxidative stress and brain aging: is zinc the link? Biogerontology, 7(5):307–314, October 2006.
- [18] Mark S. Sharpley and Judy Hirst. The Inhibition of Mitochondrial Complex I (NADH:Ubiquinone Oxidoreductase) by Zn^{2+} . Journal of Biological Chemistry, 281(46):34803–34809, November 2006.
- [19] Joseph Lemire, Ryan Mailloux, and Vasu D. Appanna. Zinc toxicity alters mitochondrial metabolism and leads to decreased ATP production in hepatocytes. Journal of Applied Toxicology, 28(2):175–182, 2008.
- [20] Wolfgang Maret. Analyzing free zinc(ii) ion concentrations in cell biology with fluorescent chelating molecules. Metallomics, 7(2):202–211, February 2015.
- [21] Tomasz Kočańczyk, Agnieszka Drozd, and Artur Krężel. Relationship between the architecture of zinc coordination and zinc binding affinity in proteins – insights into zinc regulation. Metallomics, 7(2):244–257, February 2015.
- [22] Wolfgang Maret. Zinc in Cellular Regulation: The Nature and Significance of “Zinc Signals”. International Journal of Molecular Sciences, 18(11):2285, November 2017.
- [23] Jan L. Vinkenborg, Tamara J. Nicolson, Elisa A. Bellomo, Melissa S. Koay, Guy A. Rutter, and Maarten Merkx. Genetically encoded FRET sensors to monitor intracellular Zn^{2+} homeostasis. Nature Methods, 6(10):737–740, October 2009.

- [24] Yan Qin, Jose G. Miranda, Caitlin I. Stoddard, Kevin M. Dean, Domenico F. Galati, and Amy E. Palmer. Direct Comparison of a Genetically Encoded Sensor and Small Molecule Indicator: Implications for Quantification of Cytosolic Zn²⁺. *ACS Chemical Biology*, 8(11):2366–2371, November 2013.
- [25] Yan Qin, Philip J. Dittmer, J. Genevieve Park, Katarina B. Jansen, and Amy E. Palmer. Measuring steady-state and dynamic endoplasmic reticulum and Golgi Zn²⁺ with genetically encoded sensors. *Proceedings of the National Academy of Sciences*, 108(18):7351–7356, May 2011.
- [26] J. Genevieve Park, Yan Qin, Domenico F. Galati, and Amy E. Palmer. New Sensors for Quantitative Measurement of Mitochondrial Zn²⁺. *ACS Chemical Biology*, 7(10):1636–1640, October 2012.
- [27] Dylan H. Fudge, Raymond Black, Lea Son, Kate LeJeune, and Yan Qin. Optical Recording of Zn²⁺ Dynamics in the Mitochondrial Matrix and Intermembrane Space with the GZnP2 Sensor. *ACS Chemical Biology*, 13(7):1897–1905, July 2018.
- [28] Anne M. Hessels and Maarten Merckx. Genetically-encoded FRET-based sensors for monitoring Zn²⁺ in living cells. *Metallomics*, 7(2):258–266, 2015.
- [29] Kyle P. Carter, Margaret C. Carpenter, Brett Fiedler, Ralph Jimenez, and Amy E. Palmer. Critical Comparison of FRET-Sensor Functionality in the Cytosol and Endoplasmic Reticulum and Implications for Quantification of Ions. *Analytical Chemistry*, 89(17):9601–9608, September 2017.
- [30] Yu Han, Jacob M. Goldberg, Stephen J. Lippard, and Amy E. Palmer. Superiority of SpiroZin2 Versus FluoZin-3 for monitoring vesicular Zn²⁺ allows tracking of lysosomal Zn²⁺ pools. *Scientific Reports*, 8(1):15034, October 2018.
- [31] Evan P.S. Pratt, Kelsie J. Anson, Justin K. Tapper, David M. Simpson, and Amy E. Palmer. Systematic Comparison of Vesicular Targeting Signals Leads to the Development of Genetically Encoded Vesicular Fluorescent Zn²⁺ and pH Sensors. *ACS Sensors*, 5(12):3879–3891, December 2020.
- [32] Lien H. Ho, Richard E. Ruffin, Chiara Murgia, Lixin Li, Steven A. Krilis, and Peter D. Zalewski. Labile Zinc and Zinc Transporter ZnT4 in Mast Cell Granules: Role in Regulation of Caspase Activation and NF- κ B Translocation. *The Journal of Immunology*, 172(12):7750–7760, June 2004.
- [33] Emily L. Que, Francesca E. Duncan, Amanda R. Bayer, Steven J. Philips, Eric W. Roth, Reiner Bleher, Sophie C. Gleber, Stefan Vogt, Teresa K. Woodruff, and Thomas V. O’Halloran. Zinc sparks induce physiochemical changes in the egg zona pellucida that prevent polyspermy. *Integrative Biology*, 9(2):135–144, February 2017.
- [34] Wolfgang Maret. The Function of Zinc Metallothionein: A Link between Cellular Zinc and Redox State. *The Journal of Nutrition*, 130(5):1455S–1458S, May 2000.
- [35] Hajo Haase and Wolfgang Maret. Intracellular zinc fluctuations modulate protein tyrosine phosphatase activity in insulin/insulin-like growth factor-1 signaling. *Experimental Cell Research*, 291(2):289–298, December 2003.

- [36] Tuo Zhang, Jian Liu, Matthias Fellner, Chi Zhang, Dexin Sui, and Jian Hu. Crystal structures of a ZIP zinc transporter reveal a binuclear metal center in the transport pathway. Science Advances, 3(8):e1700344, August 2017.
- [37] Taiho Kambe, Eisuke Suzuki, and Taiki Komori. Zinc Transporter Proteins: A Review and a New View from Biochemistry. In Toshiyuki Fukada and Taiho Kambe, editors, Zinc Signaling, pages 23–56. Springer, Singapore, 2019.
- [38] L. A. Gaither and D. J. Eide. Eukaryotic zinc transporters and their regulation. Biometals: An International Journal on the Role of Metal Ions in Biology, Biochemistry, and Medicine, 14(3-4):251–270, December 2001.
- [39] Maria Luisa Lopez-Redondo, Nicolas Coudray, Zhening Zhang, John Alexopoulos, and David L. Stokes. Structural basis for the alternating access mechanism of the cation diffusion facilitator YiiP. Proceedings of the National Academy of Sciences of the United States of America, 115(12):3042–3047, March 2018.
- [40] Wei Lin, Jin Chai, James Love, and Dax Fu. Selective electrodiffusion of zinc ions in a Zrt-, Irt-like protein, ZIPB. The Journal of Biological Chemistry, 285(50):39013–39020, December 2010.
- [41] Kuppuswami Girijashanker, Lei He, Manoocher Soleimani, Jodie M. Reed, Hong Li, Zhiwei Liu, Bin Wang, Timothy P. Dalton, and Daniel W. Nebert. Slc39a14 gene encodes ZIP14, a metal/bicarbonate symporter: similarities to the ZIP8 transporter. Molecular Pharmacology, 73(5):1413–1423, May 2008.
- [42] Ayako Fukunaka, Tomoyuki Suzuki, Yayoi Kurokawa, Tomohiro Yamazaki, Naoko Fujiwara, Kaori Ishihara, Hitoshi Migaki, Katsuzumi Okumura, Seiji Masuda, Yuko Yamaguchi-Iwai, Masaya Nagao, and Taiho Kambe. Demonstration and characterization of the heterodimerization of ZnT5 and ZnT6 in the early secretory pathway. The Journal of Biological Chemistry, 284(45):30798–30806, November 2009.
- [43] T. E. Thingholm, L. Rönstrand, and P. A. Rosenberg. Why and how to investigate the role of protein phosphorylation in ZIP and ZnT zinc transporter activity and regulation. Cellular and molecular life sciences: CMLS, 77(16):3085–3102, August 2020.
- [44] Tuo Zhang, Dexin Sui, and Jian Hu. Structural insights of ZIP4 extracellular domain critical for optimal zinc transport. Nature Communications, 7(1):11979, June 2016. Number: 1 Publisher: Nature Publishing Group.
- [45] Chengfeng Merriman, Qiong Huang, Guy A. Rutter, and Dax Fu. Lipid-tuned Zinc Transport Activity of Human ZnT8 Protein Correlates with Risk for Type-2 Diabetes*. Journal of Biological Chemistry, 291(53):26950–26957, December 2016.
- [46] Claudia J. Stocks, Jessica B. von Pein, James E. B. Curson, James Rae, Minh-Duy Phan, Darren Foo, Nilesh J. Bokil, Taiho Kambe, Kate M. Peters, Robert G. Parton, Mark A. Schembri, Ronan Kapetanovic, and Matthew J. Sweet. Frontline Science: LPS-inducible SLC30A1 drives human macrophage-mediated zinc toxicity against intracellular Escherichia coli. Journal of Leukocyte Biology, 109(2):287–297, 2021.

- [47] Jodi Dufner-Beattie, S. Joshua Langmade, Fudi Wang, David Eide, and Glen K. Andrews. Structure, function, and regulation of a subfamily of mouse zinc transporter genes. The Journal of Biological Chemistry, 278(50):50142–50150, December 2003.
- [48] Peter Thomas, Yefei Pang, Jing Dong, and A. Håkan Berg. Identification and characterization of membrane androgen receptors in the ZIP9 zinc transporter subfamily: II. Role of human ZIP9 in testosterone-induced prostate and breast cancer cell apoptosis. Endocrinology, 155(11):4250–4265, November 2014.
- [49] Artur Krężel and Wolfgang Maret. Dual Nanomolar and Picomolar Zn(II) Binding Properties of Metallothionein. Journal of the American Chemical Society, 129(35):10911–10921, September 2007.
- [50] Wolfgang Maret. Metallothionein/disulfide interactions, oxidative stress, and the mobilization of cellular zinc. Neurochemistry International, 27(1):111–117, July 1995.
- [51] Artur Krezel and Wolfgang Maret. Zinc-buffering capacity of a eukaryotic cell at physiological pZn. Journal of biological inorganic chemistry: JBIC: a publication of the Society of Biological Inorganic Chemistry, 11(8):1049–1062, November 2006.
- [52] Chiara Devirgiliis, Chiara Murgia, Gorm Danscher, and Giuditta Perozzi. Exchangeable zinc ions transiently accumulate in a vesicular compartment in the yeast *Saccharomyces cerevisiae*. Biochemical and Biophysical Research Communications, 323(1):58–64, October 2004.
- [53] Gerd Wellenreuther, Michele Cianci, Remi Tucoulou, Wolfram Meyer-Klaucke, and Hajo Haase. The ligand environment of zinc stored in vesicles. Biochemical and Biophysical Research Communications, 380(1):198–203, February 2009.
- [54] Glen K. Andrews. Cellular zinc sensors: MTF-1 regulation of gene expression. In W. Maret, editor, Zinc Biochemistry, Physiology, and Homeostasis: Recent Insights and Current Trends, pages 37–51. Springer Netherlands, Dordrecht, 2001.
- [55] Chih-Min Tang, Jennifer Westling, and Edward Seto. trans Repression of the Human Metallothionein IIA Gene Promoter by PZ120, a Novel 120-Kilodalton Zinc Finger Protein. Molecular and Cellular Biology, 19(1):680–689, January 1999.
- [56] Viola Günther, Uschi Lindert, and Walter Schaffner. The taste of heavy metals: Gene regulation by MTF-1. Biochimica et Biophysica Acta (BBA) - Molecular Cell Research, 1823(9):1416–1425, September 2012.
- [57] Ursula Wimmer, Ying Wang, Oleg Georgiev, and Walter Schaffner. Two major branches of anti-cadmium defense in the mouse: MTF-1/metallothioneins and glutathione. Nucleic Acids Research, 33(18):5715–5727, October 2005.
- [58] J E J Hardyman, J Tyson, K A Jackson, C Aldridge, S J Cockell, L A Wakeling, R A Valentine, and D Ford. Zinc sensing by metal-responsive transcription factor 1 (MTF1) controls metallothionein and ZnT1 expression to buffer the sensitivity of the transcriptome response to zinc[†]. Metallomics, 8(3):337–343, March 2016.
- [59] Nicholas Dietrich, Daniel L. Schneider, and Kerry Kornfeld. A pathway for low zinc homeostasis that is conserved in animals and acts in parallel to the pathway for high zinc homeostasis. Nucleic Acids Research, 45(20):11658–11672, November 2017.

- [60] Cheri M. Ackerman, Sumin Lee, and Christopher J. Chang. Analytical Methods for Imaging Metals in Biology: From Transition Metal Metabolism to Transition Metal Signaling. Analytical Chemistry, 89(1):22–41, January 2017.
- [61] Evan P. S. Pratt, Leah J. Damon, Kelsie J. Anson, and Amy E. Palmer. Tools and techniques for illuminating the cell biology of zinc. Biochimica et Biophysica Acta (BBA) - Molecular Cell Research, 1868(1):118865, January 2021.
- [62] Yan Qin, Deanne W. Sammond, Esther Braselmann, Margaret C. Carpenter, and Amy E. Palmer. Development of an Optical Zn²⁺ Probe Based on a Single Fluorescent Protein. ACS Chemical Biology, 11(10):2744–2751, October 2016.
- [63] Amanda J. Bird, Hui Zhao, Huan Luo, Laran T. Jensen, Chandra Srinivasan, Marguerite Evans-Galea, Dennis R. Winge, and David J. Eide. A dual role for zinc fingers in both DNA binding and zinc sensing by the Zap1 transcriptional activator. The EMBO Journal, 19(14):3704–3713, July 2000.
- [64] Brett L. Fiedler, Steven Van Buskirk, Kyle P. Carter, Yan Qin, Margaret C. Carpenter, Amy E. Palmer, and Ralph Jimenez. Droplet Microfluidic Flow Cytometer For Sorting On Transient Cellular Responses Of Genetically-Encoded Sensors. Analytical Chemistry, 89(1):711–719, January 2017.
- [65] Pablo Rivera-Fuentes, Alexandra T. Wrobel, Melissa L. Zastrow, Mustafa Khan, John Georgiou, Thomas T. Luyben, John C. Roder, Kenichi Okamoto, and Stephen J. Lippard. A far-red emitting probe for unambiguous detection of mobile zinc in acidic vesicles and deep tissue. Chemical Science, 6(3):1944–1948, 2015.
- [66] Amit Tuli and Mahak Sharma. How to do business with lysosomes: Salmonella leads the way. Current Opinion in Microbiology, 47:1–7, February 2019.
- [67] Thomas E Kehl-Fie and Eric P Skaar. Nutritional immunity beyond iron: a role for manganese and zinc. Current Opinion in Chemical Biology, 14(2):218–224, April 2010.
- [68] Lauren D. Palmer and Eric P. Skaar. Transition Metals and Virulence in Bacteria. Annual Review of Genetics, 50(1):67–91, 2016.
- [69] M. Indriati Hood and Eric P. Skaar. Nutritional immunity: transition metals at the pathogen–host interface. Nature Reviews Microbiology, 10(8):525–537, August 2012.
- [70] Sunil Sazawal, Robert E Black, Mahdi Ramsan, Hababu M Chwaya, Rebecca J Stoltzfus, Arup Dutta, Usha Dhingra, Ibrahim Kabole, Saikat Deb, Mashavi K Othman, and Fatma M Kabole. Effects of routine prophylactic supplementation with iron and folic acid on admission to hospital and mortality in preschool children in a high malaria transmission setting: community-based, randomised, placebo-controlled trial. The Lancet, 367(9505):133–143, January 2006.
- [71] Loretta Brabin, Bernard J Brabin, and Sabine Gies. Influence of iron status on risk of maternal or neonatal infection and on neonatal mortality with an emphasis on developing countries. Nutrition Reviews, 71(8):528–540, August 2013.
- [72] Joseph P. Zackular and Eric P. Skaar. The role of zinc and nutritional immunity in *Clostridium difficile* infection. Gut Microbes, 9(5):469–476, September 2018.

- [73] Lillian J. Juttukonda, Evelien T. M. Berends, Joseph P. Zackular, Jessica L. Moore, Matthew T. Stier, Yaofang Zhang, Jonathan E. Schmitz, William N. Beavers, Christiaan D. Wijers, Benjamin A. Gilston, Thomas E. Kehl-Fie, James Atkinson, Mary K. Washington, R. Stokes Peebles, Walter J. Chazin, Victor J. Torres, Richard M. Caprioli, and Eric P. Skaar. Dietary Manganese Promotes Staphylococcal Infection of the Heart. Cell Host & Microbe, 22(4):531–542.e8, October 2017.
- [74] Gernot Fritsche, Manfred Nairz, Igor Theurl, Sabine Mair, Rosa Bellmann-Weiler, Howard C. Barton, and Günter Weiss. Modulation of macrophage iron transport by Nramp1 (Slc11a1). Immunobiology, 212(9):751–757, January 2008.
- [75] Tomas Ganz. Iron and infection. International Journal of Hematology, 107(1):7–15, January 2018.
- [76] Yaniv Nevo and Nathan Nelson. The NRAMP family of metal-ion transporters. Biochimica Et Biophysica Acta, 1763(7):609–620, July 2006.
- [77] Olivier Cunrath and Dirk Bumann. Host resistance factor SLC11A1 restricts Salmonella growth through magnesium deprivation. Science, 366(6468):995–999, November 2019.
- [78] Manfred Nairz, Ulrike Schleicher, Andrea Schroll, Thomas Sonnweber, Igor Theurl, Susanne Ludwiczek, Heribert Talasz, Gerald Brandacher, Patrizia L. Moser, Martina U. Muckenthaler, Ferric C. Fang, Christian Bogdan, and Günter Weiss. Nitric oxide-mediated regulation of ferroportin-1 controls macrophage iron homeostasis and immune function in Salmonella infection. Journal of Experimental Medicine, 210(5):855–873, April 2013.
- [79] James E. Cassat and Eric P. Skaar. Iron in Infection and Immunity. Cell Host & Microbe, 13(5):509–519, May 2013.
- [80] Rebecca J. Abergel, Melissa K. Wilson, Jean E. L. Arceneaux, Trisha M. Hoette, Roland K. Strong, B. Rowe Byers, and Kenneth N. Raymond. Anthrax pathogen evades the mammalian immune system through stealth siderophore production. Proceedings of the National Academy of Sciences of the United States of America, 103(49):18499–18503, December 2006.
- [81] Erik Ladomersky, Aslam Khan, Vinit Shanbhag, Jennifer S. Cavet, Jefferson Chan, Gary A. Weisman, and Michael J. Petris. Host and Pathogen Copper-Transporting P-Type ATPases Function Antagonistically during Salmonella Infection. Infection and Immunity, 85(9), September 2017.
- [82] Byung-Eun Kim, Tracy Nevitt, and Dennis J. Thiele. Mechanisms for copper acquisition, distribution and regulation. Nature Chemical Biology, 4(3):176–185, March 2008.
- [83] Carine White, Jaekwon Lee, Taiho Kambe, Kevin Fritsche, and Michael J. Petris. A Role for the ATP7A Copper-transporting ATPase in Macrophage Bactericidal Activity*. Journal of Biological Chemistry, 284(49):33949–33956, December 2009.
- [84] Karrera Y. Djoko, Cheryl-lynn Y. Ong, Mark J. Walker, and Alastair G. McEwan. The Role of Copper and Zinc Toxicity in Innate Immune Defense against Bacterial Pathogens *. Journal of Biological Chemistry, 290(31):18954–18961, July 2015.

- [85] Sulman Shafeeq, Hasan Yesilkaya, Tomas G. Kloosterman, Geetha Narayanan, Michal Wandel, Peter W. Andrew, Oscar P. Kuipers, and Julie A. Morrissey. The cop operon is required for copper homeostasis and contributes to virulence in *Streptococcus pneumoniae*. Molecular Microbiology, 81(5):1255–1270, 2011. _eprint: <https://onlinelibrary.wiley.com/doi/pdf/10.1111/j.1365-2958.2011.07758.x>.
- [86] H. Irving and R. J. P. Williams. 637. The stability of transition-metal complexes. Journal of the Chemical Society (Resumed), (0):3192–3210, January 1953.
- [87] Pete Chandransu and John D. Helmann. Intracellular Zn(II) Intoxication Leads to Dysregulation of the PerR Regulon Resulting in Heme Toxicity in *Bacillus subtilis*. PLOS Genetics, 12(12):e1006515, December 2016.
- [88] H el ene Botella, Pascale Peyron, Florence Levillain, Renaud Poincloux, Yannick Poquet, Ir ene Brandli, Chuan Wang, Ludovic Tailleux, Sylvain Tilleul, Guillaume M. Charri ere, Simon J. Waddell, Maria Foti, Geanncarlo Lugo-Villarino, Qian Gao, Isabelle Maridonneau-Parini, Philip D. Butcher, Paola Ricciardi Castagnoli, Brigitte Gicquel, Chantal de Chastellier, and Olivier Neyrolles. Mycobacterial P1-Type ATPases Mediate Resistance to Zinc Poisoning in Human Macrophages. Cell Host & Microbe, 10(3):248–259, September 2011.
- [89] Claudia J. Stocks, Minh-Duy Phan, Maud E. S. Achard, Nguyen Thi Khanh Nhu, Nicholas D. Condon, Jayde A. Gawthorne, Alvin W. Lo, Kate M. Peters, Alastair G. McEwan, Ronan Kapetanovic, Mark A. Schembri, and Matthew J. Sweet. Uropathogenic *Escherichia coli* employs both evasion and resistance to subvert innate immune-mediated zinc toxicity for dissemination. Proceedings of the National Academy of Sciences, 116(13):6341–6350, March 2019.
- [90] Jennifer Angeline Gaddy and Kathryn P. Haley. Metalloregulation of *Helicobacter pylori* physiology and pathogenesis. Frontiers in Microbiology, 6, 2015.
- [91] Kavitha Subramanian Vignesh, Julio A. Landero Figueroa, Aleksey Porollo, Joseph A. Caruso, and George S. Deepe Jr. Zinc Sequestration: Arming Phagocyte Defense against Fungal Attack. PLOS Pathogens, 9(12):e1003815, December 2013.
- [92] Jessica Dade, Juwen C. DuBois, Rajamouli Pasula, Anna M. Donnell, Joseph A. Caruso, A. George Smulian, and George S. Deepe. HcZrt2, a zinc responsive gene, is indispensable for the survival of *Histoplasma capsulatum* in vivo. Medical Mycology, 54(8):865–875, November 2016.
- [93] Timothy C. Johnstone and Elizabeth M. Nolan. Beyond iron: non-classical biological functions of bacterial siderophores. Dalton Transactions, 44(14):6320–6339, 2015.
- [94] Luisa Martinez-Pomares and Siamon Gordon. Antigen presentation the macrophage way. Cell, 131(4):641–643, November 2007.
- [95] Christian Schulz, Elisa Gomez Perdiguero, Laurent Chorro, Heather Szabo-Rogers, Nicolas Cagnard, Katrin Kierdorf, Marco Prinz, Bishan Wu, Sten Eirik W. Jacobsen, Jeffrey W. Pollard, Jon Frampton, Karen J. Liu, and Frederic Geissmann. A lineage of myeloid cells independent of Myb and hematopoietic stem cells. Science (New York, N.Y.), 336(6077):86–90, April 2012.

- [96] Luke C. Davies and Philip R. Taylor. Tissue-resident macrophages: then and now. *Immunology*, 144(4):541–548, April 2015.
- [97] Antonio Sica and Alberto Mantovani. Macrophage plasticity and polarization: in vivo veritas. *The Journal of Clinical Investigation*, 122(3):787–795, March 2012.
- [98] Jia Xue, Susanne V. Schmidt, Jil Sander, Astrid Draffehn, Wolfgang Krebs, Inga Quester, Dominic De Nardo, Trupti D. Gohel, Martina Emde, Lisa Schmidleithner, Hariharasudan Ganesan, Andrea Nino-Castro, Michael R. Mallmann, Larisa Labzin, Heidi Theis, Michael Kraut, Marc Beyer, Eicke Latz, Tom C. Freeman, Thomas Ulas, and Joachim L. Schultze. Transcriptome-Based Network Analysis Reveals a Spectrum Model of Human Macrophage Activation. *Immunity*, 40(2):274–288, February 2014.
- [99] Peter J. Murray, Judith E. Allen, Subhra K. Biswas, Edward A. Fisher, Derek W. Gilroy, Sergij Goerdt, Siamon Gordon, John A. Hamilton, Lionel B. Ivashkiv, Toby Lawrence, Massimo Locati, Alberto Mantovani, Fernando O. Martinez, Jean-Louis Mege, David M. Mosser, Gioacchino Natoli, Jeroen P. Saeij, Joachim L. Schultze, Kari Ann Shirey, Antonio Sica, Jill Suttles, Irina Udalova, Jo A. van Genderachter, Stefanie N. Vogel, and Thomas A. Wynn. Macrophage Activation and Polarization: Nomenclature and Experimental Guidelines. *Immunity*, 41(1):14–20, July 2014.
- [100] Jan Van den Bossche, Jeroen Baardman, and Menno P. J. de Winther. Metabolic Characterization of Polarized M1 and M2 Bone Marrow-derived Macrophages Using Real-time Extracellular Flux Analysis. *JoVE (Journal of Visualized Experiments)*, (105):e53424, November 2015.
- [101] G. M. Tannahill, A. M. Curtis, J. Adamik, E. M. Palsson-McDermott, A. F. McGettrick, G. Goel, C. Frezza, N. J. Bernard, B. Kelly, N. H. Foley, L. Zheng, A. Gardet, Z. Tong, S. S. Jany, S. C. Corr, M. Haneklaus, B. E. Caffrey, K. Pierce, S. Walmsley, F. C. Beasley, E. Cummins, V. Nizet, M. Whyte, C. T. Taylor, H. Lin, S. L. Masters, E. Gottlieb, V. P. Kelly, C. Clish, P. E. Auron, R. J. Xavier, and L. a. J. O’Neill. Succinate is an inflammatory signal that induces IL-1 β through HIF-1 α . *Nature*, 496(7444):238–242, April 2013.
- [102] Gili Rosenberg, Dror Yehezkel, Dotan Hoffman, Camilla Ciolli Mattioli, Moran Fremder, Hadar Ben-Arosh, Leia Vainman, Noa Nissani, Shelly Hen-Avivi, Shirley Brenner, Maxim Itkin, Sergey Malitsky, Ehud Ohana, Noa Bossel Ben-Moshe, and Roi Avraham. Host succinate is an activation signal for Salmonella virulence during intracellular infection. *Science*, 371(6527):400–405, January 2021.
- [103] Silvia Galván-Peña and Luke A. J. O’Neill. Metabolic Reprograming in Macrophage Polarization. *Frontiers in Immunology*, 5, 2014.
- [104] Abhishek K. Jha, Stanley Ching-Cheng Huang, Alexey Sergushichev, Vicky Lampropoulou, Yulia Ivanova, Ekaterina Loginicheva, Karina Chmielewski, Kelly M. Stewart, Juliet Ashall, Bart Everts, Edward J. Pearce, Edward M. Driggers, and Maxim N. Artyomov. Network Integration of Parallel Metabolic and Transcriptional Data Reveals Metabolic Modules that Regulate Macrophage Polarization. *Immunity*, 42(3):419–430, March 2015.
- [105] S. M. Vidal, E. Pinner, P. Lepage, S. Gauthier, and P. Gros. Natural resistance to intracellular infections: Nramp1 encodes a membrane phosphoglycoprotein absent in macrophages from

- susceptible (Nramp1 D169) mouse strains. The Journal of Immunology, 157(8):3559–3568, October 1996.
- [106] D. E. Brown, S. J. Libby, S. M. Moreland, M. W. McCoy, T. Brabb, A. Stepanek, F. C. Fang, and C. S. Detweiler. Salmonella enterica causes more severe inflammatory disease in C57/BL6 Nramp1G169 mice than Sv129S6 mice. Veterinary Pathology, 50(5):867–876, September 2013.
- [107] Mauricio C. De Marzi, Marcos Todone, María B. Ganem, Qian Wang, Roy A. Mariuzza, Marisa M. Fernández, and Emilio L. Malchiodi. Peptidoglycan recognition protein–peptidoglycan complexes increase monocyte/macrophage activation and enhance the inflammatory response. Immunology, 145(3):429–442, 2015.
- [108] Xinghong Yang, Theresa Thornburg, Zhiyong Suo, SangMu Jun, Amanda Robison, Jinqian Li, Timothy Lim, Ling Cao, Teri Hoyt, Recep Avci, and David W. Pascual. Flagella Overexpression Attenuates Salmonella Pathogenesis. PLOS ONE, 7(10):e46828, October 2012.
- [109] Daphne A. C. Stapels, Peter W. S. Hill, Alexander J. Westermann, Robert A. Fisher, Teresa L. Thurston, Antoine-Emmanuel Saliba, Isabelle Blommestein, Jörg Vogel, and Sophie Helaine. Salmonella persists undermine host immune defenses during antibiotic treatment. Science, 362(6419):1156–1160, December 2018.
- [110] Pauline Chabosseau, Erkan Tuncay, Gargi Meur, Elisa A. Bellomo, Anne Hessels, Stephen Hughes, Paul R.V. Johnson, Marco Bugliani, Piero Marchetti, Belma Turan, Alexander R. Lyon, Maarten Merckx, and Guy A. Rutter. Mitochondrial and ER-Targeted eCALWY Probes Reveal High Levels of Free Zn²⁺. ACS Chemical Biology, 9(9):2111–2120, September 2014.
- [111] J. Genevieve Park and Amy E. Palmer. Quantitative Measurement of Ca²⁺ and Zn²⁺ in Mammalian Cells Using Genetically Encoded Fluorescent Biosensors. In Jin Zhang, Qiang Ni, and Robert H Newman, editors, Fluorescent Protein-Based Biosensors: Methods and Protocols, Methods in Molecular Biology, pages 29–47. Humana Press, Totowa, NJ, 2014.
- [112] Sian L. Stafford, Nilesh J. Bokil, Maud E. S. Achard, Ronan Kapetanovic, Mark A. Schembri, Alastair G. McEwan, and Matthew J. Sweet. Metal ions in macrophage antimicrobial pathways: emerging roles for zinc and copper. Bioscience Reports, 33(e00049), July 2013.
- [113] Serena Ammendola, Paolo Pasquali, Claudia Pistoia, Paola Petrucci, Patrizia Petrarca, Giuseppe Rotilio, and Andrea Battistoni. High-Affinity Zn²⁺ Uptake System ZnuABC Is Required for Bacterial Zinc Homeostasis in Intracellular Environments and Contributes to the Virulence of Salmonella enterica. Infection and Immunity, 75(12):5867–5876, December 2007.
- [114] Patrizia Petrarca, Serena Ammendola, Paolo Pasquali, and Andrea Battistoni. The Zur-Regulated ZinT Protein Is an Auxiliary Component of the High-Affinity ZnuABC Zinc Transporter That Facilitates Metal Recruitment during Severe Zinc Shortage. Journal of Bacteriology, 192(6):1553–1564, March 2010.
- [115] Kaisong Huang, Dan Wang, Rikki F. Frederiksen, Christopher Rensing, John E. Olsen, and Ana H. Fresno. Investigation of the Role of Genes Encoding Zinc Exporters zntA, zitB, and fieF during Salmonella Typhimurium Infection. Frontiers in Microbiology, 8, 2018.

- [116] Aimin Wu, Piotr Tymoszek, David Haschka, Simon Heeke, Stefanie Dichtl, Verena Petzer, Markus Seifert, Richard Hilbe, Sieghart Sopper, Heribert Talasz, Dirk Bumann, Cornelia Lass-Flörl, Igor Theurl, Keying Zhang, and Guenter Weiss. Salmonella Utilizes Zinc To Subvert Antimicrobial Host Defense of Macrophages via Modulation of NF- κ B Signaling. Infection and Immunity, 85(12), December 2017.
- [117] Ronan Kapetanovic, Nilesh J. Bokil, Maud E. S. Achard, Cheryl-lynn Y. Ong, Kate M. Peters, Claudia J. Stocks, Minh-Duy Phan, Mercedes Monteleone, Kate Schroder, Katharine M. Irvine, Bernadette M. Saunders, Mark J. Walker, Katryn J. Stacey, Alastair G. McEwan, Mark A. Schembri, and Matthew J. Sweet. *Salmonella* employs multiple mechanisms to subvert the TLR-inducible zinc-mediated antimicrobial response of human macrophages. The FASEB Journal, 30(5):1901–1912, May 2016.
- [118] Susana Campoy, Mónica Jara, Núria Busquets, Ana M. Pérez de Rozas, Ignacio Badiola, and Jordi Barbé. Role of the High-Affinity Zinc Uptake znuABC System in *Salmonella enterica* Serovar Typhimurium Virulence. Infection and Immunity, 70(8):4721–4725, August 2002.
- [119] Antoine-Emmanuel Saliba, Lei Li, Alexander J. Westermann, Silke Appenzeller, Daphne A. C. Stapels, Leon N. Schulte, Sophie Helaine, and Jörg Vogel. Single-cell RNA-seq ties macrophage polarization to growth rate of intracellular *Salmonella*. Nature Microbiology, 2(2):16206, February 2017.
- [120] Aravind Subramanian, Pablo Tamayo, Vamsi K. Mootha, Sayan Mukherjee, Benjamin L. Ebert, Michael A. Gillette, Amanda Paulovich, Scott L. Pomeroy, Todd R. Golub, Eric S. Lander, and Jill P. Mesirov. Gene set enrichment analysis: A knowledge-based approach for interpreting genome-wide expression profiles. Proceedings of the National Academy of Sciences, 102(43):15545–15550, October 2005.
- [121] Arthur Liberzon, Chet Birger, Helga Thorvaldsdóttir, Mahmoud Ghandi, Jill P. Mesirov, and Pablo Tamayo. The Molecular Signatures Database Hallmark Gene Set Collection. Cell Systems, 1(6):417–425, December 2015.
- [122] Kirsten Schaffer and Cormac T. Taylor. The impact of hypoxia on bacterial infection. The FEBS Journal, 282(12):2260–2266, 2015.
- [123] Marie Wrande, Kim Vestö, Speranta Puiac Banesaru, Naeem Anwar, Johan Nordfjell, Lifeng Liu, Gerald M. McInerney, and Mikael Rhen. Replication of *Salmonella enterica* serovar Typhimurium in RAW264.7 Phagocytes Correlates With Hypoxia and Lack of iNOS Expression. Frontiers in Cellular and Infection Microbiology, 10, November 2020.
- [124] G. Bugla-Płoskońska, A. Kiersnowski, B. Futoma-Kołoch, and W. Doroszkiewicz. Killing of Gram-Negative Bacteria with Normal Human Serum and Normal Bovine Serum: Use of Lysozyme and Complement Proteins in the Death of *Salmonella* Strains O48. Microbial Ecology, 58(2):276–289, August 2009.
- [125] Jason R. Dunkelberger and Wen-Chao Song. Complement and its role in innate and adaptive immune responses. Cell Research, 20(1):34–50, January 2010.
- [126] D. M. Monack, B. Raupach, A. E. Hromockyj, and S. Falkow. *Salmonella typhimurium* invasion induces apoptosis in infected macrophages. Proceedings of the National Academy of Sciences, 93(18):9833–9838, September 1996.

- [127] Can G. Pham, Concetta Bubici, Francesca Zazzeroni, Salvatore Papa, Joy Jones, Kellean Alvarez, Shanthi Jayawardena, Enrico De Smaele, Rong Cong, Carole Beaumont, Frank M. Torti, Suzy V. Torti, and Guido Franzoso. Ferritin Heavy Chain Upregulation by NF- κ B Inhibits TNF α -Induced Apoptosis by Suppressing Reactive Oxygen Species. Cell, 119(4):529–542, November 2004.
- [128] Philip J. Dittmer, Jose G. Miranda, Jessica A. Gorski, and Amy E. Palmer. Genetically Encoded Sensors to Elucidate Spatial Distribution of Cellular Zinc. Journal of Biological Chemistry, 284(24):16289–16297, June 2009.
- [129] Lech Kiedrowski. Cytosolic zinc release and clearance in hippocampal neurons exposed to glutamate – the role of pH and sodium. Journal of Neurochemistry, 117(2):231–243, 2011.
- [130] Jeeyon Jeong, Joel M. Walker, Fudi Wang, J. Genevieve Park, Amy E. Palmer, Cecilia Giunta, Marianne Rohrbach, Beat Steinmann, and David J. Eide. Promotion of vesicular zinc efflux by ZIP13 and its implications for spondylocheiro dysplastic Ehlers–Danlos syndrome. Proceedings of the National Academy of Sciences, 109(51):E3530–E3538, December 2012.
- [131] Sophie Helaine, Angela M. Cheverton, Kathryn G. Watson, Laura M. Faure, Sophie A. Matthews, and David W. Holden. Internalization of Salmonella by Macrophages Induces Formation of Nonreplicating Persisters. Science, 343(6167):204–208, January 2014.
- [132] Ming-Jie Liu, Shengying Bao, Marina Gálvez-Peralta, Charlie J. Pyle, Andrew C. Rudawsky, Ryan E. Pavlovicz, David W. Killilea, Chenglong Li, Daniel W. Nebert, Mark D. Wewers, and Daren L. Knoell. ZIP8 Regulates Host Defense through Zinc-Mediated Inhibition of NF- κ B. Cell Reports, 3(2):386–400, February 2013.
- [133] Denise M. Monack, Donna M. Bouley, and Stanley Falkow. Salmonella typhimurium persists within macrophages in the mesenteric lymph nodes of chronically infected Nramp1+/+ mice and can be reactivated by IFN γ neutralization. The Journal of Experimental Medicine, 199(2):231–241, January 2004.
- [134] Gabriel Núñez, Kei Sakamoto, and Miguel P. Soares. Innate Nutritional Immunity. The Journal of Immunology, 201(1):11–18, July 2018.
- [135] Kavitha Subramanian Vignesh, Julio A. Landero Figueroa, Aleksey Porollo, Joseph A. Caruso, and George S. Deepe. Granulocyte Macrophage-Colony Stimulating Factor Induced Zn Sequestration Enhances Macrophage Superoxide and Limits Intracellular Pathogen Survival. Immunity, 39(4):697–710, October 2013.
- [136] Ahmed Sayadi, Anh-Tuan Nguyen, Frederic A. Bard, and Emilie A. Bard-Chapeau. Zip14 expression induced by lipopolysaccharides in macrophages attenuates inflammatory response. Inflammation Research, 62(2):133–143, February 2013.
- [137] Mauro Cerasi, Janet Z Liu, Serena Ammendola, Adam J Poe, Patrizia Petrarca, Michele Pesciaroli, Paolo Pasquali, Manuela Raffatellu, and Andrea Battistoni. The ZupT transporter plays an important role in zinc homeostasis and contributes to Salmonella enterica virulence \dagger . Metallomics, 6(4):845–853, April 2014.
- [138] Madeleine A. Wemyss and Jaclyn S. Pearson. Host Cell Death Responses to Non-typhoidal Salmonella Infection. Frontiers in Immunology, 10, 2019.

- [139] Marco Orecchioni, Yanal Ghosheh, Akula Bala Pramod, and Klaus Ley. Macrophage Polarization: Different Gene Signatures in M1(LPS+) vs. Classically and M2(LPS-) vs. Alternatively Activated Macrophages. Frontiers in Immunology, 10, 2019.
- [140] Kyle A. Jablonski, Stephanie A. Amici, Lindsay M. Webb, Juan de Dios Ruiz-Rosado, Phillip G. Popovich, Santiago Partida-Sanchez, and Mireia Guerau-de Arellano. Novel Markers to Delineate Murine M1 and M2 Macrophages. PLOS ONE, 10(12):e0145342, December 2015.
- [141] Nicholas A. Eisele, Thomas Ruby, Amanda Jacobson, Paolo S. Manzanillo, Jeffery S. Cox, Lilian Lam, Lata Mukundan, Ajay Chawla, and Denise M. Monack. Salmonella Require the Fatty Acid Regulator PPAR δ for the Establishment of a Metabolic Environment Essential for Long-Term Persistence. Cell Host & Microbe, 14(2):171–182, August 2013.
- [142] Aravind Subramanian, Heidi Kuehn, Joshua Gould, Pablo Tamayo, and Jill P. Mesirov. GSEA-P: a desktop application for Gene Set Enrichment Analysis. Bioinformatics, 23(23):3251–3253, December 2007.
- [143] Enhui Pan, Xiao-an Zhang, Zhen Huang, Artur Krezel, Min Zhao, Christine E. Tinberg, Stephen J. Lippard, and James O. McNamara. Vesicular Zinc Promotes Presynaptic and Inhibits Postsynaptic Long-Term Potentiation of Mossy Fiber-CA3 Synapse. Neuron, 71(6):1116–1126, September 2011.
- [144] Kyle Pierce Carter. Engineering and Evaluating Fluorescent Tools for Endoplasmic Reticulum Zinc.
- [145] Ritika Mohan, Arnab Mukherjee, Selami E. Sevgen, Chotitath Sanpitakseree, Jaebum Lee, Charles M. Schroeder, and Paul J. A. Kenis. A multiplexed microfluidic platform for rapid antibiotic susceptibility testing. Biosensors & Bioelectronics, 49:118–125, November 2013.
- [146] Sophie Helaine, Jessica A. Thompson, Kathryn G. Watson, Mei Liu, Cliona Boyle, and David W. Holden. Dynamics of intracellular bacterial replication at the single cell level. Proceedings of the National Academy of Sciences, 107(8):3746–3751, February 2010.
- [147] J. M. Goepfert, I. K. Iskander, and C. H. Amundson. Relation of the Heat Resistance of Salmonellae to the Water Activity of the Environment 1. Applied Microbiology, 19(3):429–433, March 1970.
- [148] Johnathan Canton, Rojyar Khezri, Michael Glogauer, and Sergio Grinstein. Contrasting phagosomal pH regulation and maturation in human M1 and M2 macrophages. Molecular Biology of the Cell, 25(21):3330–3341, November 2014.